GR-79

SSCL-SR-1138

PRELIMINARY LABORATORY TESTING,

SAMPLES FROM

SUPERCONDUCTING SUPER COLLIDER PROJECT

FINAL REPORT

Submitted to
Earth Technology Corporation
P. O. Box 22785
Long Beach, CA 90802-5785

Contract SP-3133

Submitted by

Roy E. Olson
4901 Ridge Oak Drive
Austin, TX 78731

July 31, 1990

SECTION 1

INTRODUCTION

Contract Provisions

The contract provides for a final report "characterizing the behavior of the geologic materials from the site" and also "including all raw data, computations and laboratory notes".

Several points may be made regarding "raw data forms":

1. the raw data forms have gone through an evolution based on our experience and comments from the Earth Technology Corporation, so presentation of photocopies of those forms would lead to a variety of forms for the same purpose.

2. reproduction of data forms containing original pencil data entry often leads to illegible copy.

3. the raw data forms are relatively inefficient in terms of the amount of paper generated.

4. at perhaps the first third point of the testing, we switched to data forms in the form of spreadsheets so data reduction would involve simply transcribing the pencilled-in material directly to the computer, thus making the computer copy a duplicate of the "raw" data.

As a result of the above circumstances, the computer spreadsheets have become the "raw" data forms and will be included in this report. In most cases, no other data form now exists.

The contract provided for the performance of at least two one-dimensional consolidation tests, two one-dimensional swelling tests, two drained direct shear tests, and two drained triaxial

SECTION 2

REVIEW OF CORES RECEIVED AND TESTING PROGRAM

Introduction

A listing of cores received and tests finished or in progress was included in Report No. 5, and a detailed presentation of the testing procedures was presented in Report Nos. 3 and 4. Brief comments are included here for the benefit of readers who may not have access to earlier reports.

Cores Received

A log of the cores received is presented in Table 2.1.

The symbolism used in the column entitled "Test Description" is as follows:

C one-dimensional consolidation including swelling pressure

CD "drained" triaxial compression tests

DS "drained" direct shear tests.

The test numbers were assigned in the sequence the tests were performed.

The procedure we followed in handling cores is presented in Report No. 4. All cores were stored in a moist room during this contract and core weights were recorded initially and at the times that material was removed for testing, to ensure that no measurable weight changes occurred during storage. No weight changes, beyond the accuracy of the measurement, were found.

Boring ID	our Sample ID	Sample Depth (ft)	Sample Formation	Test Description
SIR 3B	10	190.6-191.9	Bentonitic shale, bentonite	C5,DS14,DS15,DS16
BIR 44	11	227.5-229.1	Eagleford Shale	C8,C9,CD5-CD8
	12	184.1-184.9	Eagleford Shale	
BIR 43	13	182.7-184.0	Eagleford Shale	C6,DS4-DS10
	14	189.0-190.0	Eagleford Shale	C7, CD2-CD4
	15	251.0-252.5	Eagleford Shale	DS11-DS13, C10, C11. CD9, CD10
	16	313.4-314.8	Eagleford Shale	
BIR 14	17	219.8-220.8	Eagleford Shale	
	18	220.8-221.8	Eagleford Shale	
	19	249.6-250.6	Eagleford Shale	
	20	252.0-252.9	Eagleford Shale	
BIR 13	21	216.0-216.75	Eagleford Shale	
	22	259.0-260.0	Eagleford Shale	
B1 527	23	201.8-202.8	Eagleford Shale	
BI 533	24	175.8-177.2	Eagleford Shale	
	25	235.0-236.0	Eagleford Shale	
BI 540	26	239.7-240.5	Eagleford Shale	
	27	271.6-272.9	Eagleford Shale	
B1 737	28	184.0-184.6	Eagleford Shale	
	29	184.6-185.4	Eagleford Shale	
	30	243.5-244.6	Eagleford Shale	
B1 807	31	168.4-170.2	Eagleford Shale	
BIR 45	32	170.3-174.4	Eagleford Shale	
	33	174.5-175.8	Eagleford Shale	
	34	201.9-203.0	Eagleford Shale	
	35	298.0-299.7	Eagleford Shale	
SE1 8	1	197.1-197.5	Eagleford Shale	C1
BIR51	2	88.9-90.6	Taylor Marl	
BIR41	3	128.4-128.8	Austin Chalk	
BE6	4	34.3-35.6	Taylor Marl	C2, C3, CD1, DS1- DS3
	5	172.9-174.7	Taylor Marl	C4
	6	52.5-53.6	Taylor Marl	
	7	111.6-112.8	Taylor Marl	
	8	110.6-111.6	Taylor Marl	
BF7	9	55.6-56.6	Taylor Marl	

Table 2.1 Summary of Cores Received and Tests Performed

Testing Program

The testing program is shown in Table 2.2. The tests, their intended purposes, and brief comments on testing procedures, are presented below:

Consolidation. The one-dimensional consolidation properties were measured following essentially standard procedures. Samples had nominal dimensions of 1.5 inches in diameter by 0.6 inch high.

The consolidation samples were subjected to the field overburden effective stress initially, to help close up any fissures that may have opened during coring, handling, shipping, storage, or trimming. The dial indicator used to measure change in thickness was then mounted and zeroed and tap water was added to the cell. The total stress was then adjusted to maintain essentially a constant thickness. When equilibrium was re-established, the applied total stress is considered to be the swelling pressure. The sample was then unloaded in suitable steps to a minimum pressure around 300 psf, then reloaded in increments to a peak pressure of about 178,000 psf, and then unloaded to the minimum pressure in steps. Generally, pressures were doubled for successive steps during loading, and were reduced by a factor of four during unloading.

The above procedure is now modified slightly to require that the dial indicator be mounted and zeroed under a small seating pressure, so that readings of the compression can be measured when the field overburden stress is applied.

Properties measured include the swelling pressure, the stress-strain relationship (in the form of void ratio versus log of effective stress) in one-dimensional compression, and the time-rate properties backed out of the data using Terzaghi's theory (coefficients of consolidation and hydraulic conductivity). The fitting operation was based on the square-root-of-time method as a first step, but then the experimental and theoretical curves were compared on a microcomputer screen and adjustments were made to obtain the "best" fit. Hand checks of selected data confirmed the validity of the resulting parameters.

Hydraulic conductivity. The hydraulic conductivities of some of the one-dimensional consolidation samples were measured, in the

Test ID	Samp. No.	Test Type	Formation	Boring	Core Depth (ft.)	Test Purpose
C1	1	Std. Consol.	Eagleford	SE1-8	197.1-197.5	Consol. Properties
C2	4	Consol., Hyd. Cond.	Taylor	BE6	34.3-35.7	Consol. Prop., Compare k's
C3	4	Std. Consol.	Taylor	BE6	34.3-35.7	Consol. Properties
C4	5	Std. Consol.	Taylor	BE6	172.9-174.7	Consol. Properties
C5	10	Consol., Hyd. Cond.	Bentonite	SIR3B	190.6-191.9	Consol. Prop., Compare k's
C6	13	Std. Consol.	Eagleford	BIR43	182.7-184	Consol. Properties
C7	14	Consol., Hyd. Cond.	Eagleford	BIR43	189-190	Consol. Prop., Compare k's
C8	11	Std. Consol.	Eagleford	BIR44	227.5-229.1	Consol. Properties
C9	11	Consol., Hyd. Cond.	Eagleford	BIR44	227.5-229.1	Consol. Prop., Compare k's
C10	15	Std. Consol.	Eagleford	BIR43	251-252.5	Consol. Properties
C11	15	Consol.,Hyd.Cond.	Eagleford	BIR43	252-252.5	Consol. Prop., Compare k's
DS1	4	Direct Shear	Taylor	BE6	34.3-35.7	Failure Envelope
DS2	4	Direct Shear	Taylor	BE6	34.3-35.7	Failure Envelope
DS3	4	Direct Shear	Taylor	BE6	34.3-35.7	Failure Envelope
DS4	13	Direct Shear	Eagleford	BIR43	182.7-184	10-psi strain rate study
DS5	13	Direct Shear	Eagleford	BIR43	182.7-184	10-psi strain rate study
DS6	13	Direct Shear	Eagleford	BIR43	182.7-184	10-psi strain rate study
DS7	13	Direct Shear	Eagleford	BIR43	182.7-184	50-psi strain rate study
DS8	13	Direct Shear	Eagleford	BIR43	182.7-184	10-psi strain rate study
DS9	13	Direct Shear	Eagleford	BIR43	182.7-184	10-psi strain rate study
DS10	13	Direct Shear	Eagleford	BIR43	182.7-184	10-psi strain rate study
DS11	15	Direct Shear	Eagleford	BIR43	251-252.5	Failure Envelope
DS12	15	Direct Shear	Eagleford	BIR43	251-252.5	Failure Envelope
DS13	15	Direct Shear	Eagleford	BIR43	251-252.5	Failure Envelope
DS14	10	Direct Shear	Eagleford	SIR3B	190.6-191.9	Failure Envelope
DS15	10	Direct Shear	Eagleford	SIR3B	190.6-191.9	Failure Envelope
DS16	10	Direct Shear	Eagleford	SIR3B	190.6-191.9	Failure Envelope
CD1	4	CD Shear	Taylor	BE6	34.3-35.7	Preliminary Test
CD2	14	CD Shear	Eagleford	BIR43	189-190	Failure Envelope
CD3	14	CD Shear	Eagleford	BIR43	189-190	Failure Envelope
CD4	14	CD Shear	Eagleford	BIR43	189-190	Failure Envelope
CD5	11	CD Shear	Eagleford	BIR44	227.5-229.1	10 psi strain rate study
CD6	11	CD Shear	Eagleford	BIR44	227.5-229.1	10 psi strain rate study
CD7	11	CD Shear	Eagleford	BIR44	227.5-229.1	10 psi strain rate study
CD8	11	CD Shear	Eagleford	BIR44	227.5-229.1	10 psi strain rate study
CD9	15	CD Shear	Eagleford	BIR43	251-252.5	100-psi strain rate study
CD10	15	CD Shear	Eagleford	BIR43	251-252.5	100-psi strain rate study

Table 2.2 Tests Completed

consolidation cells, using a constant-head technique. The samples were not backpressured.

We added the hydraulic-conductivity tests to the testing program to allow us to compare the measured hydraulic conductivities with values obtained by fitting Terzaghi's theory to the time-settlement curves and thus to provide an estimate of the applicability of Terzaghi's theory to prediction of time-rates-of movement in the field. These measurements turned out to be important when we interpreted both consolidation and shear data.

Direct Shear. Direct shear samples were consolidated in stages with measurement of consolidation properties, and then sheared at essentially a constant rate of deformation up to failure. The nominal sample dimensions were the same as for one-dimensional consolidation.

The interest here was in defining the Coulomb failure envelope both at peak shearing stress and in the immediate post-failure condition. Many of the samples underwent a sudden failure with nearly constant shearing stress after failure. The post-failure condition was here defined as the condition after displacements of the order of 0.2 inch; no cyclic loading tests with stress reversals were performed.

Most of the direct shear tests were performed to get an estimate of the times-to-failure that would be recommended for production testing but tests were performed at a range in pressures to obtain preliminary data on failure envelopes as well.

Triaxial Compression. The triaxial compression tests were performed using samples with nominal dimensions of 1.5 inches in diameter by 3 inches high (actual heights ranged from 2.64 to 3.05 inches). Early tests involved consolidation under several stresses so as to obtain consolidation data, but the consolidation times were too long to allow this practice to continue. Some of the last tests involved consolidation at once under the final pressure.

The tests were performed to obtain Mohr-Coulomb failure envelopes and to obtain preliminary data on the influence of the testing time on the "drained" strength. In addition, there was an interest in defining stress-strain behavior and in comparing the failure envelopes in triaxial and direct shear.

SECTION 3

INDEX TESTS

Grain Size Analyses

Although grain size analyses were not planned as part of this contract, we performed two hydrometer analyses in accord with ASTM D422, "Standard Method for Particle Size Analysis of Soils". We used 5 gm/liter of sodium hexametaphosphate as the dispersant and allowed samples to soak overnight prior to testing. One test was performed on a sample of Taylor marl and one of Eagleford shale. The grain size curves are shown in Fig. 3.1 and the raw data are included in the appendix. The material is fine grained with 40-50 percent finer than 2 microns.

Specific Gravity Tests

We performed tests for the specific gravity of solids using ASTM D854, "Standard Test Method for Specific Gravity of Soils". Tests were performed on both oven dried material and material that started at the natural field moisture content.

The results of specific gravity tests are included in Table 3.1 and the data forms are included in the appendix.

Duplicate tests, e.g., 8 and 9, 10A and 10B, and 11A and 11B, were performed in an effort to estimate the probable scatter in test results. The duplicates indicated no significant scatter.

The relatively high values of specific gravity apparently resulted from the presence of pyrite, at least in some cases. We found, and removed, some pieces of pyrite that were more than an inch in diameter, from Eagleford cores, and we detected fine grained pyrite in a number of samples of Eagleford shale.

Test No.	Core Number	Formation	Boring	Depth Feet	Oven Dried	Gs
1	4	Taylor	B6	34.3	no	2.67
2	4	Taylor	B6	34.3	no	2.88
3	1	Eagleford	SE 1.8	197.1	yes	2.62
4	4	Taylor	BE6	34.3	yes	2.87
5	1	Eagleford	SE 1.8	197.1	yes	2.56
6	14	Eagleford	BIR 43	189.5	no	2.77
7	14	Eagleford	BIR 43	189.5	no	2.77
8	14	Eagleford	BIR 43	189.5	yes	2.78
9	14	Eagleford	BIR 43	189.5	yes	2.79
10A	11	Eagleford	BIR 44	228	no	2.76
10B	11	Eagleford	BIR 44	228	no	2.78
11A	13	Eagleford	BIR 43	183	no	2.78
11B	13	Eagleford	BIR 43	183	no	2.78
12A	15	Eagleford	BIR 43	228	no	2.78
12B	15	Eagleford	BIR 43	228	no	2.77
13A	10	Bentonite	SIR 3B	191.3	no	2.87
13B	10	Bentonite	SIR 3B	191.3	no	2.87

Table 3.1 Specific Gravity Test Results

The data do not show any clear effect of oven drying on the specific gravity.

Generally, it appears that the specific gravity of the Eagleford is about 2.78 and the Taylor is about 2.87.

Atterberg Limits

Atterberg limit tests were performed in accord with ASTM D4318, "Standard Test Method for Liquid Limit, Plastic Limit, and Plasticity Index of Soils". The samples were oven dried prior to testing and had been used previously for measurement of other properties.

The Atterberg limit data are summarized in Table 3.2 and are plotted in a Casagrande plasticity chart in Fig. 3.2. The original data forms are included in the appendix. The points in the plasticity chart plot in a zone that is essentially parallel to the A line, in accord with engineering experience. The material is a highly plastic clay when it is disaggregated and mixed with water.

Overnight soaking had no apparent effect on the Atterberg limits, contrary to other experience. The effect of oven drying was to raise the Atterberg limits in comparison with tests started at the natural water content, in accord with limited previous experience.

Unit Weights

The unit weights were determined for each sample used for consolidation, direct shear, and triaxial shear tests. Values of the total, dry, and submerged unit weights for all samples are included in Table 3.3. The total unit weight is plotted against sample depth in Fig. 3.3. Except for the bentonite, the total unit weights are generally in the range of 130 to 140 pcf.

Test No.	Sample No.	Boring	Depth Feet	Formation	LL %	PL %	PI %	Oven Dried	Engineering Tests	Notes
1	1	SE 1.8	197.4	Eagleford	62	26	36	no	none	negligible soaking
2	1	SE 1.8	197.4	Eagleford	62	26	36	no	none	soaked overnight
3	4	BE6	34.8	Taylor	73	26	47	yes	DS1+DS2	
4	4	BE6	34.5	Taylor	63	27	36	yes	DS3	
5	13	BIR 43	183.5	Eagleford	86	32	54	yes	DS4	
6	13	BIR 43	183.4	Eagleford	87	31	56	yes	DS5	
7	13	BIR 43	183.3	Eagleford	82	29	53	yes	DS6	
8	13	BIR 43	183.0	Eagleford	82	30	52	yes	DS7	
9	13	BIR 43	182.9	Eagleford	86	35	51	yes	DS8	
10	13	BIR 43	182.8	Eagleford	82	33	49	yes	DS9	
11	13	BIR 43	182.7	Eagleford	90	29	61	yes	DS10	
12	15	BIR 43	251.0	Eagleford	64	24	20	yes	DS11	
13	15	BIR 43	252.2	Eagleford	63	24	39	yes	DS12	
14	15	BIR 43	251.6	Eagleford	63	29	34	yes	DS13	
15	10	SIR 3B	191.5	Bentonite	108	58	50	yes	DS14	
16	10	SIR 3B	191.1	Bentonite	113	58	55	yes	DS15	
17	10	SIR 3B	191.0	Bentonite	120	50	70	yes	DS16	
18	1	SE 1.8	197.1	Eagleford	70	27	43	yes	C1	
19	4	BE6	35.2	Taylor	69	29	40	yes	C2	
20	4	BE6	34.3	Taylor	66	29	37	yes	C3	
21	5	BE6	173.0	Taylor	77	25	52	yes	C4	
22	10	SIR 3B	191.7	Bentonite	110	53	57	yes	C5	
23	13	BIR 43	183.8	Eagleford	88	30	58	yes	C6	
24	14	BIR 43	189.0	Eagleford	75	29	46	yes	C7	
25	11	BIR 44	228.4	Eagleford	64	25	39	yes	C8	
26	11	BIR 44	229.0	Eagleford	73	28	45	yes	C9	
27	15	BIR 43	251.4	Eagleford	59	28	31	yes	C10	
28	15	BIR 43	252.4	Eagleford	66	27	39	yes	C11	
29	4	BE6	35.4	Taylor	67	27	40	yes	CD1	effect of drying
30	4	BE6	35.4	Taylor	64	27	37	no	CD1	effect of drying
31	14	BIR 43	189.3	Eagleford	83	26	57	yes	CD2+CD3	effect of drying
32	14	BIR 43	189.3	Eagleford	78	31	47	no	CD2+CD3	effect of drying
33	14	BIR 43	189.2	Eagleford	80	32	48	yes	CD2	
34	14	BIR 43	189.5	Eagleford	94	29	65	yes	CD3	
35	14	BIR 43	189.8	Eagleford	82	29	53	yes	CD4	noticeable pyrite
36	11	BIR 44	227.7	Eagleford	80	31	49	yes	CD5	noticeable pyrite
37	11	BIR 44	228.0	Eagleford	85	29	56	yes	CD6	
38	11	BIR 44	228.6	Eagleford	80	30	50	yes	CD7	
39	11	BIR 44	228.5	Eagleford	77	31	46	yes	CD8	
40	15	BIR 43	251.7	Eagleford	64	28	36	yes	CD9	
41	15	BIR 43	252.0	Eagleford	67	30	37	yes	CD10	

Table 3.2 Summary of Atterberg Limits

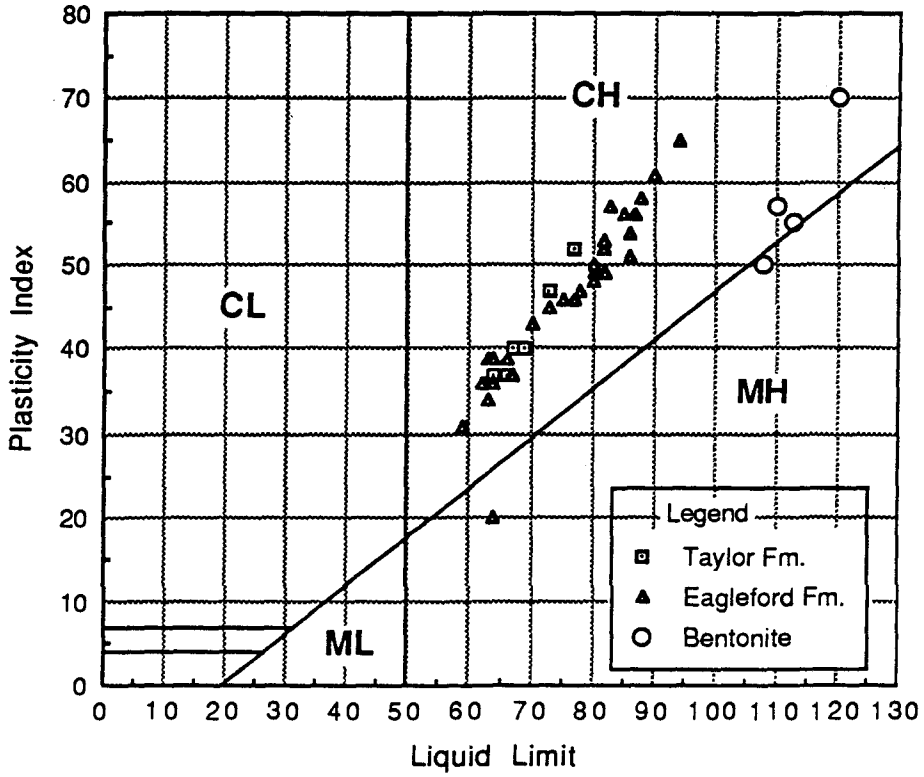

Fig. 3.2 Casagrande Plasticity Chart

Test ID	Sample No.	Formation	Boring	Depth (ft.)	wc %	Total Unit Wt. (pcf)	Dry Unit Wt. (pcf)	Subm. Unit Wt. (pcf)
C1	1	Eagleford	SE1-8	197.2	15.5	137.1	118.7	74.7
C2	4	Taylor	BE6	35.2	20.6	131.9	109.4	69.5
C3	4	Taylor	BE6	35.0	19.8	132.0	110.2	69.6
C4	5	Taylor	BE6	173.0	17.6	138.0	117.3	75.6
C5	10	Bentonite	SIR3B	191.7	38.0	117.4	85.1	55.0
C6	13	Eagleford	BIR43	183.8	18.9	133.2	112.0	70.8
C7	14	Eagleford	BIR43	189.0	16.1	139.4	120.1	77.0
C8	11	Eagleford	BIR44	228.4	13.2	139.7	123.4	77.3
C9	11	Eagleford	BIR44	229.0	17.5	134.2	114.2	71.8
C10	15	Eagleford	BIR43	251.4	18.3	136.0	115.0	73.6
C11	15	Eagleford	BIR43	252.3	16.1	137.9	118.8	75.5
DS1	4	Taylor	BE6	34.9	20.2	131.6	109.5	69.2
DS2	4	Taylor	BE6	34.7	24.3	131.6	105.9	69.2
DS3	4	Taylor	BE6	34.5	20.7	134.1	111.1	71.7
DS4	13	Eagleford	BIR43	183.5	18.6	134.1	113.1	71.7
DS5	13	Eagleford	BIR43	183.4	17.7	134.2	114.1	71.8
DS6	13	Eagleford	BIR43	183.3	17.6	132.6	112.8	70.2
DS7	13	Eagleford	BIR43	183.0	19.0	134.0	112.6	71.6
DS8	13	Eagleford	BIR43	182.9	17.5	133.6	113.7	71.2
DS9	13	Eagleford	BIR43	182.8	17.5	132.3	112.6	69.9
DS10	13	Eagleford	BIR43	182.7	17.1	134.2	114.6	71.8
DS11	15	Eagleford	BIR43	251.0	16.7	129.3	110.8	66.9
DS12	15	Eagleford	BIR43	252.2	14.0	127.7	112.0	65.3
DS13	15	Eagleford	BIR43	251.5	16.0	134.7	116.1	72.3
DS14	10	Bentonite	SIR3B	191.5	39.4	115.2	82.7	52.8
DS15	10	Bentonite	SIR3B	191.1	40.0	111.9	79.9	49.5
DS16	10	Bentonite	SIR3B	191.0	36.8	113.9	83.3	51.5
CD1	4	Taylor	BE6	35.4	19.7	130.4	108.9	68.0
CD2	14	Eagleford	BIR43	189.2	16.2	136.5	117.5	74.1
CD3	14	Eagleford	BIR43	189.5	16.9	137.6	117.7	75.2
CD4	14	Eagleford	BIR43	189.8	15.9	138.2	119.3	75.8
CD5	11	Eagleford	BIR44	227.7	16.7	137.3	117.6	74.9
CD6	11	Eagleford	BIR44	228.0	16.6	137.4	117.8	75.0
CD7	11	Eagleford	BIR44	228.6	16.2	137.9	118.7	75.5
CD8	11	Eagleford	BIR44	228.9	16.1	137.2	118.1	74.8
CD9	15	Eagleford	BIR43	251.7	15.7	138.0	119.3	75.6
CD10	15	Eagleford	BIR43	252.0	15.8	139.0	120.0	76.6

Table 3.3 Densities

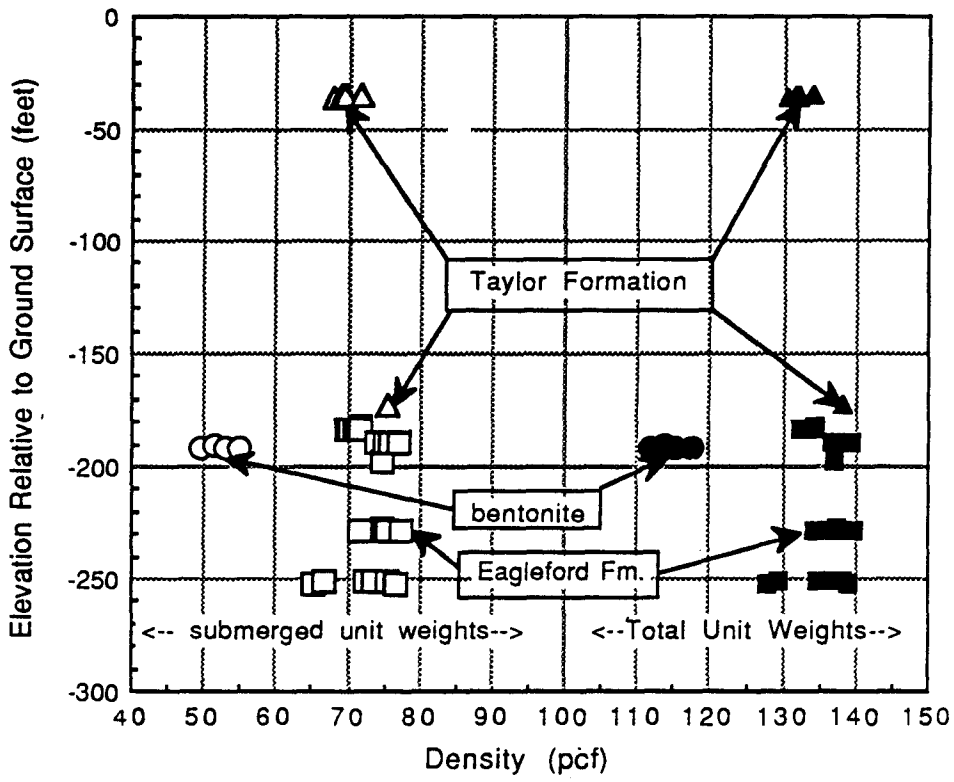

Fig. 3.3 Depth Dependency of Unit Weights

SECTION 4

ONE-DIMENSIONAL CONSOLIDATION

PRESENTATION OF DATA

Consolidation data are presented in the appendix in the following sequence:

First section. The first section is entitled "Summary Data and Plots for One-Dimensional Consolidation Tests".

The information in this section is intended to be a brief summary of the results of the test. The material includes:

1. output from a spreadsheet that contains sample identification information (boring number, sample depth, formation name, sample description), data collected at set-up time (sample thickness and weight), relevant index properties, and relevant data for each of the loading or unloading stages.

2. the stress-strain curves of the sample, in the form of a plot of void ratio versus log of the vertical effective stress.

3. the coefficients of consolidation for the loading phase only (to avoid a confusing number of points) plotted versus log of effective stress, with the e-log($\bar{\sigma}$) relationship included for comparison.

4. plots of void ratio versus the log of the hydraulic conductivity. When values of hydraulic conductivity were measured, then both calculated (Terzaghi's theory) and measured hydraulic conductivities are included.

5. all coefficients of volume compressibility (m_v) plotted versus the log of the effective stress.

Second section. The second section contains the source readings of the dial indicators and time, with any notes included at observation time. The dial readings have been converted to negative numbers for use in a plotting program later. The dial readings are then plotted versus time, square root of time, and the log (base 10) of time so the reader can better judge the time response of the samples.

Third section. The third section contains data for measured hydraulic conductivity and exists only for tests where such measurements were made.

Measurement of Hydraulic Conductivity

The technique for measurement of hydraulic conductivity was reported in Report No. 4. One essential aspect of that technique was that a constant head be used and that measurements of incremental hydraulic conductivity be continued until essential equilibrium was established. Data were collected for volume of flow through the sample, as a function of time, and the incremental hydraulic conductivity was calculated for the time period between successive readings. Spreadsheets used to collect data are included in the appendix. Values of the hydraulic conductivity are plotted against time to show the scatter inherent in the measurements, as well as to show the time-dependency of the measurements. The scatter results from the need to measure tiny flows coupled with normal fluctuations in laboratory temperature and probably other such minor effects as well.

Long periods of time were required to establish steady-state flow. The cause of the delay is that imposition of an excess pore pressure on the base of the sample results in a reduction in effective stress and the beginning of a rebound cycle. Some of the inflow of water is involved in volume change. Steady state seepage is established only after swelling has come to an end.

CUMULATIVE DATA

Data on the consolidation test identification numbers, samples, depths, formation, and certain sample properties, are summarized in Table 4.1.

In the material to follow, the discussion will be more detailed the first time some issue arises but thereafter will be brief.

SAMPLES C2 AND C3 (TAYLOR MARL)

Reasons for Testing Taylor Marl

It was not intended that samples of Taylor marl be tested but inclement weather at the SSC site resulted in a delay in recovery of cores of the Eagleford shale so we began the testing program using cores of Taylor marl that had been supplied for visual examination. The tests with marl were mainly to develop experimental procedures.

Special Purpose for Duplicate Tests

Tests C2 and C3 were performed using samples from the same core. These tests were performed in part, to obtain some idea of the reproducibility of test data, and also to examine the influence of using variations in the technique for estimating the swelling pressure.

Swelling Pressures

For sample C2, we applied a small pressure of about 350 psf, mounted the dial indicator used to measure deformation, innundated

Test ID	Sample No.	Formation	Boring	Depth (ft.)	w c (%)	Gs	LL (%)	PL (%)	Vert. Eff. Stress (psf)	Swelling Pressure (psf)
C2	4	Taylor	BE6	35.2	20.6	2.87	69	29	2750	3000
C3	4	Taylor	BE6	35.0	19.8	2.87	66	29	2750	17000
C4	5	Taylor	BE6	173.0	17.6	2.87	77	25	12000	11000
C5	10	Bentonite	SIR3B	191.7	38.0	2.87	110	53	13000	11000
C6	13	Eagleford	BIR43	183.8	18.9	2.78	88	30	13000	10000
C7	14	Eagleford	BIR43	189.0	16.1	2.78	75	29	13000	9000
C1	1	Eagleford	SE1-8	197.2	15.5	2.67	62	26	14000	35000
C8	11	Eagleford	BIR44	228.4	13.2	2.77	64	25	16000	30000
C9	11	Eagleford	BIR44	229.0	17.5	2.77	73	28	16000	12000
C10	15	Eagleford	BIR43	251.4	18.3	2.78	59	28	18000	17000
C11	15	Eagleford	BIR43	252.4	16.1	2.78	66	27	18000	17000

Table 4.1 Summary of General Consolidation Data

the sample, and then added load as required to maintain constant volume (see discussion below). For sample C3, we applied a rather large pressure of about 5560 psf and duplicated the above process. The field effective overburden pressure was believed to be about 2750 psf.

The initial void ratio of sample C2 was calculated to be 0.639 using a specific gravity of 2.87. The initial degree of saturation was calculated to be 92.6%. Because the sample came from a depth considerably below the water table, many engineers would expect the degree of saturation to be 100%. Several possible explanations exist for the calculated value being less than 100%: (1) the field degree of saturation is actually less than 100%, (2) fissures have opened during coring and subsequent handling and the air voids are actually concentrated in microfissures (no fissures could be seen), or (3) there were errors in defining the specific gravity or sample thickness. However, the fact that all samples had degrees of saturation less than 100% tended to eliminate the possibility of significant experimental errors.

In performing the tests, we have assumed that the sample had microfissures. Thus, when we innundated the sample, and it swelled slightly, we would double the applied load. There would then be an immediate compression which generally exceeded our estimate of apparatus deflection. The sample would then typically have a small amount of time-dependent compression and then begin to swell. We interpreted the compression as being due to closure of fissures and thus we set a new "zero", i.e., we took the new dial reading as corresponding to no real reduction in void ratio of the sample. Eventually, the sample would compress and continue compressing so we were clearly past the swelling pressure. The swelling pressure would then be defined using the compression or swelling index, C:

$$C = \frac{e_1 - e_2}{\log\left(\frac{\bar{\sigma}_2}{\bar{\sigma}_1}\right)} \qquad (4.1)$$

where $e_1 > e_2$ and $\bar{\sigma}_2 > \bar{\sigma}_1$. If point 2 is the known void ratio and effective stress at equilibrium, and e_1 is the initial void ratio, then $\bar{\sigma}_1$ is the swelling pressure (effective stress for no swelling) and is given by:

$$\bar{\sigma}_s = \frac{\bar{\sigma}}{10^{**}\left(\frac{e_i - e}{C}\right)} \qquad (4.2)$$

where $\bar{\sigma}_s$ is the swelling pressure, $\bar{\sigma}$ is the effective stress at the first point where the sample comes to equilibrium and e is the associated void ratio, and e_i is the initial void ratio.

We will use test C2 as an example. The calculated initial void ratio is 0.639. The sample first came to equilibrium at 11,100 psf at an apparent void ratio of 0.625. The first rebound decrement was from 11,100 psf to 2778 psf with a void ratio increase of 0.007. From Eq. 4.2, the swelling pressure was 760 psf, a value significantly less than the apparent field effective stress of about 2750 psf.

If, however, we assume that the net compression of 27 dial divisions (at 0.0001 inch each) under the pressure of 5550 psf was actually closing of fissures and should be ignored, then the void ratio of the non-fissures was less than 0.639 - 0.0027/0.363 = 0.632. The calculated swelling pressure now becomes about 2900 psf, a value in excess of the apparent field effective stress.

The laboratory swelling pressures are usually less than the field overburden effective stress because of the effects of disturbance. The swelling pressure in the lab can exceed the apparent field effective stress if the pore water pressures are reduced in the field, e.g., from pumping an aquifer, or from effects of cementation. If the soil was loaded to an elevated pressure in the field and then cemented to form rock, then removal of overburden pressure might lead to negligible increase in volume in the field. The measured swelling pressure for a perfect sample would then be almost undefinable due to the relative incompressibility of the sample, but might approximate the field overburden stress in an ideal case. On the other hand, rupture of some of the cement during coring and subsequent handling, would mean that the applied pressure in the laboratory would have to correspond to the overburden stress during the cementing process, a value that might exceed the existing overburden stress. Laboratory swelling pressures may be less than actual field values if the cores swelled during the coring operation by imbibation of drilling fluid, and may be too high if the cores were allowed to partially desiccate at any stage prior to setting up the test.

Clearly there is a level of uncertainty in calculating the apparent swelling pressure that cannot be resolved with available data. We will calculate swelling pressures for consolidation tests using Eq. 4.5 and assuming that essentially instantaneous compressions, when loads are applied, are the result of partial closing of fissures that were closed in the field but slightly open in the laboratory. The swelling pressures may thus exceed the field overburden pressure. It must be recognized, however, that the rebound slopes (swelling indices) are so small that significant ranges in swelling pressure result from apparently trivial differences in sample thickness.

On the basis of these comments, sample C2 has a swelling pressure of about 2900 psf.

For sample C3, we applied 5560 psf and set the dial indicator in place, thus trying to close the fissures at once. The sample showed signs of swelling at 5560 psf and 11,100 psf but underwent continued compression for 12 minutes under 22,000 psf. We rebounded back to 16,700 psf and the sample underwent no measurable movement (to 0.00001 inch) during 920 minutes of observation. For this procedure, the swelling pressure was thus 16,700 psf (or thereabouts). This sample had a calculated initial degree of saturation of 90%. As before, it seems impossible to determine with certainty whether the apparent air voids represent a field condition or resulted from opening of microfissures.

The "swelling pressure" is thus seen to vary considerably, in this case from about 3000 psf to about 17000 psf, depending on an apparently minor variation in laboratory procedure.

Comparison of Stress-Strain Curves

The complete e-log($\bar{\sigma}$) curves for tests C2 and C3 are compared in Fig. 4.1. A striking feature of these curves is that the void ratios at low stress are essentially unaffected by loading to almost 180,000 psf and rebounding back again. The implication is that the material might be closer to linearly elastic on a natural stress scale than a log scale. The e-$\bar{\sigma}$ curves (Fig. 4.2) are slightly closer to linear than

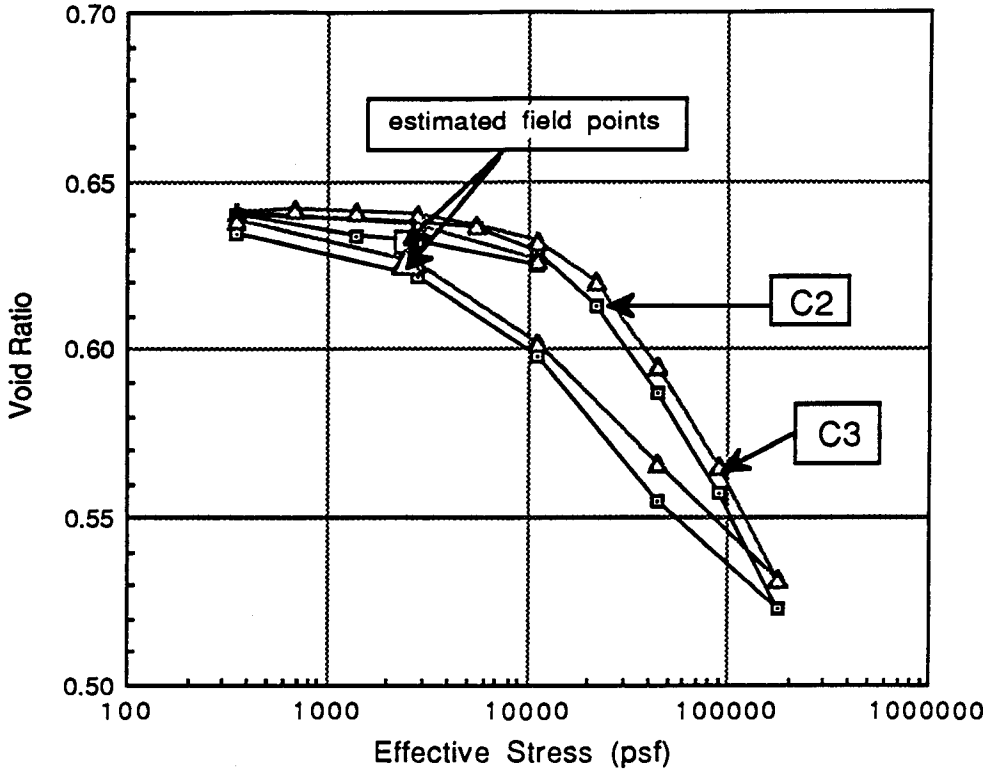

Fig. 4.1 Comparison of Stress-Strain Curves in One-Dimensional Compression for Duplicate Tests C2 and C3

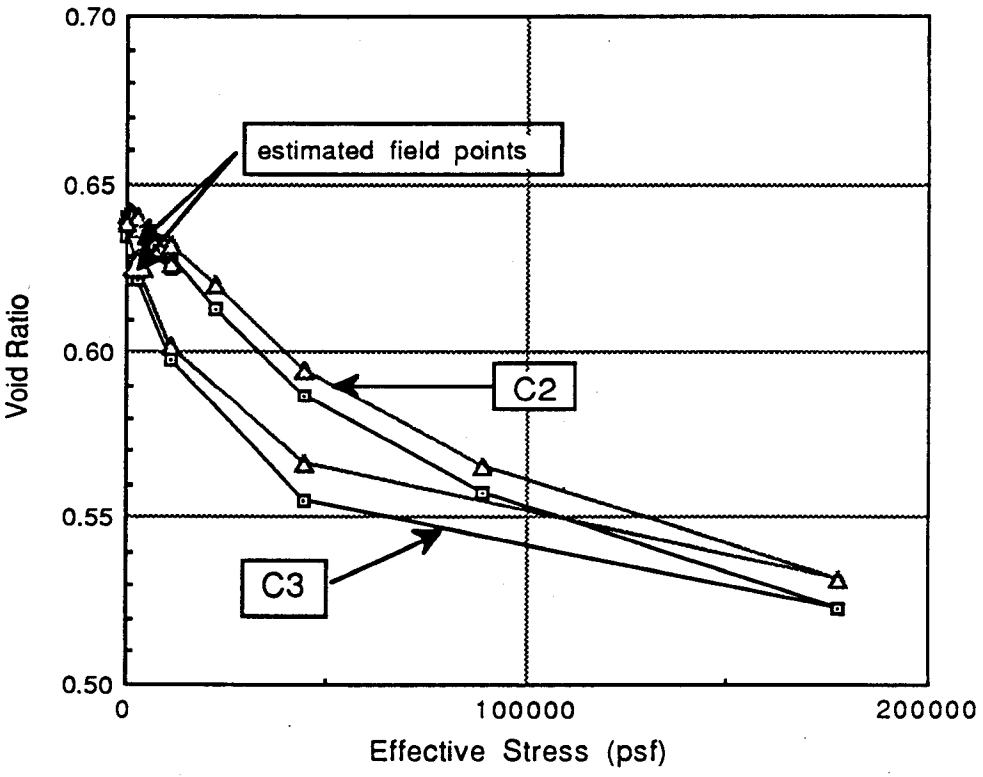

Fig. 4.2 Comparison of Stress-Strain Curves in One-Dimensional Compression for Duplicate Tests C2 and C3

the e-log($\bar{\sigma}$) curves but the natural scale tends to obscure data at low stress levels and thus will not be used further.

The void ratios for tests C2 and C3 differ by less than about 0.01 throughout most of the pressure range .

The procedure used for sample C3 was to apply a significant pressure of 5550 psf and then set the dial indicator in place. Compression that occurred under the 5550 psf was deliberately not measured, assuming it resulted from the closing of fissures. However, the associated reduction in void ratio from the calculated initial value was not measured and cannot be accounted for. For sample C2, the measured compression up to 5550 psf was 36 dial divisions and the height of solids was 0.363 inch so the apparent change in void ratio was about 0.01. The difference in void ratios of samples C2 and C3 is thus most likely the result of variations in the initial loading procedure.

Differences in void ratio can also result from minor experimental errors or variations in material properties.

For example:

$$\Delta e = \frac{w}{S_r}\Delta G_s \qquad (4.3)$$

where Δe is a change in void ratio resulting from an error in specific gravity of solids of ΔG_s, for a sample with a water content of w and degree of saturation of S_r. For an initial water content of 20% and degree of saturation of 100%, a difference of 0.01 in void ratio is a difference of 0.05 in specific gravity of solids. For samples with random amounts of pyrite, such a difference is possible.

Further:

$$\Delta e = \frac{\Delta S}{H_s} \qquad (4.4)$$

where ΔS is an error in thickness or settlement, and H_s is the height of solids. For a height of solids of 0.363 inch (test C2), an error in void ratio of 0.01 corresponds to an error in thickness of 0.004 inch.

ratio because we did not have data on the amount of compression required to close the microfissures. Both the field and laboratory void ratios are likely to be about 0.01 too high for sample C3 as discussed previously.

The field void ratios are slightly lower than those on the reloading curve because of hysteresis associated with the fact that we loaded samples to beyond the swelling pressure and then rebounded. There is no evidence of effects of sample disturbance and we tentatively conclude that the samples can be treated as being undisturbed.

Coefficients of Consolidation

Coefficients of consolidation for tests C2 and C3 are compared in Fig. 4.3. The curves have the same general shape, indicating a gradual reduction in c_v as the consolidation pressure increases.

The differences between the c_v values for samples C2 and C3 may just represent slight differences in material properties but it may also result in part from the difficulty of fitting Terzaghi's theory to measured consolidation curves when the rate of consolidation is probably not controlled by the factors used in developing the theory. Examination of the S-$\sqrt{t}$ curves in the appendix will show that many do not have a well defined early linear portion, as required by Terzaghi's theory, but instead are concave upwards throughout the range of times of measurement. Attempts to fit the theory then lead to scatter depending on which range of times the engineer chooses to assume represents a pseudo-linear portion of the curve.

Hydraulic Conductivities

The question of the applicability of Terzaghi's consolidation theory to any data set is to find a property in the theory that is subject to independent measurement. For the time rate of consolidation, the critical parameter is the hydraulic conductivity which, fortunately, can be measured independently of the time-settlement curve.

Hydraulic conductivities were measured for test C2 and for several other consolidation tests. The measured hydraulic conductivities

are compared with the values obtained by fitting Terzaghi's theory to S-t data, in Fig. 4.4 (same as Fig. C2.4 in the appendix). The measured hydraulic conductivities are plotted against the ultimate void ratios whereas the calculated hydraulic conductivities are plotted against the mean void ratio during consolidation, on the assumption that hydraulic conductivity ought to vary with void ratio.

At low pressures (at void ratios around 0.64), the ratio of measured to calculated hydraulic conductivity, k_m/k_c, is about three but at higher pressures it is closer to ten. The hydraulic conductivity, obtained by fitting Terzaghi's theory to measured S-t data, is too low because actual consolidation is delayed both by hydrodynamic effects and by ill-defined secondary effects but the theory ignores secondary effects, thus requiring a reduced value of hydraulic conductivity to explain the delayed consolidation. The large secondary effect in the laboratory probably results from the high strain rate in the laboratory. With vastly smaller strain rates in the field, secondary effects may be reduced to negligible proportions in the field. As a result, the coefficients of consolidation appropriate to field use may be significantly higher than the values obtained from laboratory tests.

Rebound Properties

For unloading problems, the properties of the samples during rebound are of major interest. Rebound from the peak pressure leads to better defined properties than for the initial unloading from the swelling pressure but loading to pressures near 180,000 psf (but less than the apparent maximum previous consolidation pressure) may result in breakage of cement bonds or other changes in properties that would cause departure from current field conditions.

The rebound slopes of the stress-strain curves are so flat that graphical comparisons may not be very meaningful. Instead, it is convenient to examine the numerical values of the slopes of the stress-strain curves. The slopes can be defined as:

$$\text{coefficient of compressibility} = a_v = \frac{\Delta e}{\Delta \bar{\sigma}} \qquad (4.6)$$

For test C2 the values of C for initial rebound range from 0.006 to 0.011, whereas for test C3 the same range is from 0.007 to 0.013. When the probable errors are considered, these slopes are the same.

For rebound from the peak pressure of 178,000 psf, the (irrelevant) values of C at high pressures are considerably more, but for the pressure range from say 2800 psf to 350 psf (around the field in situ stresses) , the values of C for C2 are 0.014 to 0.040 and for C3 are 0.015 to 0.041, essentially identical values.

It is worth noting that ring friction values are typically quite high for rebound at low pressures, because of stresses built in during the high-pressure loading, so the measured rebound slopes are too small.

By way of comparison, we may note that the virgin value of C is likely to be near 0.5 (see previous discussion). The slope for rebound is likely to be significantly less, perhaps by a factor of 1.5 (highly plastic soils with no non-clay minerals) to 20 (sensitive inorganic clays). The measured slopes are thus in about the range one would expect.

Conclusions Regarding Tests C2 and C3

The following conclusions seem warranted:

1. it was possible to duplicate test results for two samples of Taylor clay that were close together in a single core.

2. the swelling pressure is sensitive to small changes in set-up procedure, because of the relative incompressibility of the samples. In the absence of any mechanism for determining whether or not microfissures have opened in the samples during or after sampling, it is not possible to select a "correct" method of initial loading. We decided to place the field overburden effective stress on subsequent samples, prior to mounting the dials, but the lack of information on compression from the initial void ratio means that our calculated void ratios are likely to be too high by a small amount.

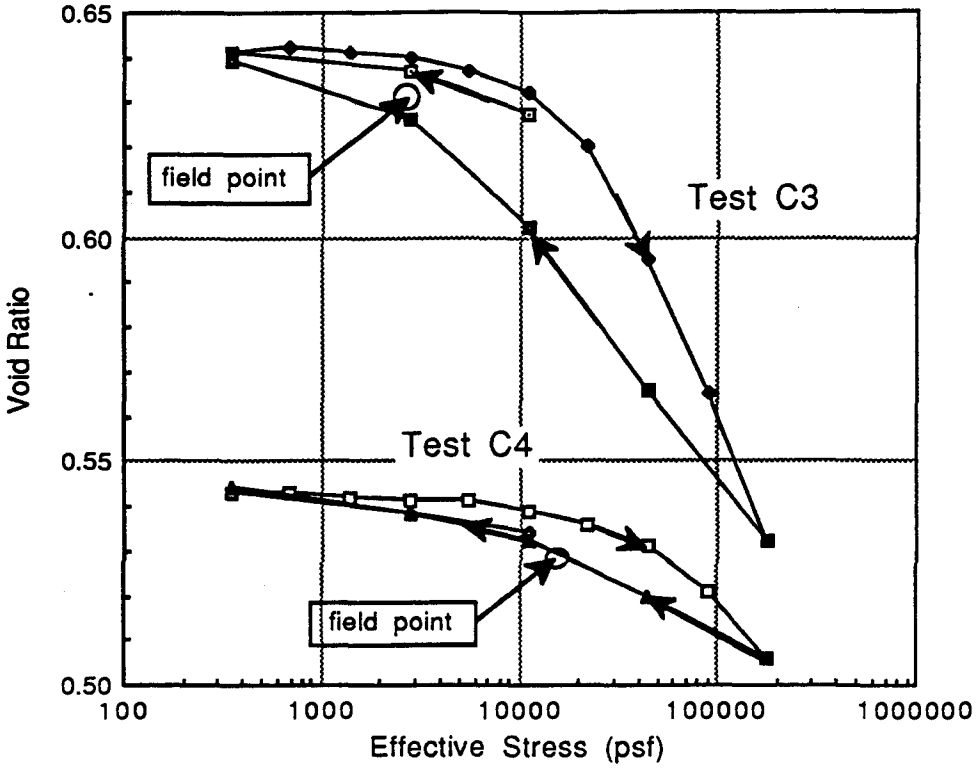

Fig. 4.5 Comparison of Stress Strain Curves for Samples C3 (depth 35 ft) and C4 (depth 173 ft), both of Taylor Marl

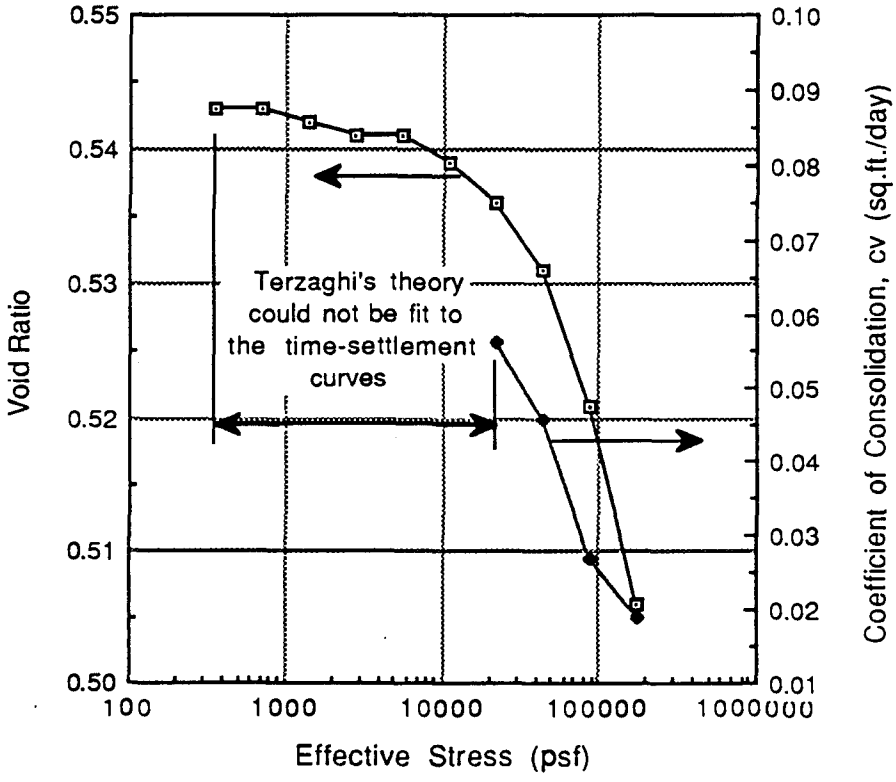

Fig. 4.6 cv and e versus Effective Stress, Test C4

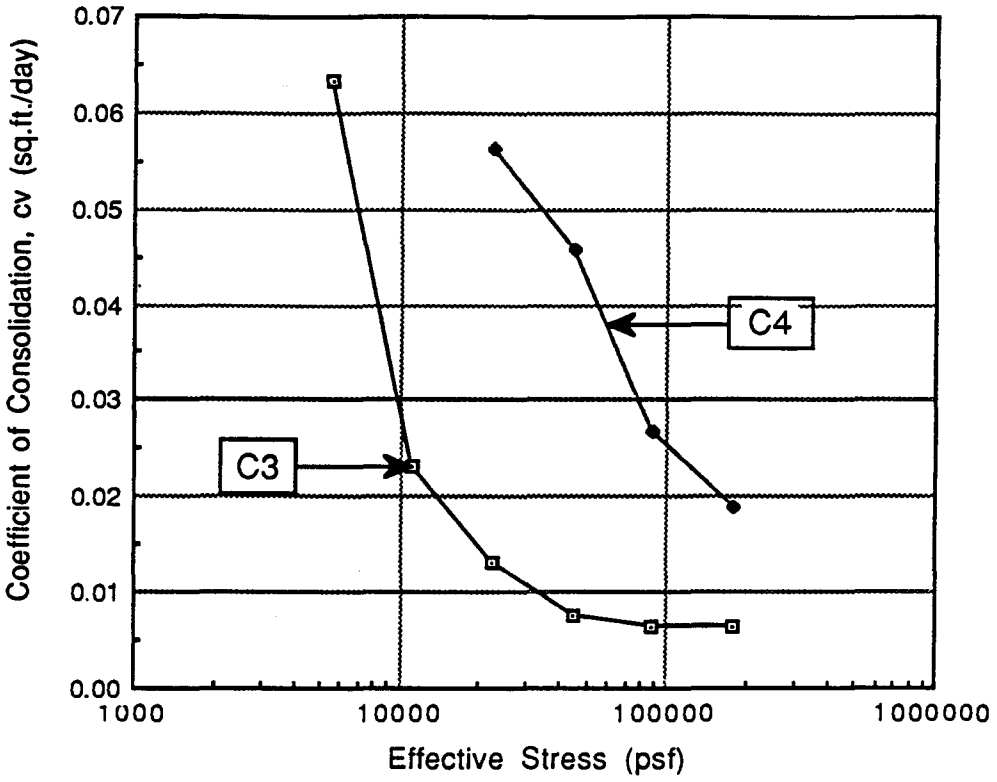

Fig. 4.7 Comparison of Coefficients of Consolidation for Tests C3 (depth 35 ft) and C4 (depth 173 ft) for Taylor Marl

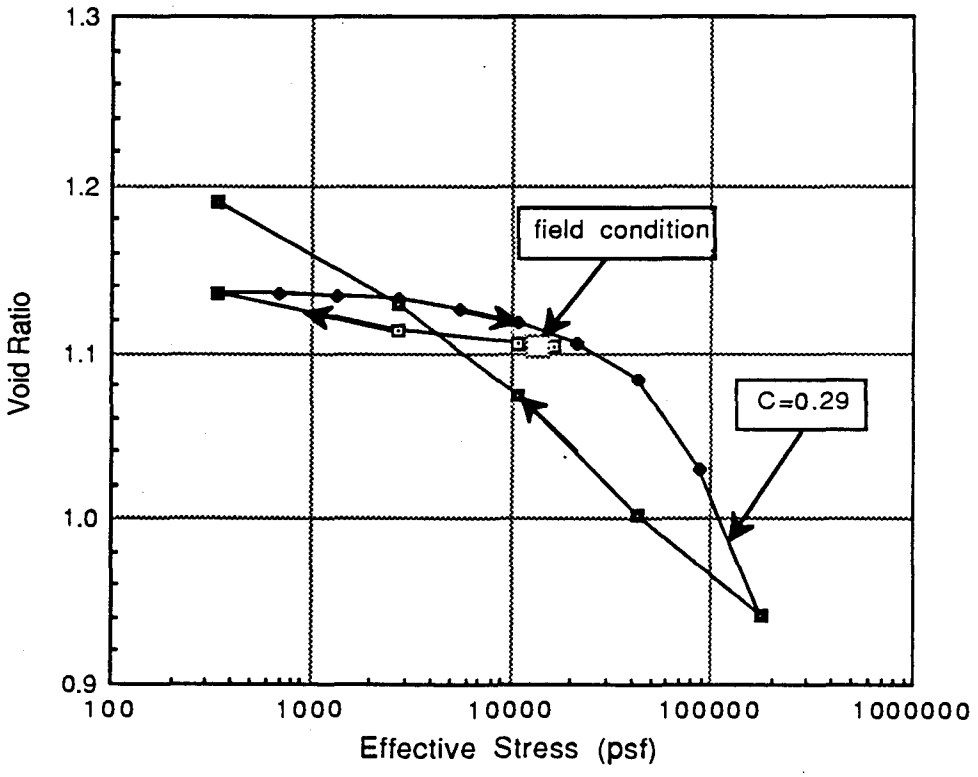

Fig. 4.8 Stress-Strain Curve for Test C5 on Bentonite

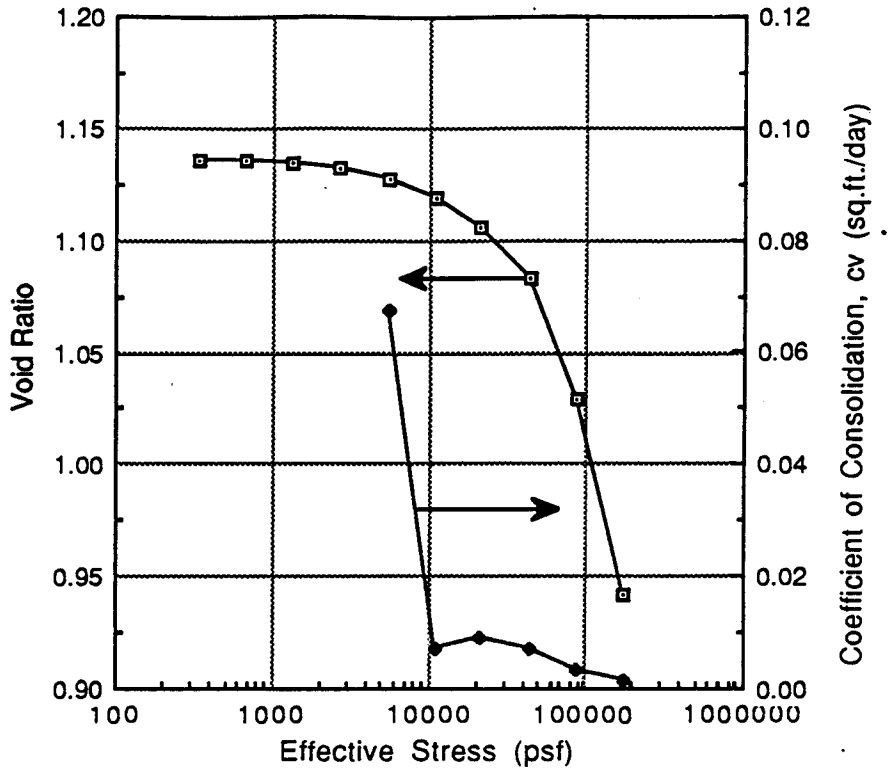

Fig. 4.9 cv and e versus Effective Stress for Test C5 on Bentonite

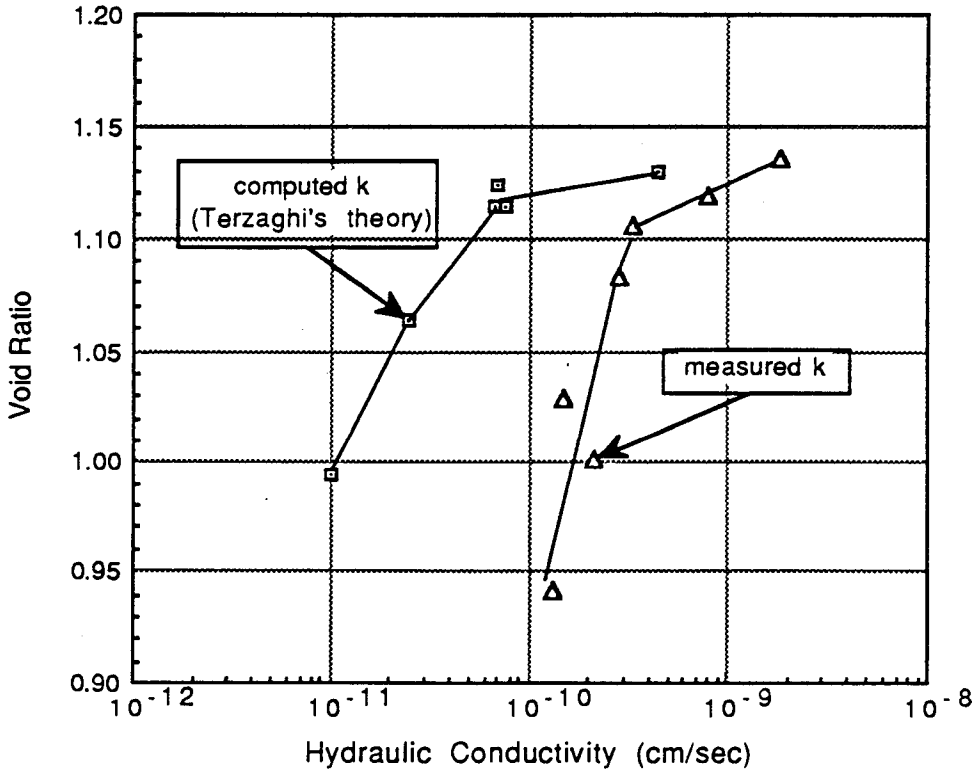

Fig. 4.10 Comparison of Measured and Computed Values of Hydraulic Conductivity for Bentonite

Stress-Strain Relationships

The main loading and unloading stress-strain curves are compared in Fig. 4.11. The initial unloading and reloading curves, and the points representing the field void ratio and effective stress, have been eliminated to improve clarity. The range in initial void ratio is small, only about 0.2, and the curves all have the same basic appearance. The slopes are quite flat for pressures under about 10,000 psf (overburden effective stresses were in the range of about 12,000 psf to 18,000 psf). The slopes increased for larger stresses but never came close to the expected slopes of virgin curves so all of the materials appear to be highly overconsolidated. The swelling curves generally rise to void ratios higher than the loading curves for the final pressure of about 350 psf.

Incremental values of the compression indices are compared in Table 4.2. The indices are remarkably similar for materials from such a wide range in depths, with the largest indices only about twice the smallest ones.

Incremental values of the compression indices for various ranges of pressure tend to increase as the liquid limit increases (Fig. 4.12), with the slopes perhaps a bit low for samples with liquid limits of 64% (C8), 66% (C11), and 70% (C1). The sample for test C8 was slightly too small for the ring (see previous discussion), thus being different from the other samples. Indices for test C11 (LL=60%) tend to be low because they are averaged over a larger range in pressure and the e-log($\bar{\sigma}$) curve is turning downwards. Slopes for test C1 (LL=70%) are also a bit low but that sample was part of the procedures development phase and may have been influenced by its different stress history compared to the other samples.

It is worth noting that an error of 10 dial divisions (0.001 inch) in machine deflections corresponds to an error in compression index of 0.01 (using a height of solids of 0.4 inch and a load increment ratio of 2). Thus, for the expanded scale used in Fig. 4.12, the compression indices for the lowest pressure range could have been influenced visably by errors as minor as those associated with measurement of apparatus deflections. As the pressure increases, the scatter diminishes.

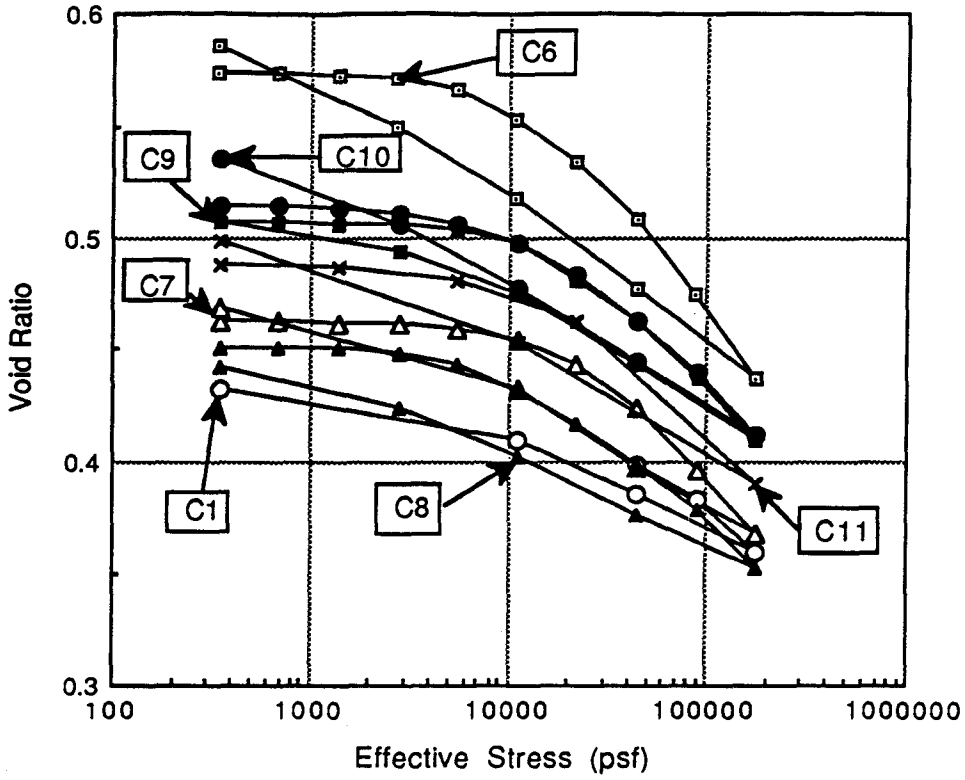

Fig. 4.11 Stress-Strain Curves for Eagleford Shale for Main Loading and Rebound

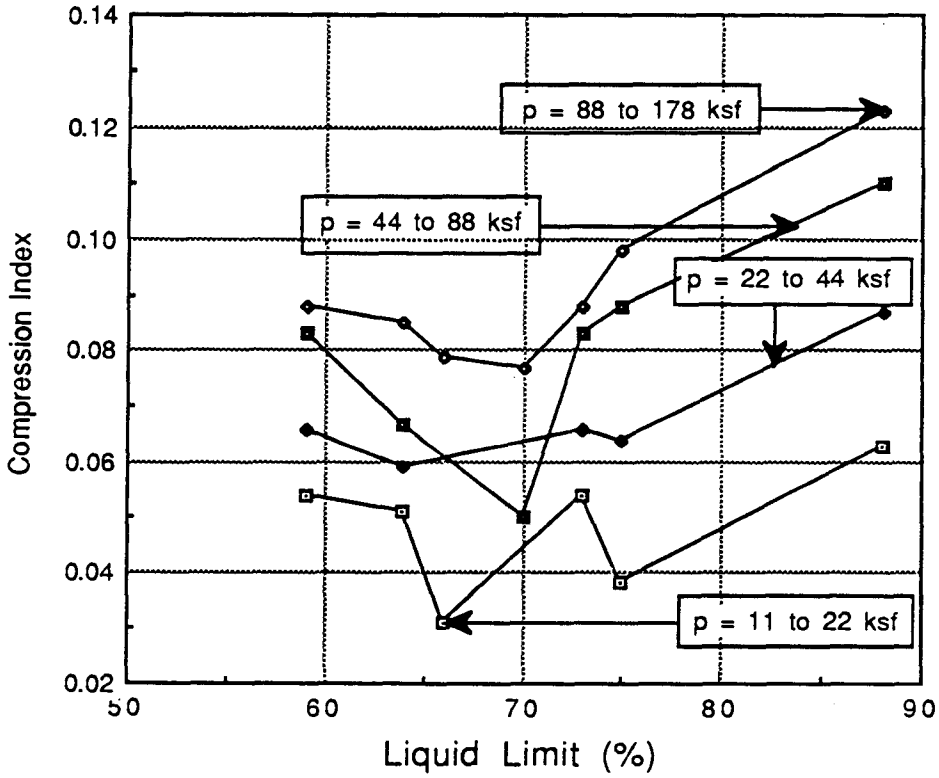

Fig. 4.12 Influence of Liquid Limit on Compression Indices for the Main Loading Curve

Finally, it may be noted that for normally consolidated materials, the compression indices would be expected to range from 0.36 to 0.72 for the range of liquid limits encountered here. The measured slopes are thus considerably less than the values expected for normally consolidated materials.

The shapes and positions of the stress strain curves are in accord with expectations, and the slopes increase generally with increases in plasticity of the material.

Coefficients of Consolidation

Scatter. The curves of settlement versus $\sqrt{\text{time}}$ were often gently curved during the stage when they should have been linear according to Terzaghi's theory. As a result, a wide range in values of c_v can be obtained for any load depending on what part of the curve is assumed to be linear by the person reducing the data. No benefit can be achieved by using the log(time) fitting method because it utilizes the same assumption for the shape of the primary part of the curve. We therefore anticipate significant amounts of scatter for any one test and more scatter when data for a group of tests are compared.

Loading curve. For the loading part of the consolidation tests, the calculated coefficients of consolidation scatter surprisingly little (Fig. 4.13). For stresses near the field overburden pressures the values of c_v range from about 0.001 sq.ft./day to 0.03 sq.ft./day.

Rebound curve. For rebound from the peak pressure, the coefficients of consolidation are lower than for the loading curve (Fig. 4.14). If the material was preloaded in the past, the rebound values may be closer to the actual field values than would be found by applying the field pressure and then rebounding (the procedure we actually followed). For pressures near the field overburden stress, the coefficients of consolidation are around 0.001 sq.ft/day. These values are quite low but are consistent amoung the various samples of Eagleford shale.

Initial rebound. Values of the coefficient of consolidation for the initial rebound are not likely to be accurate because of the problem of closing up microfissures that we suspect opened in the

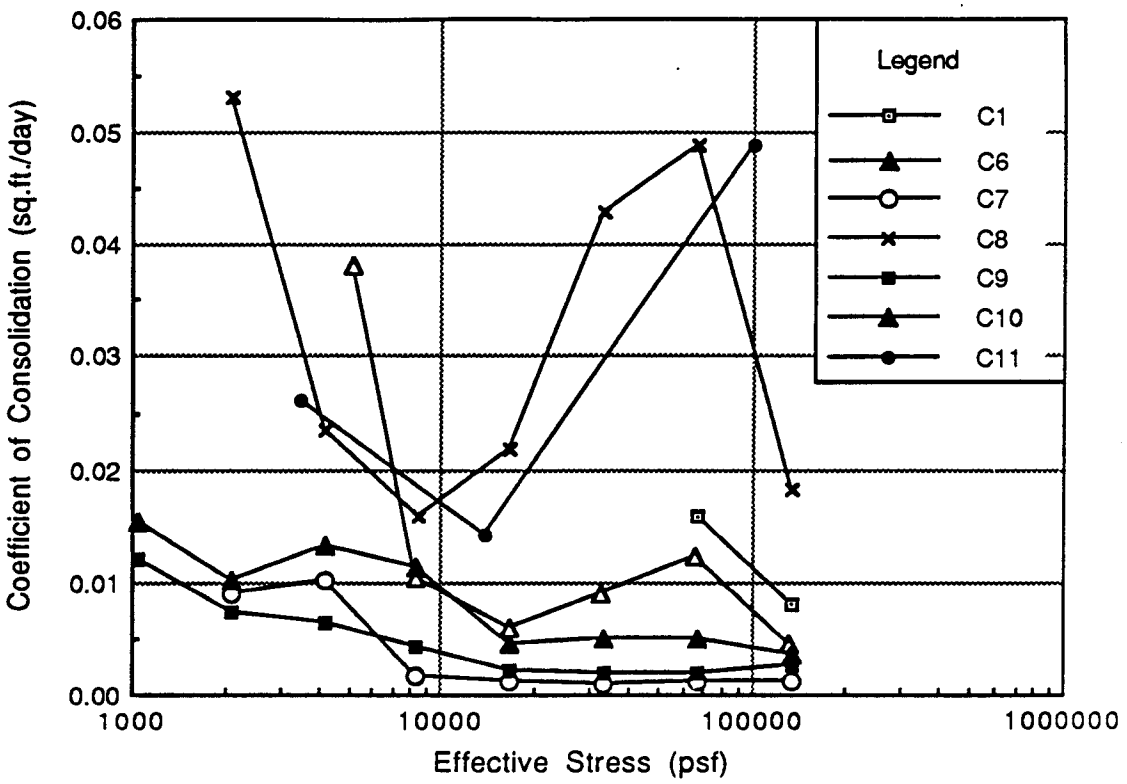

Fig. 4.13 Variation of Coefficient of Consolidation with Mean Effective Stress for Eagleford Shale

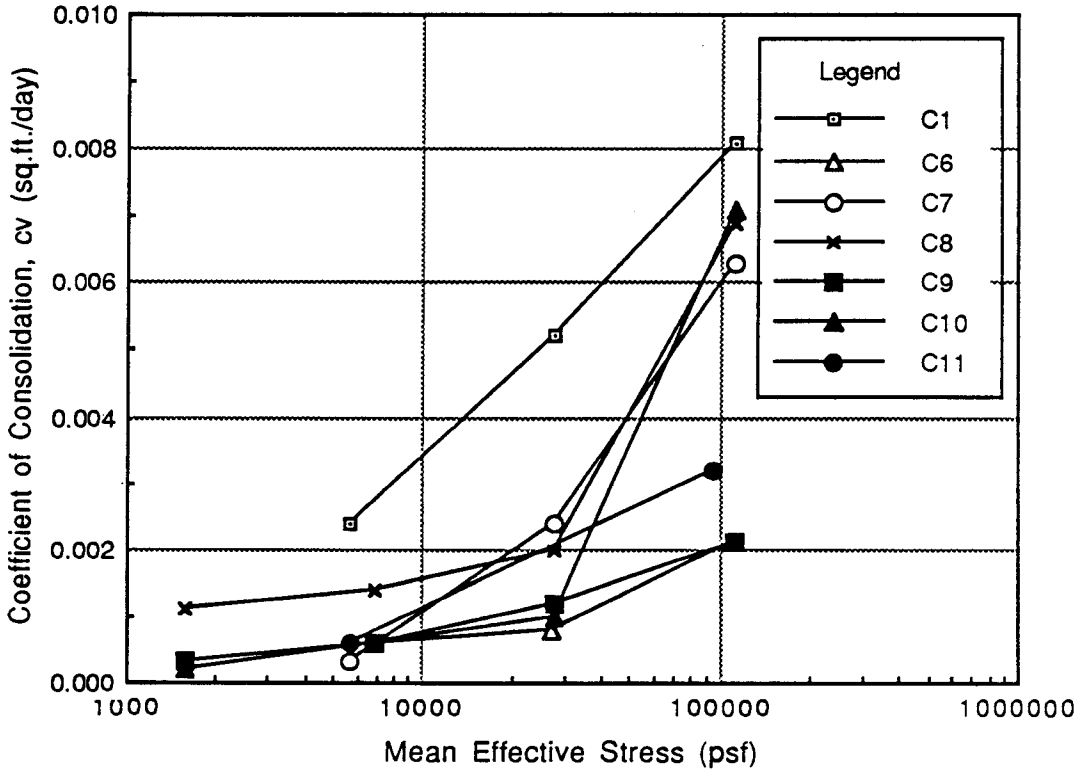

Fig. 4.14 Coefficients of Consolidation for Rebound from 178,000 psf for Eagleford Shale

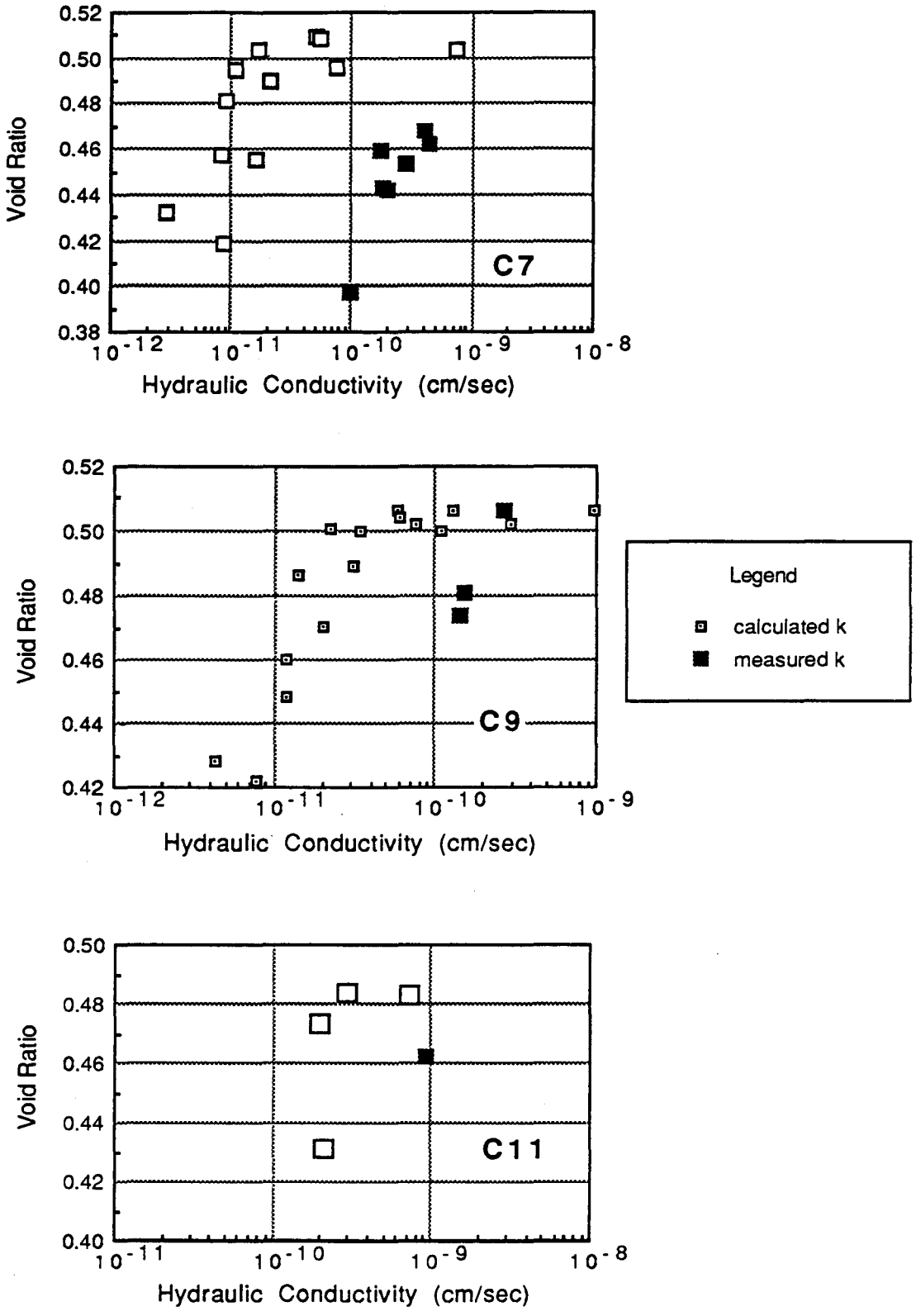

Fig. 4.15 Comparison of Measured and Computed Hydraulic Conductivities for Eagleford Shale

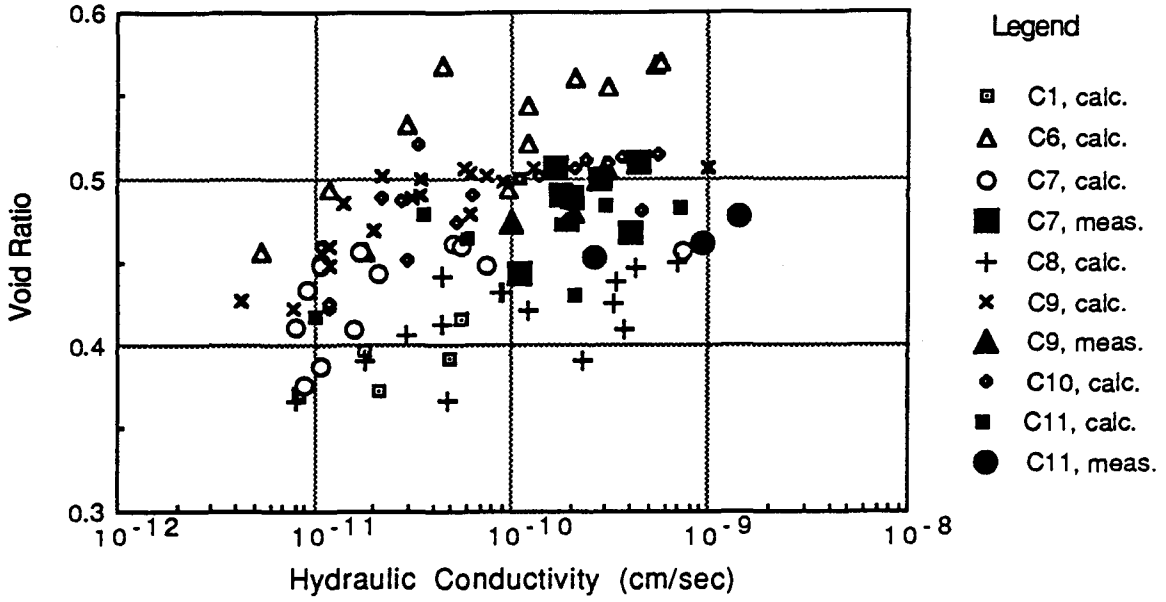

Fig. 4.16 Comparison of Measured and Calculated Values of Hydraulic Conductivity for Eagleford Shale

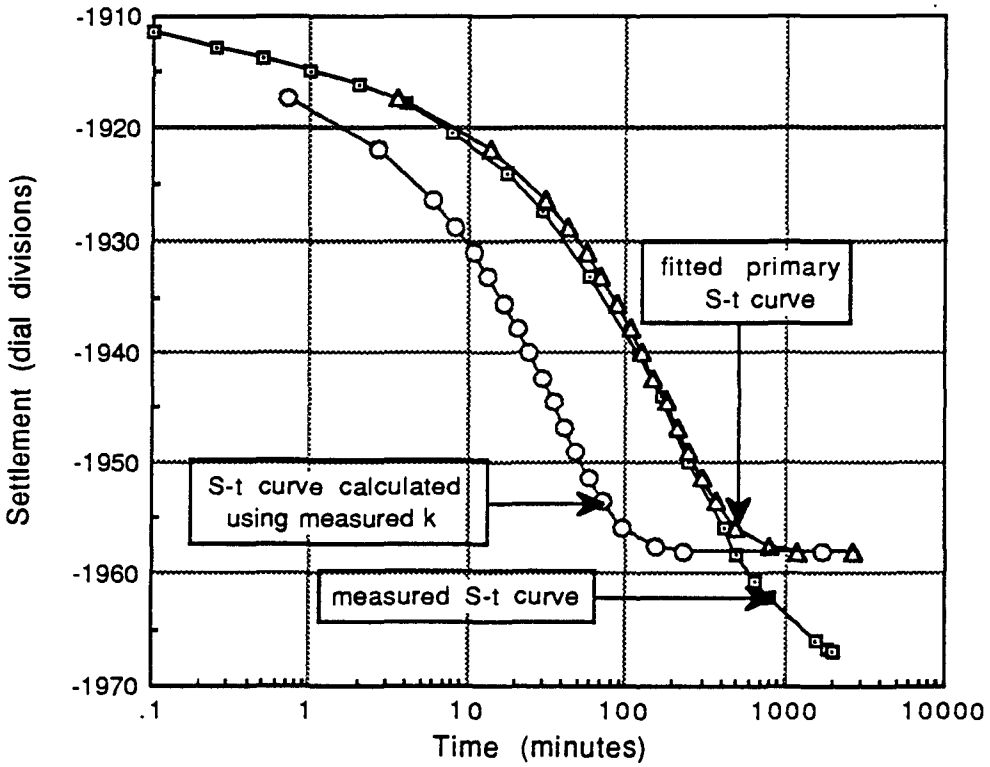

Fig. 4.17 Comparisons of the Fitted S-t Curve and an S-t Curve Calculated using Measured Values of k, with a Measured S-t Curve

3. the coefficients of consolidation found by fitting Terzaghi's theory to the measured S-t curves are also quite low, often below 0.01 sq.ft./day.

4. measured values of hydraulic conductivity are substantially larger than the values obtained by fitting Terzaghi's theory to the measured S-t curves, indicating the presence of substantial secondary effects. We have not had time to investigate these effects nor to consider the implication for predicting time rates of movement in the field.

TESTS USING TAYLOR MARL

Introduction

The first set of three direct shear tests was performed using Taylor marl and was part of the equipment and procedures development phase. The data were reported in Report No. 2 but will be included here for completeness. The data forms are included in the appendix.

Consolidation Stage

For optimal results, the samples should have been subjected to a procedure similar to that followed for the one-dimensional consolidation tests, with determination of the swelling pressure first, and then rebound or loading to the desired normal stress with recording of changes in sample thickness with time. In such a way the coefficients of consolidation could have been defined. Such a procedure was not followed with the Taylor samples because:

1. the goal of these preliminary tests was to develop the shearing procedures, not study the strength.

2. the samples were provided only for initial examination; they had not been sealed to prevent moisture loss, nor handled in any particular fashion to minimize disturbance.

3. the time period available for these tests was too short to allow the preferred testing procedure.

As a result, the samples were placed in the shear boxes and loaded to the final pressure in a single step. In the absence of knowledge of the previous effective stress, it was impossible to define any compressibility term or the hydraulic conductivity, but the coefficient of consolidation could be defined. However, the samples

were so stiff that only a few dial divisions of change in thickness occurred and thus the time-settlement curves would be ill-defined.

The sample for test DS3 underwent the largest volume change during consolidation (see appendix) so an effort was made to estimate its coefficient of consolidation. The estimated value of c_v was 0.04 sq.ft./day, a value that agrees quite well with results from one dimensional consolidation tests (see Figs. 4.3 and 4.6).

Shearing Results

The first test (DS1) was dismantled when the measured shearing force became so high that we thought that the apparatus was binding. However, no evidence of such binding was found in this, or any subsequent test. The apparatus was reassembled and the sample sheared further. Unfortunately, it appeared (see stress-deformation curve in the appendix) that the sample was on the verge of failure when we dismantled the apparatus because it failed at a lower stress upon second loading. Tests DS2 and DS3 were sheared to failure without intermediate unloading.

The curves of shearing stress versus horizontal displacement are shown in Fig. 5.1. All samples underwent sudden failures, indicating that the marl was cemented. The curves are inconsistent in that the post-failure shearing stresses are the same for tests DS2 and DS3 although the normal stresses differed widely (2700 psf for DS2 and 21,000 psf for DS3).

Accordingly, the Coulomb diagram (Fig. 5.2) indicates considerable scatter. The low strengths of the first sample may have been due to the loading-unloading-dismantling-reassembly-reloading process but that process cannot explain the existence of essentially the same residual shearing stresses for tests DS2 and DS3.

Because of the small sample size, material from tests DS2 and DS3 were combined for index tests so Atterberg limits cannot be used in comparing the samples. The initial water content is lowest, and the density highest, for the sample for DS3, observations inconsistent with the comparative results for tests DS2 and DS3.

The average degree of dissipation of excess pore water pressures at failure (U_f) can be estimated using:

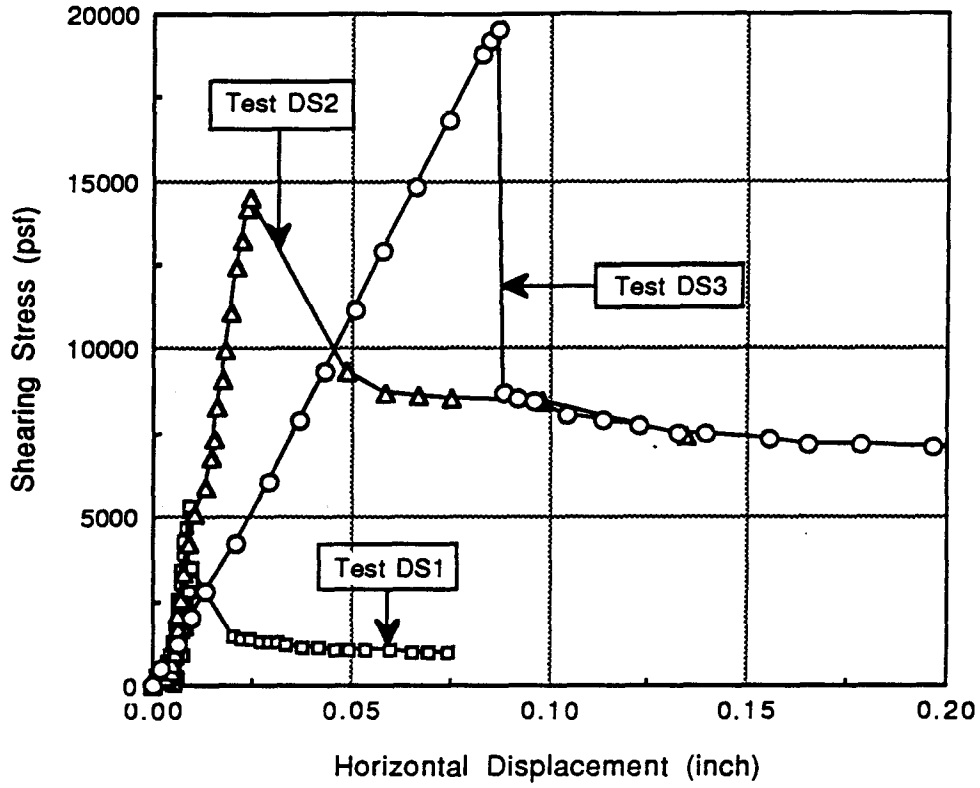

Fig. 5.1 Stress-Deformation Curves for Three Direct Shear Tests on Taylor Marl

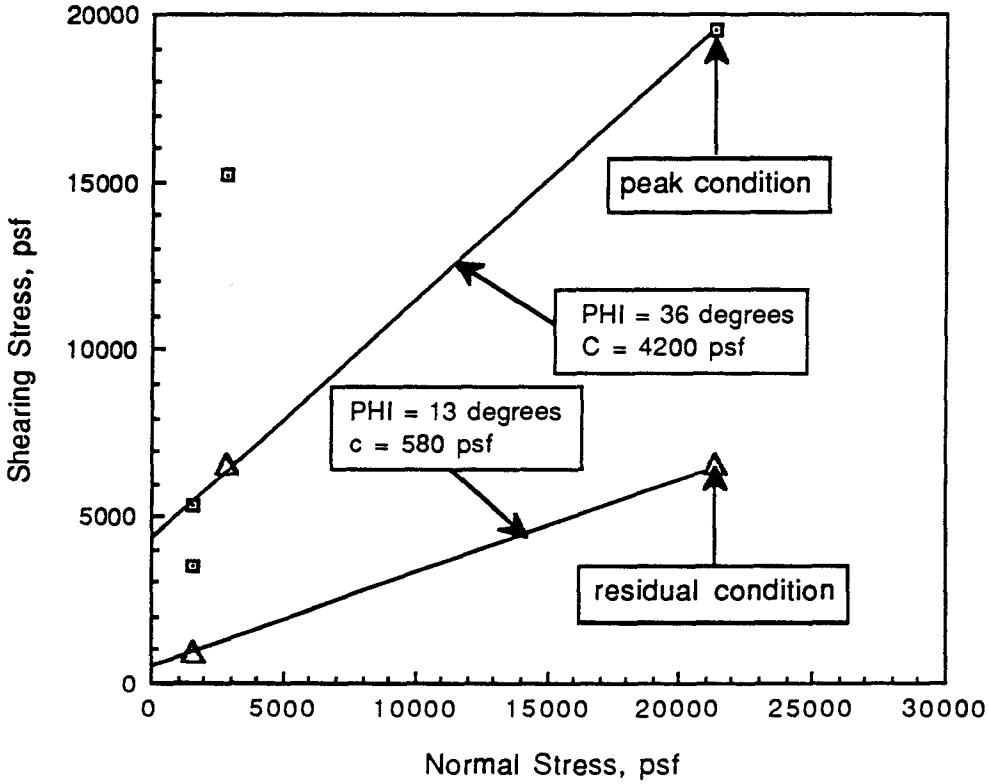

Fig. 5.2 Coulomb Failure Envelope for Taylor Marl

$$U_f = 1 - \frac{H^2}{2c_v t_f} \qquad (5.1)$$

where H is the drainage distance, c_v is the coefficient of consolidation, and t_f is the time to failure. Equation 5.1 is reasonably accurate only if the degree of consolidation at failure is reasonably large, say about 60%. If c_v=0.04 sq.ft./day and H=0.3 inch, then the calculated degrees of dissipation at failure for tests C1, C2, and C3 are 85%, 95%, and 95%, respectively, all reasonable values. It does not appear, therefore, that the scatter of data results from some samples being more completely drained than other samples.

Because the strength of the Taylor material was not a major consideration on this project, no other tests were performed on the Taylor samples. In the absence of other data, and considering that these were preliminary tests on a core that had deliberately not been treated like later cores, we have to conclude that we cannot determine the cause of the scatter.

In the absence of other information, tests DS1 and DS3 seem to have yielded more reasonable results than DS2. If we use data from DS1 and DS3, then the failure envelope is defined as:

peak failure envelope $\bar{\phi}$ = 36 degrees $\bar{c}$ = 4200 psf

residual envelope $\bar{\phi}$ = 13 degrees $\bar{c}$ = 580 psf

The failure surfaces of all three samples were irregular (rough). This observation will be considered further based on later tests on Eagleford shale and bentonite.

TESTS WITH EAGLEFORD SHALE TO DETERMINE THE EFFECTS OF TIME TO FAILURE ON THE MEASURED SHEARING STRENGTH

Expected Behavior

For highly overconsolidated materials, it is expected that application of shearing stresses will cause generation of negative

pore water pressures, which will thus increase the effective stresses and shearing strengths. Time dependent dissipation of these negative pore water pressures should then lead to reductions in shearing strength as the testing time increases. After some shearing time, the shear-induced negative pore water pressures should have dissipated and further increases in time to failure should lead to a reduction in strength due to material viscosity.

Shearing Strengths

The study of effects of deformation rate on "drained" strength was performed using seven tests (DS4-DS10) on samples of Eagleford shale from boring BIR43 at a depth of about 183 feet. Detailed data are presented in the appendix. Peak shearing stresses are summarized in Table 5.1. There is no obvious effect of time to

Table 5.1 Summary of Direct Shear Tests used in Deformation-Rate Study for Eagleford Shale

Test No.	Time to Failure (minutes)	Shearing Strength (psf)
DS5	8	2820
DS4	92	4330
DS6	430	1320
DS7	440	4150
DS8	858	980
DS9	2340	730
DS10	7260	4560

failure on shearing strength. The shearing strengths are plotted against time to failure in Fig. 5.3. The shearing strengths for four of the tests (DS5, DS6, DS8, DS9) seem to fall on a relationship of the expected type but three tests (DS4, DS7, and DS10) yield substantially higher strengths.

The shearing stress-horizontal deformation curves are compared in Fig. 5.4. For these curves, the displacements of some of the tests were corrected by up to 0.006 inch to eliminate problems associated with establishing firm initial contact between the loading head and the shear box. No shearing stresses were altered.

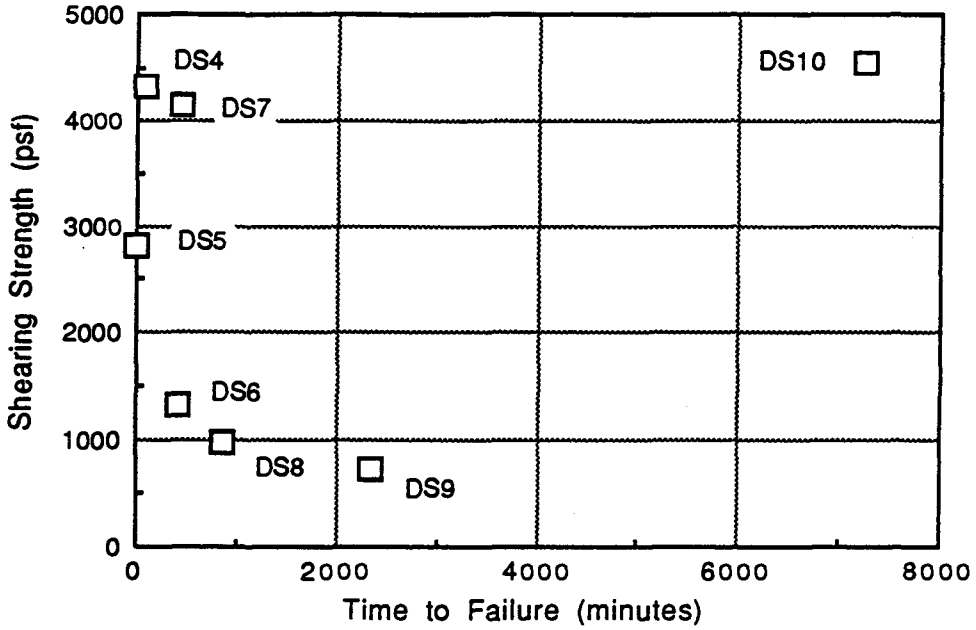

Fig. 5.3 Influence of Time to Failure on Strength of Eagleford Shale from Boring BIR43 at a Depth of 183 Feet

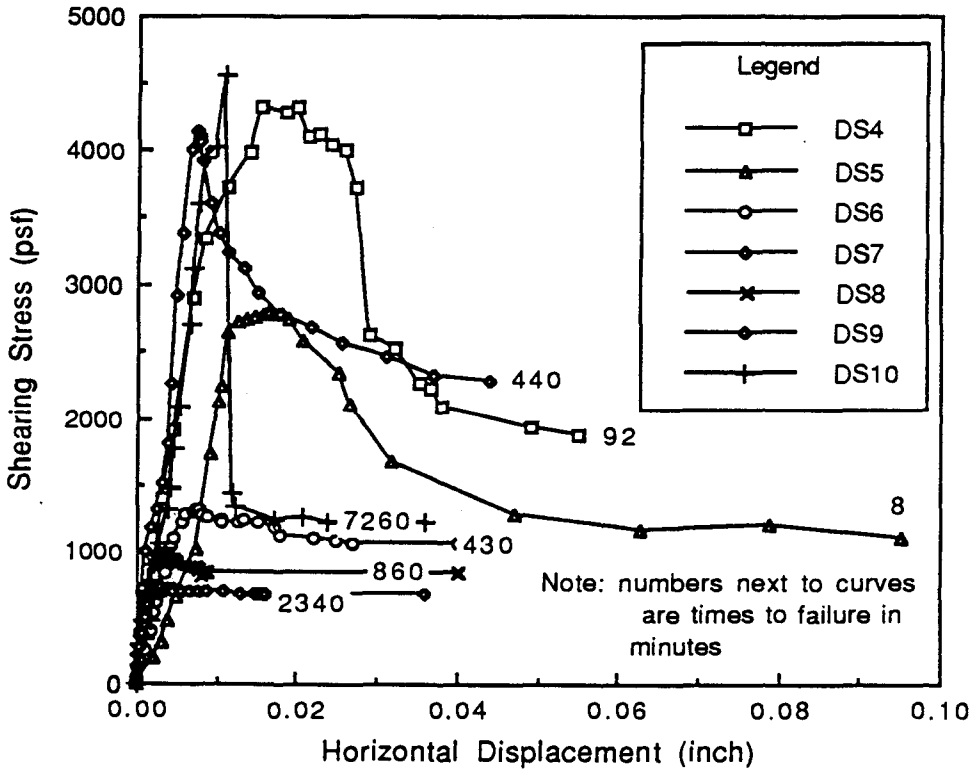

Fig. 5.4 Shearing Stress-Horizontal Displacement Curves for Tests on Eagleford Shale from Boring BIR43 at a Depth of 183 Feet

The stress-deformation behavior of the samples falls in two distinct groups. Samples for tests DS4, DS5, DS7, and DS10 experienced a large reduction in shearing stress after reaching a peak stress. It is noticeable that these four samples had the highest strengths (Fig. 5.3). Samples for tests DS6, DS8, and DS9 had relatively little strength loss after failure and these samples showed the expected behavior regarding dissipation of shear induced pore water pressures (Fig. 5.3).

Shapes of Shearing Surfaces

The specimens used in the shear tests were ground up for use in index testing and thus are not available for further examination. However, the persons who ran the tests noted that the failure surface was quite irregular for tests DS4 and DS10, meaning that the shearing surface was not smooth but instead had a bumpy appearance with a top-to-bottom amplitude of perhaps 0.05 inch. The surface for test DS5 were slightly irregular. No condition was recorded for DS7. The surfaces for the other specimens were essentially smooth.

The cores had numerous horizontal planes of weakness that caused unexpected failure periodically during the trimming operation. We have used the term "fissile" to apply to this condition. We do not know whether these planes of weakness result from very thin layers of a different material or just from parallelism of platey particles and thus do not use the term "fissile" to denote the cause of the behavior.

For the direct shear tests, we infer that the smooth failure surfaces resulted from shearing on fissile surfaces. The higher strengths of other specimens then resulted from the specimen being forced to shear through harder material. The roughness may indicate that the shear is entirely through harder material or that the failure planes are migrating up and down between fissile surfaces.

Residual Condition

As a result of a lack of sufficient time, we did not try to shear the samples back and forth cyclically to define residual failure

envelopes. In any case, a torsion shearing device would be more appropriate for such tests.

However, as a first approximation, we can use the final readings from each test to estimate "residual" stresses. The resulting plot of shearing stress versus time to the last reading (Fig. 5.5) shows reductions in strength down to times of the order of 4000 minutes. Except for DS7, there is a relatively minor effect of time-to-failure on the residual shearing stress.

It should be noted that the observed irregular surfaces existed at essentially the time of the final deformation reading. The condition of the failure surfaces at the peak shearing stress are unknown.

Theory

Equation 5.1 will again be used to estimate the degrees of dissipation of pore water pressures at failure. Unfortunately, the S-t curves (see appendix) are not generally in accord with Terzaghi's theory.

In the case of Test DS8, we consolidated the sample under a pressure of 14,400 psf and then rebounded it in a single step to 1440 psf, hoping that the large load decrement ratio of ten (compared with the usual value of four) would lead to a better defined S-t curve.

The curves of S-t, S-$\sqrt{t}$, and S-log(t) for test DS8 are shown in Fig. 5.6. Efforts to make a reasonable fit of Terzaghi's theory to the data were unsuccessful. Accordingly, we arbitrarily set S0=20 dial divisions and S100=140 dial divisions and obtained a t_{50} of 105 minutes. For a value 2H=0.645 inch, the calculated coefficient of consolidation (c_v) was 0.002 sq.ft/day. That value of c_v was used to recalculate the theoretical curve. The measured and calculated S-t curves are compared in Fig. 5.7 to show the poor quality of the fit. In any case, if we use the same sample dimensions and the resulting value of c_v, with Eq. 5.1, we find that achieving the usual degree of equilization of 95% would require a testing time of 10,000 minutes (one week). The experimental data suggest that a shorter time is acceptable, perhaps about two days. Such a conclusion can easily be supported by theory, in retrospect, by simply fitting Terzaghi's theory to the S-t curve in a lower time range and attributing the remaining swell to secondary effects.

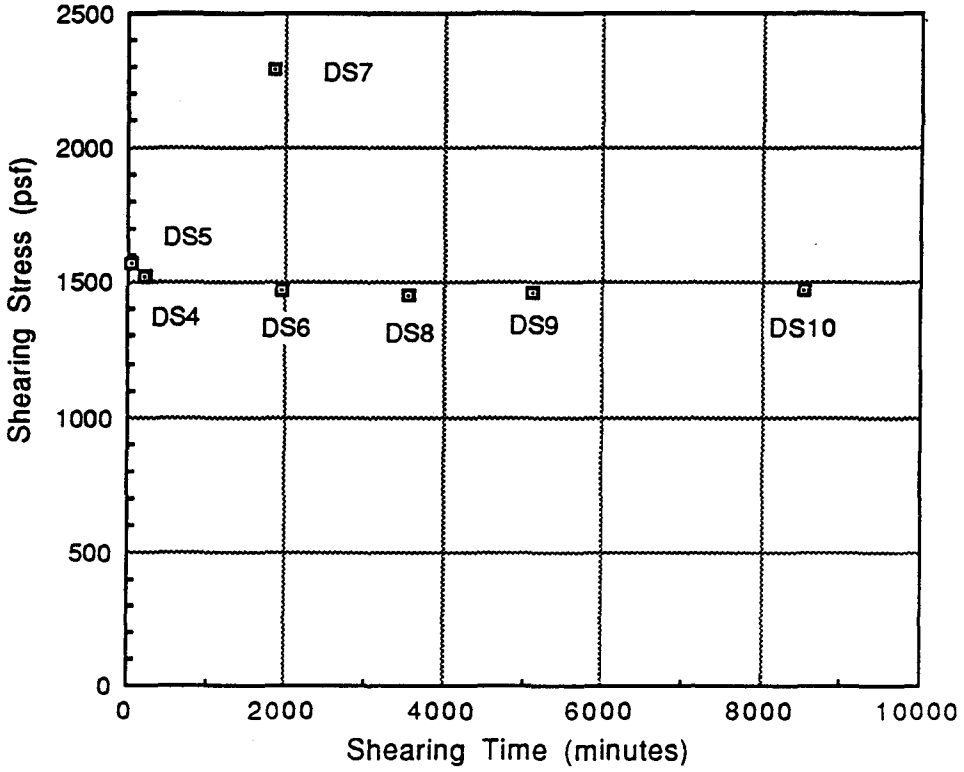

Fig. 5.5 Influence of Shearing Time on the Residual Shearing Stress

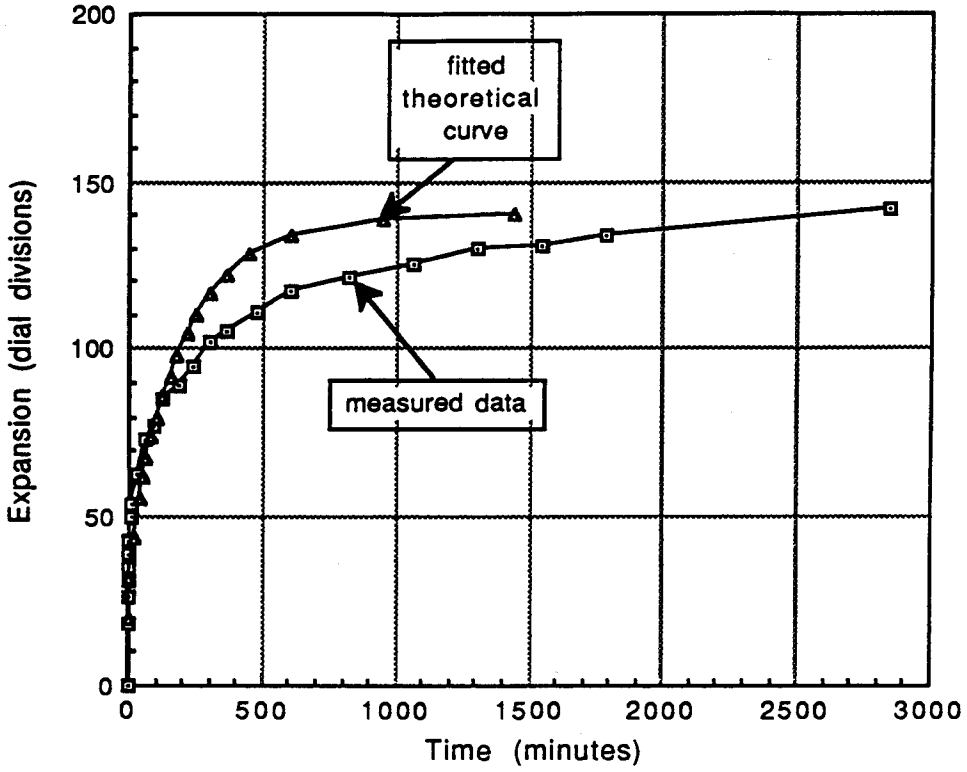

Fig. 5.7 Comparison of Measured and Computed S-t Curves for Sample DS8 (S0=20 div., S100=140 div., t50=105 minutes)

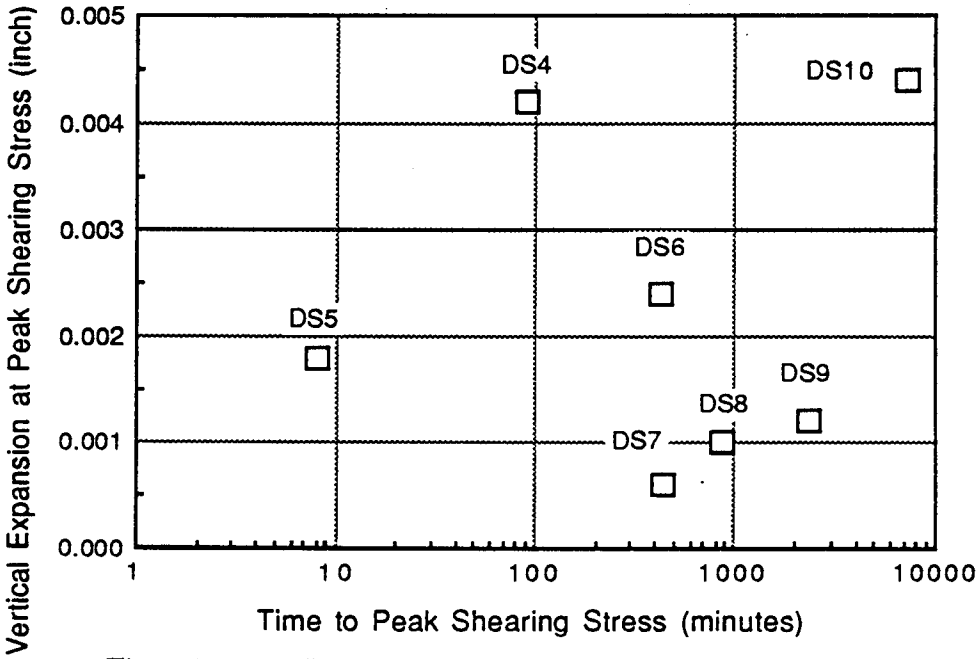

Fig. 5.8 Influence of Shearing Time on Vertical Expansion at the Peak Shearing Stress

It is worth noting that the magnitude of the error associated with incomplete dissipation of excess pore water pressures, is proportional to the excess pore water pressure developed in an undrained test. This undrained excess pore water pressure cannot be measured in direct shear. However, we do know that shear-induced excess pore water pressures are generally positive for normally consolidated materials and negative for highly overconsolidated materials. For some intermediate condition of overconsolidation, the undrained excess pore water pressure is negligible and thus the testing time becomes irrelevant (viscosity effects should still be consider, however).

We tested samples under normal stresses of about 10 psi where we expected large negative pore water pressures. Evidence in support of the existence of negative pore water pressures is found in the volume change data in that all samples expanded during shear (see appendices). There was, however, no relationship between the amount of expansion and the time to failure (Fig. 5.8). On the other hand, the two samples with distinctly irregular failure surfaces (DS4 and DS10) expanded more than 0.004 inch, the sample with a slightly irregular surface (DS6) expanded 0.0025 inch, and the samples with smooth failure surfaces (DS5, DS8, DS9) all expanded less than 0.002 inch. The data on shear-induced expansion are thus in general accord with other observations.

Conclusions

Tentative conclusions and inferences, from the deformation-rate study include:

1. the fissile nature of these samples has a major influence on their shearing strengths (an inference).

2. samples that have smooth failure surfaces probably failed on pre-existing planes of weakness. Those samples have peak and residual strengths that do not differ greatly.

3. samples with highly irregular failure surfaces probably failed, at least in part, through intact material. The failure planes may shift up and down to include fissile surfaces above and below the forced failure plane. These samples experience a major post-failure loss in strength.

4. these tests suggest that times to failure of about two days will suffice for dissipation of shear-induced excess pore water pressures.

5. theoretical estimates of required times to failure, based on a modified form of Terzaghi's theory, seem to correlate with the measurements if curve fitting is done at an early range of times on the S-t plots.

FAILURE ENVELOPE FOR EAGLEFORD SHALE (BORING BIR43, DEPTH 252 FEET)

A series of three direct shear tests (DS11-DS13) was performed on the core from boring BIR43 at a depth of about 252 feet to obtain a failure envelope. Raw data and test-specific plots are in the appendix.

Consolidation Data

Test DS11. The specimen for DS11 had a swelling pressure of about 17000 psf and was sheared under a normal stress of 14,400 psf. The amount of rebound in that stress range was too small to allow analysis of any time-rate information.

Test DS12. Test DS12 was carried out at the lowest pressure of about 1440 psf. The sample had a swelling pressure of about 17000 psf. It was rebounded directly back to 1440 psf. The coefficient of consolidation was estimated to be 0.024 sq.ft./day. The fitted theoretical time-rebound curve is shown in the appendix as a solid line without data points.

Test DS13. The specimen for test DS13 was rebounded directly from the swelling pressure of almost 20,000 psf back to 7200 psf. The time-expansion curves do not correspond to Terzaghi's theory sufficiently to engage in any meaningful fitting.

Shearing Data

The failure surfaces for all three samples were irregular and rough.

All samples expanded slightly during shear but the amounts of expansion were small, ranging from 0.0001 inch for DS11 at a normal stress of 14,400 psf to 0.0026 inch for DS12 at 1440 psf.

The curves of shearing stress versus horizontal displacement (Fig. 5.9) involved considerably less post-failure strength loss than for the specimens used in the strain rate-study. Contrary to reasonable expectations, the sample at the highest pressure had the greatest post-failure strength loss.

It is unclear whether substantial rebound broke a weak cement and left specimen DS12 (lowest stress) in an uncemented condition, thus explaining its flat shear-displacement curve, or whether that specimen just happened to have a fissile surface aligned with the shear plane of the device. The gradual progression in shapes of of shear-displacement curves with respect to applied normal stress implies that the behavior is real and not the result of accidental location of fissile surfaces.

The failure envelopes at both peak and "residual" condition (Fig. 5.10) had unexpectedly small amounts of scatter in the data points. Considering the scatter found in the deformation-rate study, the small scatter is likely to be fortuitous. However, the samples seemed to be reasonably uniform, with liquid limits ranging from 63% to 64%.

The cohesion intercepts were quite small, around 150 psf and the friction angles were 33 degrees at the peak shearing stress and 24 degrees in the "residual" condition.

The times to failure were in the range of 2400 minutes (DS13) to 2750 minutes (DS11). If c_v is assumed to be 0.024 sq.ft./day for all specimens, then Eq. 5.1 leads to calculated degrees of consolidation at failure of 99%.

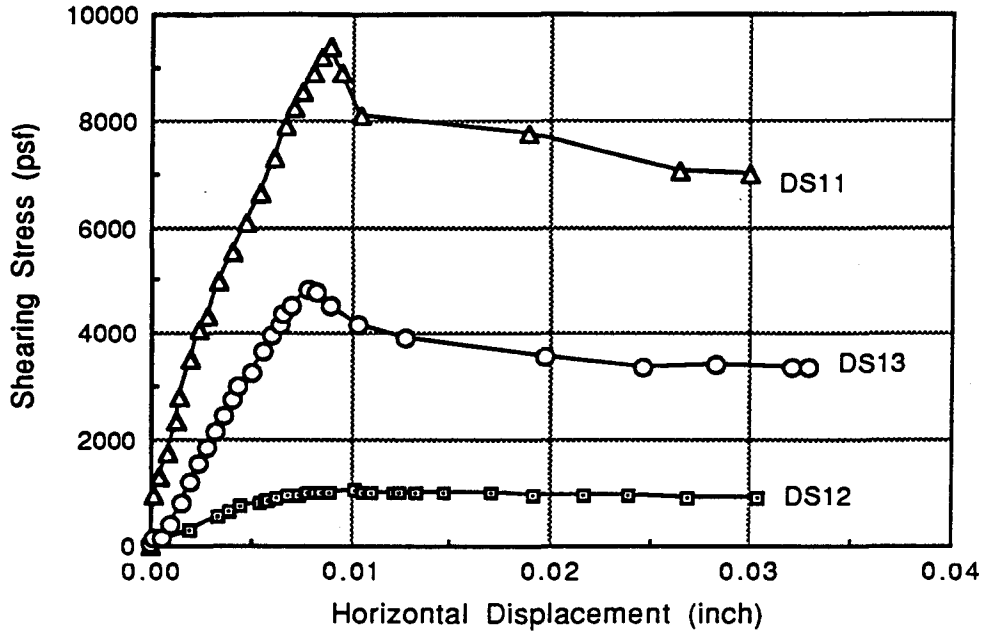

Fig. 5.9 Shearing Stress-Horizontal Displacement Curve for Tests on Samples of Eagleford Shale from Boring BIR43 at Depth 252 feet

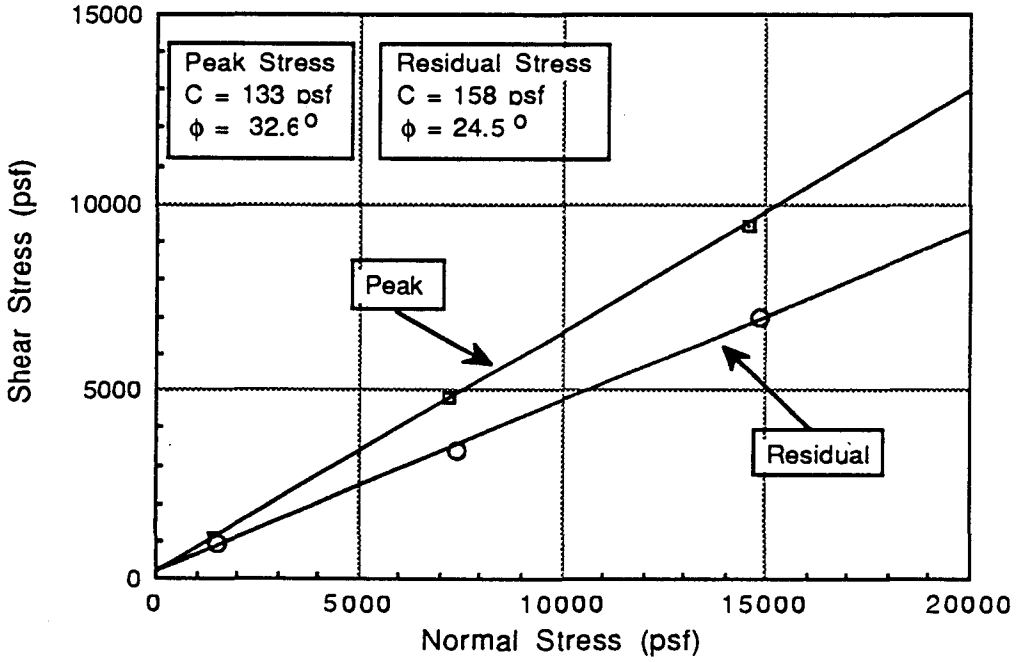

Fig. 5.10 Failure Envelope of Direct Shear Test on Sample No. 15

TESTS WITH BENTONITIC SHALE

Introduction

A series of three direct shear tests (DS14-DS16) was performed on the core from boring SIR3B at a depth of about 191 feet. The material was described in the boring logs as bentonite and bentonitic shale. The tests were performed to obtain a failure envelope. Raw data and test-specific plots are in the appendix.

Consolidation Data

Test DS14. The specimen for DS14 was subjected to the final normal stress of 14,400 psf at once, to speed up the testing process. The resulting volume change was too small to produce useful consolidation data.

Test DS15. Test DS15 was carried out at the lowest pressure of about 1440 psf. The sample was first equilibrated at a pressure of 14,400 psf, where it underwent a negligible volume change. It was then rebounded directly back to 1440 psf. The coefficient of consolidation was estimated to be 0.005 sq.ft./day. The fitted theoretical time-rebound curve is shown in the appendix as a solid line without data points. The theoretical curve was clearly fitted through data points at elapsed times ranging from 8 to 200 minutes. The result was a very poor fit of theory and measured settlements for times less than 8 minutes. It would have been possible to fit a theoretical curve through the early data, say less than 15 minutes, and get a good fit in that range but conclude that there was a large amount of secondary compression. A valid conclusion seems to be that Terzaghi's theory doesn't fit the data.

Test DS16. The specimen for test DS16 was rebounded directly from the swelling pressure of about 14,000 psf back to 7200 psf. The estimated coefficient of consolidation was 0.031 sq.ft./day.

Coefficients of consolidation. The swelling behavior of these samples did not correspond well with Terzaghi's theory and

coefficients of consolidation as low as 0.005 sq.ft./day resulted from fitting through a major part of the measured settlements and values above 0.1 sq.ft./day would be obtained by fitting to the very early parts of the curves. The value of 0.03 sq.ft./day may be a good compromise for all three samples.

Shearing Data

Stress-deformation behavior. All samples expanded slightly during shear but the amounts of expansion were small, ranging from 0.001 inch for DS14 at a normal stress of 14,400 psf to 0.004 inch for DS15 at 1440 psf.

The curves of shearing stress versus horizontal displacement (Fig. 5.11) are similar to those from sample number 15 (DS11-DS13), with a small strength loss after failure. The sample at the lowest stress level again behaved in the most "plastic" fashion with only a small strength loss after failure.

Failure envelopes. The failure envelopes at peak and "residual" condition (Fig. 5.12) seem to have had moderate scatter. The envelope drawn through the three peak points would be curved and concave downwards. However, considering the scatter in previous tests, we have arbitrarily passed a straight line through the points for the tests with the highest and lowest normal stress. The residual envelope was drawn as a straight line through the origin. For the peak condition, the failure envelope drawn through the two end points yields $\bar{\phi}$=31 deg. and $\bar{c}$= 700 psf. The envelope for residual conditions (Fig. 5.12) had the properties $\bar{\phi}$=33 degrees and $\bar{c}$=0.

The samples had similar liquid limits (Table 3.2) but the plasticity index was much higher for DS16. The Atterberg limits are high but not as high as for real bentonite, in our view, so this material might be called a bentonitic shale. The effective friction angle is higher than one would expect for such a material.

Theoretical degrees of consolidation at failure. The times to failure were in the range of 2900 minutes (DS16) to 4050 minutes (DS14). If c_v is assumed to be 0.03 sq.ft./day for all specimens, then Eq. 5.1 leads to calculated degrees of consolidation at failure of

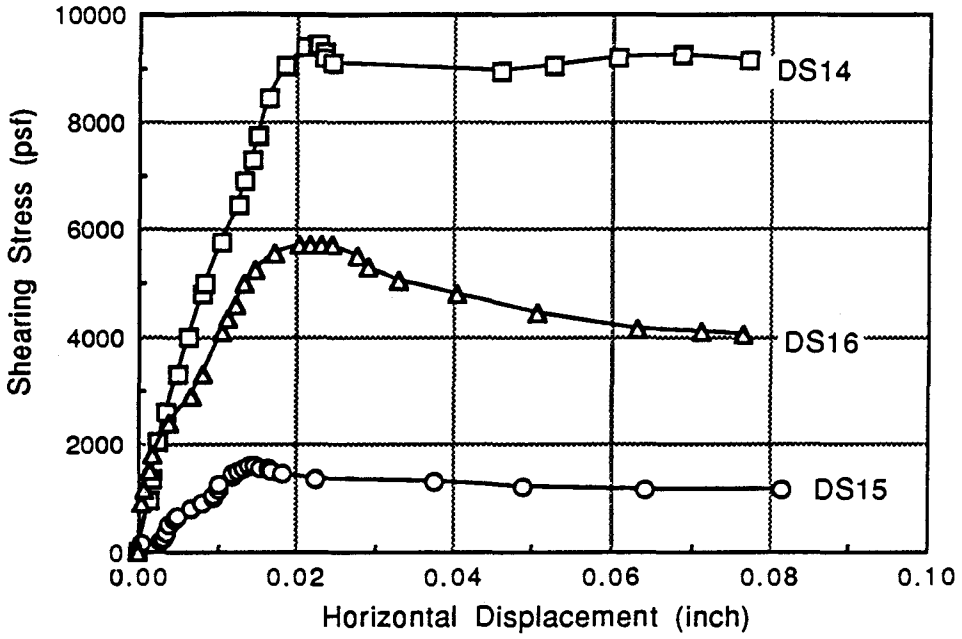

Fig. 5.11 Shearing Stress-Horizontal Displacement Curve for Tests on Samples of Bentonitic Shale from Boring SIR3B at Depth 191 Feet

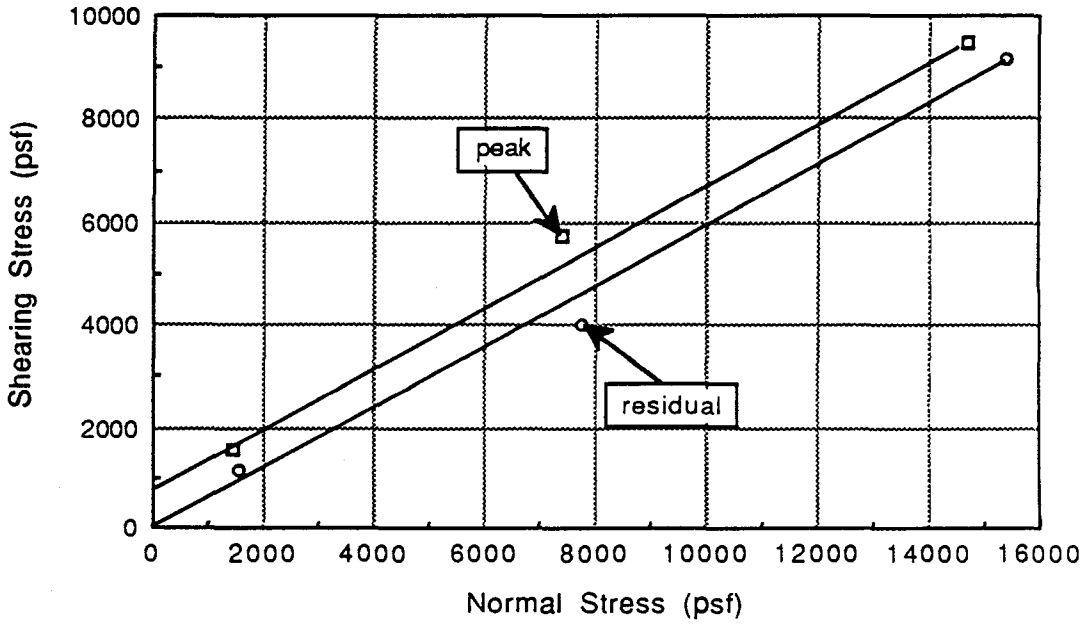

Fig. 5.12 Failure Envelopes from Direct Shear Tests on Bentonitic Shale from Boring SIR43 at Depth 191 Feet

99%. If the coefficient of consolidation is taken as 0.005 sq.ft./day, then the degrees of consolidation ranged from 97% to 98%. All values are higher than the 95% usually considered acceptable.

Condition of failure surfaces. The failure surfaces for these three tests are sketched in Fig. 5.13. We have never before encountered failure modes such as encountered for DS14 and DS16. Apparently the shear began on a fissile surface and then must have encountered a sloping surface of weakness. However, no fissure was found in the lower half of the samples nor did that particular core show signs of fissures. Our supposition is that shearing stresses developed completely across the sample in the usual assumed condition, right up to the moment of failure, and then a strength loss occurred on the sloping planes.

The changes in sample thickness during shear would be expected to reflect the strange failure modes (see appendix). However, at horizontal displacements of about 0.08 inch (essentially the end of the test), the measured vertical expansion was only about 0.003 inch for DS14 and 0.008 inch for DS16, both of which had the unusual failure surfaces. By contrast, the expansion was about 0.018 for DS15 with a more usual failure mode. Thus, the vertical expansion data support the view that the block failure occurred at the end of the test, perhaps during dismantling.

At present, we do not know whether some sort of special consideration is required for samples with the unusual failure modes. In the absence of unusual failure envelopes, we will not alter the usual interpretation but will give further consideration to test interpretation if this failure mode continues.

Summary, Conclusions, and Inferences for Bentonitic Shale

As for the Eagleford shale, the data have unusual aspects. In the absence of more complete data, any conclusions must be tentative.

1. The friction angle of the bentonitic shale was apparently in excess of 30 degrees, a value that is high compared with previous experience for bentonites.

2. The failure mode of two of the three specimens, involving a partial horizontal shearing surface and then a sloping plane up to the top cap, is quite unusual in our experience. The measured vertical movements were too small for this mode to have occurred during shear but we cannot be sure that a full horizontal shearing surface developed either.

3. The S-t curves again did not conform well with Terzaghi's theory. A crude fit of theory and measurement leads to the conclusion that pore water pressure dissipation was adequate for these tests.

COMMENTS ABOUT DIRECT SHEAR TESTS IN GENERAL FOR THIS SITE

Direct shear tests offer the advantages of having reasonably short testing times because of the relatively small drainage distance, and of giving data on shear on predefined surfaces. Because of the small size of the cores, we had to perform the shear tests so that failure occurred on horizontal planes. Conditions around underground openings involve shear on vertical and sloping surfaces as well. Thus, it would be useful to have direct shear (or other types of shear tests) on samples oriented to force failure on other surfaces.

The effective angles of internal friction were relatively high compared with our previous experience with more weathered zones of these formations.

The large amounts of scatter found in the shearing strengths measured in direct shear correlate generally with the stress-deformation behavior. Samples with abnormally high shearing strengths also experienced substantial post failure losses in strength. We believe that the large strengths resulted from shearing, at least partially, in non-fissile zones. There are advantages in performing shear tests using an apparatus that does not force shear on a particular surface. We believe that it would be useful to perform a limited number of direct simple shear tests using apparatus specially designed for this rock-like material, and for the size cores available on this project.

The samples were relatively stiff, with deformations at failure generally in the range of 0.005 inch to 0.020 inch.

It appears that shearing times of the order of two days will allow adequate dissipation of shear induced excess pore water pressures.

problems in estimating the proper area of the specimen after a significant axial strain, and tilting of samples which have rotated planes of weakness. Further, while the triaxial device allows for control of two of the principal stresses, it doesn't allow control of all three, nor does it allow for gradual rotation of principal stresses.

In spite of its problems, the triaxial device has been in substantial use in geotechnical engineering since the mid 1940's. Part of the reason for its wide usage is that devices that allow for application of more general states of stress are even more difficult and expensive to use, and have found negligible application.

Main Purposes of this Investigation

The major purposes of this phase of the project were:

1. develop appropriate triaxial testing techniques.

2. estimate reasonable testing times for future tests.

3. obtain preliminary data on the stress-strain properties and the failure envelopes of the rocks at the SSC site.

Tests Performed

Ten consolidated-drained (CD) triaxial compression tests were performed (Table 6.1). No tests were scheduled for the Taylor marl but receipt of cores of the Eagleford shale was delayed by inclement weather at the site so we began the procedure-development phase with a test (CD1) on Taylor marl. Tests CD2-CD10 were performed using the Eagleford shale.

Tests CD2 through CD4 were performed for purposes of development of testing procedures but a range in confining pressures was used so a failure envelope could be drawn. Testing times were short because of the exploratory nature of these first tests with Eagleford shale.

Test ID	Sample No.	Formation	Boring	Depth (ft.)	initial wc (%)	final wc (%)	Gs	LL (%)	PL (%)	Vert. Eff. Stress (psf)	Consol. Stress History (psi)
CD1	4	Taylor	BE6	35.4	19.7	18.4	2.87	67	27	3059	80,50,25,12,6,12,25,50,100
CD2	14	Eagleford	BIR43	189.2	16.2	17.1	2.78	80	32	14994	100,50,10
CD3	14	Eagleford	BIR43	189.5	16.9	15.5	2.78	83	26	15017	100
CD4	14	Eagleford	BIR43	189.8	15.9	16.7	2.78	82	29	15040	100,50
CD5	11	Eagleford	BIR44	227.7	16.7	18.6	2.77	80	31	17982	100, 120, 140, 50, 10
CD6	11	Eagleford	BIR44	228.0	16.6	19.7	2.77	85	29	18005	140, 50, 10
CD7	11	Eagleford	BIR44	228.6	16.2	19.0	2.77	80	30	18051	10
CD8	11	Eagleford	BIR44	228.9	16.1	19.2	2.77	77	31	18075	10
CD9	15	Eagleford	BIR43	251.7	15.7	15.6	2.78	64	28	19844	140, 100
CD10	15	Eagleford	BIR43	252.0	15.8	15.2	2.78	67	30	19867	140, 100

Table 6.1 Summary of General Data for Triaxial Tests

Tests CD5 through CD8 were performed using a single confining pressure of 10 psi and with a wide range in times to failure to obtain information on testing rates that might be used in production testing.

Similarly, tests CD9 and CD10 were performed using a range in times to failure but with a larger confining pressure of 100 psi.

Data Presentation

Data forms are presented in the appendix for the consolidation and shearing stages. The original data, which were either collected by hand or were recorded using an electronic data acquisition system, are not likely to be useful to anyone else. The hand-recorded data are often hard to read when photocopied, and contain random notes only to the experimenter. The computer-recorded data involve readings taken about every ten to fifteen minutes for tests that sometimes lasted for many days. The short time period between readings was used to ensure that the peak conditions were defined if the samples failed suddenly but the mass of often repetitious numbers, typically in units of volts, does not help someone reading this report.

Accordingly, we set up spreadsheets to handle most of the data. We then transcribed all useful data, including hand-written notes, to these spreadsheets and hand checked the data to ensure accuracy. The spreadsheets were then printed on a laser printer to ensure readability. Plots were also computer generated. The reader thus has access to the full source data in a comprehensible and readable form.

Considerations Regarding Number of Tests

The consolidation/swelling times of the samples of Eagleford shale were quite long (one sample was maintained at a single pressure for 1.5 months without apparently reaching the end of consolidation), thus severely limiting the number of tests that could be performed in the available time period. The limited number of tests then places limits on the conclusions and recommendations relating to

the production phase testing times. However, the experience gained in this preliminary testing program has provided significant insight into the time rate and stress-strain-strength response of the Eagleford shale.

EXPERIMENTAL PROCEDURES

Introduction

The experimental procedures used for the triaxial tests were discussed in detail in the Fourth Progress Report on April 24, 1990. The procedures will be summarized here as an aid to the reader of this report.

Trimming

The cores were slightly less than 2 inches in diameter. The outer zone of most of the cores was irregular. The exterior surfaces of the cores used for tests CD2, CD9, and CD10 were softened, presumably by contact with drilling fluid. To form a smooth outside surface and remove disturbed or softened material, the cores were trimmed down to 1.50 inches in diameter for triaxial shear testing.

We planned to use sample lengths of 3.00 inches but the weak horizontal planes caused considerable difficulty in trimming the end surfaces. When parts of the ends flaked off, we trimmed further to obtain smooth uniform end surfaces. As a result, the sample lengths varied between about 2.6 and 3.1 inches.

The trimming process was designed to minimize evaporation by encasing the trimmed material in a plastic membrane and keeping the remaining core encased in wax, except a short distance that was in the process of being trimmed.

Cells

Triaxial cells were of the usual design, with the piston passing through two ball bushings and with a floating O-ring seal.

The first eight tests were set up using slotted filter paper drains and dual prophylactic membranes. In spite of years of previous success with this procedure, we had a high failure rate of the membranes, often after the sample had been under confining pressure for a number of hours and, in one case (CD8) when the sample was in the shearing stage. Because of previous success and because of the time required to receive commercial membranes, we stayed with the prophylactic membranes for the first eight tests and tried to protect them better, e.g., we encased the samples in continuous filter paper drains with vertical slits, but no slots. After a few continued membrane failures, we added a sheet of slit plastic film, between the filter paper and the membrane, for some of the tests in the middle part of the sequence, with apparent success. Meantime, we ordered commercial triaxial membranes (Wykeham-Farrance) and used them for the final two tests, with no failures. On the last test (CD10) we discontinued use of the plastic film.

One reason why only the last two tests utilized the heavier membranes was that most of the tests were set up in the cells during the early part of the experimental program and occupied the cells for prolonged periods of time.

The only other serious problem with the equipment involved failure of the floating bushing on one test. Under low cell pressures, if the tiny O-ring around the piston freezes against the floating bushing, the cell fluid escapes around the bushing and it becomes necessary to tear down the cell, apply grease to the piston, and perhaps replace the O-ring.

Consolidation Stage

Samples were consolidated under an all-around hydrostatic pressure and volume change was measured by recording the amount of water entering or leaving the samples, using glass pipets. Samples typically underwent measurable volume changes for prolonged

periods of time. The plots of volume change (ΔV) versus time (t) typically showed little, or no, evidence of the end of consolidation even for times up to a month. In an effort to obtain a reasonable amount of data in the time available, most tests were performed with samples that were still undergoing apparent primary consolidation on ΔV-log(t) plots but where the rate of volume change was very small, e.g., less than 0.03 ml/day.

In a few cases, we had consolidation followed by expansion, under constant confining pressure. The initial consolidation may have been from remaining softened material on the outside of the specimen with subsequent expansion from an inner core of unsoftened material. The outer zone may have softened from moisture in the filter drain and trapped under the membrane during test set-up. The apparent expansion may also have resulted from diffusion of gas from the sample through the membrane into deaired water of the cell. The diffusion process usually stops within about a week. In any case, this problem tended to exist only with early tests.

Shearing Stage

The axial deformation was applied using a motor driven loading press. Axial deformation was measured using an LVDT. Axial force was measured outside the cell using an electronic load cell. Volume change was recorded using a pipet provided with a pressure transducer at its base, so the head of water in the pipet was calibrated against volume change.

Data were collected by a data acquisition system that was based on an IBM model XT microcomputer. The system allowed for playback of data during a test and for plotting of data on the monitor using engineering units so the data could be checked for reasonableness during the shearing stage. Electronic components were recalibrated several times during each test to ensure that no electrical drift had occurred. The sensors were found to be quite stable.

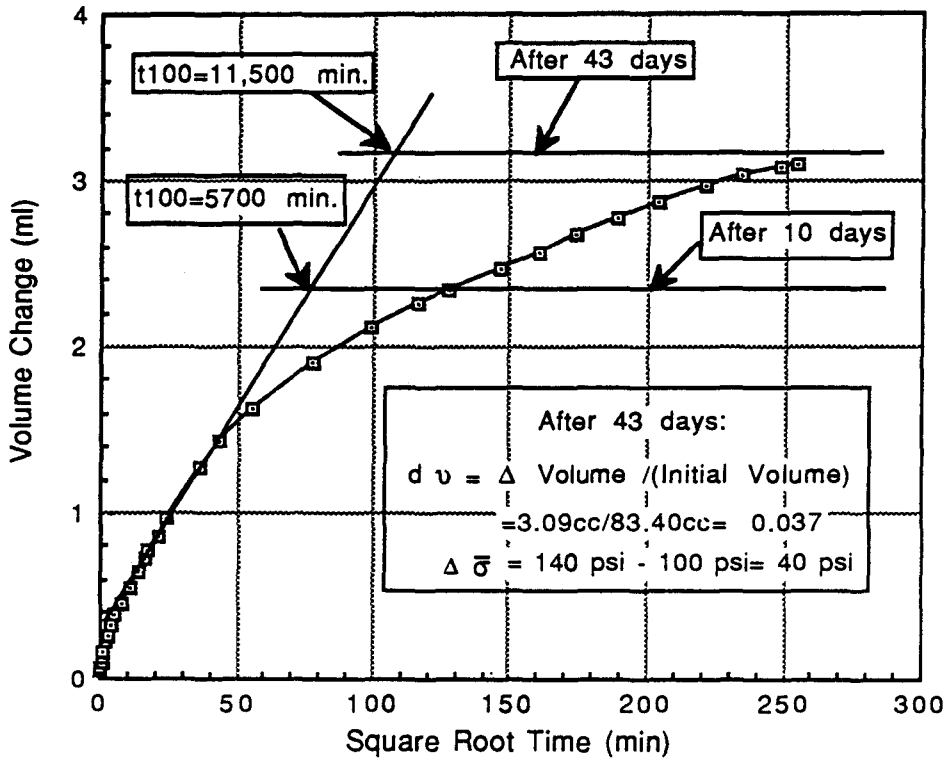

Fig. 6.1 Fitting of the Last Swell Increment for Test CD5 to obtain t100 for Computation of the Coeff. of Consol.

$$c = \frac{\pi(\frac{L}{2})^2}{4(t_{100})}\left[\frac{1}{\{1+\frac{L}{R}\}^2}\right] \qquad (6.1)$$

where L is the sample length (height), R is the sample radius and t_{100} was defined previously.

Bishop and Henkel had observed no secondary effects during consolidation so the use of V_{100} seemed reasonable. However, their published data, and most of their experience, was with remolded soils which normally have negligible secondary effects even in one-dimensional consolidation. Their method is easy and quick to apply by hand, but it becomes ambiguous when applied to undisturbed materials that may have major secondary effects. Further, the user has no equally simple way of determining how well the theoretical and experimental ΔV-t curves compare.

Analysis Using the Entire Time-Volume Change Curve

For the case of a cylindrical sample encased in a filter paper drain, Bishop and Gibson (1963) presented the following solution for the consolidation stage:

$$U = 1 - \frac{32}{\pi^2} \sum_{n=0}^{\infty} \sum_{m=1}^{\infty} \frac{\exp\left[-\beta_{mn}^2 - \frac{(1+2n)^2\pi^2a^2}{4\alpha^2d^2}\frac{c\,t}{a^2}\right]}{(1+2n)^2\beta_{mn}^2\left[1+\beta_{mn}^2 v^{-2}(1+2n)^{-4}\right]} \qquad (6.2)$$

where: $$v = \frac{\pi^2}{4}\frac{k_p}{k_r}\frac{a\delta}{d^2} \qquad (6.3)$$

and: $$\alpha = \sqrt{\frac{k_r}{k_z}} \qquad (6.4)$$

where k_p is the hydraulic conductivity of the filter paper drain, k_z is the vertical hydraulic conductivity of the soil, k_r is the radial hydraulic conductivity of the soil, c is the coefficient of consolidation of the soil (assumed isotropic), t is time, "a" is the sample radius, d is the vertical drainage distance (half the sample height if drained top and bottom), and δ is the thickness of the filter paper. In addition, m denotes successive roots of the equation:

$$v(1+2n)^2 J_o(\beta_{mn}) - \beta_{mn} J_1(\beta_{mn}) = 0 \qquad (6.5)$$

Analyses were planned for use with partially draining filter paper but preliminary data indicated that the soil was so impervious that the drains were probably freely draining. All data were reduced assuming freely draining filter paper.

The analysis allows for the existence of anisotropy in terms of hydraulic conductivity but no measurements were made of flow in the horizontal direction so it was assumed that the samples were isotropic.

The measured time-volume change data were fed into a computer program and plotted on the monitor. Trial values of the volume change at the beginning and end of primary consolidation were then fed into the program and the theoretical time-volume change curve was compared, on the monitor, with the measured curve. Repeated trials were used to obtain the best overall fit. The computer used for these analyses could only be connected to a 9-pin dot matrix printer. Printer outputs are included in the appendix.

Comparison of the Two Methods

Values of the coefficients of consolidation obtained using the two methods were always essentially equal. Comparisons will be made in discussion of several individual tests but the values obtained by fitting the entire curves will be used in the subsequent analyses.

Membrane Leakage

For "normal" consolidation and shearing times, and soils of typical compressibility, problems associated with membrane leakage are of no interest. For materials as incompressible as the rocks from the SSC site, and for consolidation/shearing times that lasted weeks, problems with membrane leakage become more significant. For the consolidation phase of the test, leakage just increases the amount of water flowing out of the specimen. For samples that are swelling, as for most of the consolidation stages for this project, leakage may reverse the apparent flow. For cases involving sample compression, leakage may show up as apparent secondary consolidation.

Because the main interest with the triaxial tests involved shearing strengths, considerations involving leakage were deferred. Leakage problems will be discussed after discussion of shearing properties and recommendations will be made in a later section on how to deal with the problem in future tests.

DATA REDUCTION FOR SHEARING STAGE

Sample Area

During the shearing stage, the horizontal area of the sample (A_ε) at any axial strain (ε) was calculated assuming the sample deformed as a right circular cylinder:

$$A_\varepsilon = A_o \frac{1+v}{1-\varepsilon} \qquad (6.6)$$

where A_o is the area at the beginning of shear, v is the volumetric strain (positive for expansion), and ε is the axial strain (positive for compression).

The area at the beginning of shear was calculated by dividing the volume by the sample length. The volume was determined as the

initial volume of the sample corrected for measured volume changes during consolidation. The initial volume was determined from measurements of the height and diameter. The sample length at the beginning of shear was measured using a cathetometer.

Secant Young's Modulus and Poisson's Ratio

Shearing data were reduced using a spreadsheet (see appendices). For each set of readings, the secant value of Young's modulus was calculated as:

$$E = \frac{\sigma_1 - \sigma_3}{\varepsilon} \tag{6.7}$$

where $\sigma_1 - \sigma_3$ is the stress difference and ε is axial strain. A value of Poisson's ratio (μ) was also defined using:

$$\mu = -\frac{\varepsilon_{lateral}}{\varepsilon_{vertical}} = \frac{1}{2}\left(\frac{v}{\varepsilon} + 1\right) \tag{6.8}$$

We used μ for Poisson's ratio to avoid confusion with the standard use of v to represent volumetric strains.

Average Degree of Consolidation at Failure

The average degree of consolidation at failure (U_f) during the shearing stage can be calculated using Gibson's equation:

$$U_f = 1 - \frac{(L/2)^2}{\eta c t_f} \tag{6.9a}$$

or:

$$t_f = \frac{(L/2)^2}{\eta c (1 - U_f)} \tag{6.9b}$$

where L is the length (height) of the sample, η is 40 for all around drainage, c is the coefficient of consolidation, and t_f is the time to failure, provided that the degree of consolidation is high, say 80% or more. For lower degrees of consolidation, we used the T-U plot in Fig. 4 from Blight (1963).

Effects of Membrane Leakage

Membrane leakage during long term shearing stages resulted in measured amounts of fluid outflow being too large. The effect on calculated sample area is trivial and thus the error in definition of the failure envelope is negligible. The problem will be discussed further after presentation of the shearing data.

PRESENTATION OF RESULTS

Consolidation and Stress-Strain Data

The appendices generally contain the following for each test:

1. a spreadsheet showing data collected during test set-up
2. a spreadsheet showing data for the shearing stage
3. a plot showing the stress differences and volumetric strains plotted against axial strain.
4. tables containing individual volume change readings during consolidation/swell.
5. plots of volume change versus time, square root of time, and log of time for each consolidation stage.
6. comparisons of measured and computed volume change.

The samples were subjected to isotropic consolidation stress histories (Table 6.1) that would allow the computation of

coefficients of consolidation and volumetric compressibility. In some of the tests (CD1, CD2, CD3, CD8) the membranes leaked or the time-volume curves began to indicate consolidation after an extended period of swelling (CD4). Coefficients of consolidation for the final pressure are included in Table 6.2.

Mohr-Coulomb Failure Envelopes

Historically, failure envelopes were defined using Mohr's circles. However, the circles are awkward to plot and cause severe difficulties when there are many tests or when data from several types of tests are to be plotted in the same diagram.

Accordingly, since about 1960, failure envelopes are often plotted using modified Mohr-Coulomb diagrams in which the axes have been transformed to allow a single point to be used to represent the entire Mohr circle. The slope and intercept of the resulting failure envelope are then transformed to give the usual Coulomb parameters. Because we performed multiple tests at identical consolidation pressures, it is convenient to plot the compressive stresses, $(\sigma_1 - \sigma_3)$, on the y axis, and the confining pressure, $\bar{\sigma}_3$, as the x axis. If the slope of the failure envelope in the modified diagram is ψ and the cohesion intercept is d, then the usual shearing properties are obtained from the equations:

$$\phi = \sin^{-1}\left(\frac{\tan\psi}{2+\tan\psi}\right) \qquad (6.10)$$

and

$$c = d\left(\frac{1-\sin(\phi)}{2\cos(\phi)}\right) \qquad (6.11)$$

Values of stress difference at failure, axial and volumetric strains at failure, and times to failure are summarized in Table 6.2.

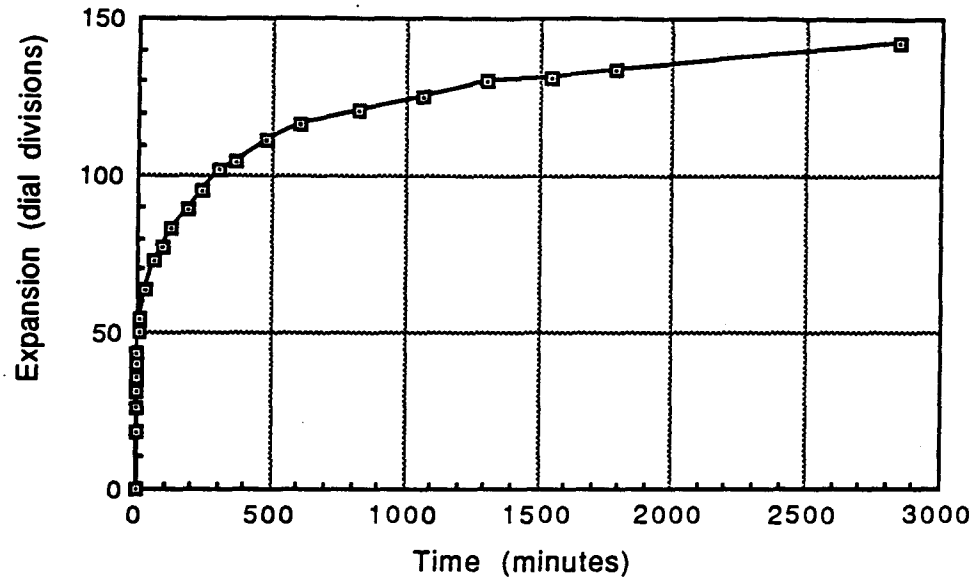

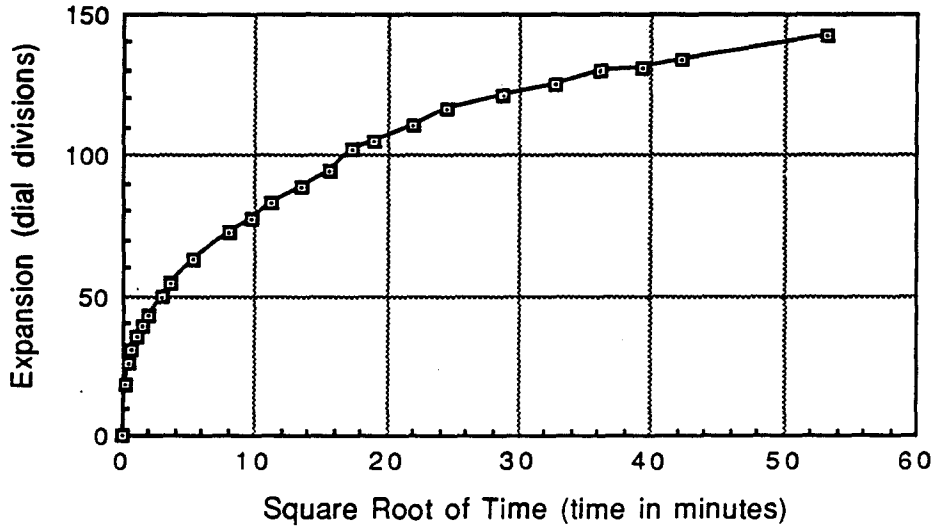

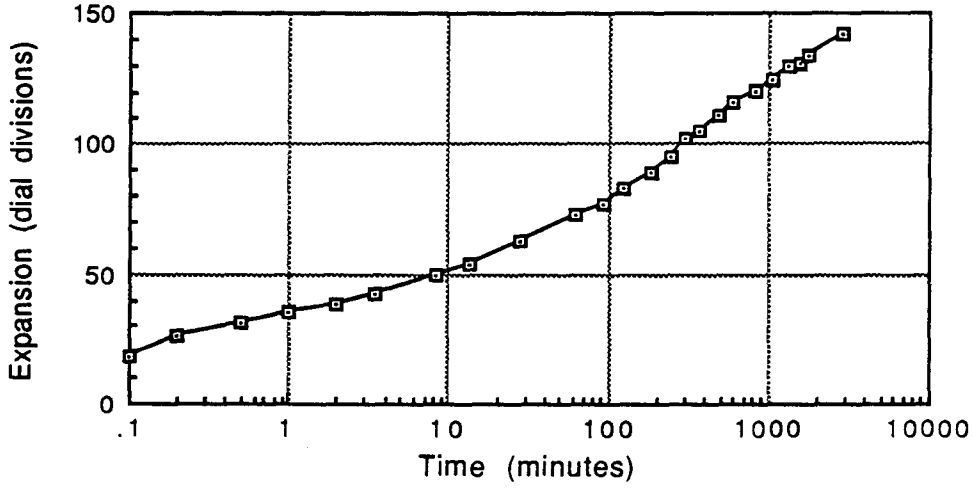

Fig. 5.6 S-t Curves for Test DS8 for a Pressure Decrease from 14,400 psf to 1440 psf

Test No.	Formation	Consol. Pressure psi	Final Coeff. of Consolidation sq.ft./day	Failure Strain %	Volumetric Strain %	Peak Stress Difference psi	Normal Stress on Failure Plane psi	Shearing Stress on Failure Plane psi
CD1	Taylor	100	0.00130	3.1	-0.39	362	343	170
CD2	Eagleford	10	0.00250	4.6	-2.20	180	165	63
CD3	Eagleford	100	0.00140	4.3	-3.23	601	498	284
CD4	Eagleford	50	0.00012	3.4	-2.40	463	331	226
CD5	Eagleford	10	0.00010	4.0	-2.50	336	198	167
CD6	Eagleford	10	0.00005	4.4	-2.73	332	57	116
CD7	Eagleford	10	0.00056	3.5	-1.84	295	208	138
CD8	Eagleford	10	0.00250	3.3	0.20	231	62	97
CD9	Eagleford	100	0.00370	2.7	-0.95	318	250	159
CD10	Eagleford	100	0.00300	2.5	-1.82	400	355	192

Table 6.2 Summary of Consolidation and Shear Data

TAYLOR FORMATION (TEST CD1)

Special Conditions

The only triaxial test performed using Taylor material was CD1. The core was provided to us only for visual examination but delay in receipt of cores, occasioned by inclement weather at the site, led us to perform this initial test as part of an effort to develop appropriate procedures. Problems included:

1. Because the core was intended only for visual examination, it was not sealed and preserved in wax as were the other cores. Consequently, the material was probably partially dried and was probably disturbed by handling.

2. The data acquisition system was not yet in operation, and the data forms used for subsequent tests were not in use so some items of data were not collected.

3. We had membrane failures as discussed earlier.

4. In order to gain some preliminary knowledge of consolidation properties under isotropic stresses, we subjected this sample to a series of pressures, using 80, 50, 25, 12.5, 6.2, 12.5, 25, 50, and 100 psi. For many of the stages where the sample was compressing, the flow direction reversed for the final few readings, i.e., water flowed back into the sample. We were not able to determine the cause of this reversal. It could have resulted from diffusion of dissolved gas from the sample into the deaired water in the cell. It could have been some sort of chemical reaction that caused the sample to swell. It could have been a problem with the measuring system. In any case, the problem disappeared for later tests.

5. With no preliminary knowledge of the shearing properties of this material, we began the shearing stage using a 600-pound proving ring to measure axial load. The load at failure exceed 700 pounds so, in the middle of the shearing stage, we had to lock the piston in place and change to a larger proving ring.

As a result of the problems, particularly problems with leaking and rupturing membranes, we were not able to calculate a useful relationship between void ratio and effective stress.

Coefficients of Consolidation

We did try to fit the Bishop and Gibson (1963) consolidation theory to the readings of volume change versus time, just to try to recover approximate values of the coefficients of consolidation. The theoretical and measured curves of volume change versus time are included in the appendix. The resulting coefficients of consolidation were as follows:

Load No.	Pressure psi	Coeff. of Consol. sq.ft./day
5	50	.0031
6	25	.0062
7	13	.0044
8	6	.0029

By way of comparison, the coefficients of consolidation from one-dimensional consolidation tests (tests C2-C4) for pressures between 6 psi (860 psf) and 80 psi (11,500 psf) were generally in the range of 0.02-0.06 sq.ft./day, with lower values at higher pressures.

Void Ratio

The water content of the sample after the shear test was 18.4%. If we assume a density of solids of 2.87 grams/cc, a degree of saturation of 95% (in accord with consolidation test data), then the void ratio at the end of the shear test was (18.4)(2.87)/95=0.556. The sample decreased in volume during shear by 1.56 cc. For a volume of solids of 19.04 cc, the calculated void ratio at the beginning of shear was 0.556+(1.56/19.04)=0.638. This void ratio is precisely on the one-dimensional consolidation curves (Fig. 4.1 at a pressure of 80 psi=11,500 psf).

Shearing Stage

The sample underwent a decrease in volume during shear (see Fig. CD1.3 in the appendix), but of less than 0.5%. Failure occurred at about 3% axial strain, after which the sample began expanding. The failure plane began at one corner of the top cap and made an angle of about 35 degrees with the horizontal, before flattening out on a probable fissile surface (Fig. CD1.4). The time to failure was 1463 minutes. If the coefficient of consolidation is about 0.0002 sq.in./minute, then the estimated degree of consolidation at failure is 81%.

Values of the secant Young's modulus and Poisson's ratio are included in Fig. CD1.2. At half the stress difference at failure, E=12,000 psi and ν=0.44. A failure envelope cannot be defined using a single test. However, the secant value of $\bar{\phi}$ is 44 degrees based on a confining pressure of 80 psi and a stress difference of 362 psi.

EAGLEFORD FORMATION (TESTS CD2-CD4)

General Comments

Tests CD2-CD4 were performed as part of an effort to develop acceptable testing procedures. They were incidently used to obtain a preliminary estimate of the position of the failure envelope. Confining pressures were 10, 50, and 100 psi.

The times to failure were less than the theoretical times corresponding to 95% consolidation because of the need to proceed with development of procedures as opposed to defining the envelope with high accuracy. Tests CD2 and CD3 experienced problems with membrane leakage. We were finally forced to use a slit plastic sheet between the filter paper and the membranes (CD2-CD4).

Repeated membrane failures in test CD2 probably caused significant disturbance.

Comments on Test CD2

Condition of core. The outside of the core used for this specimen was softened, apparently by the presence of drilling fluid.

Consolidation stage. The sample was subjected to 100 psi of pressure initially. After about thirty minutes the membrane failed. The test was dismantled and the specimen was examined. Tiny openings existed, apparently associated with the fissile surfaces. We thought that the membrane might have been blown into one of these openings so we packed cuttings into visible voids. As a result of the added soil plus imbibation of moisture from the leak, the "original" weight of the sample was increased to 180.83 grams (original weight was 177.50 grams).

The specimen was mounted in the triaxial cell again and subjected to successive pressures of 100 psi, 50 psi, and 10 psi. The sample seems to have consolidated fully under 100 psi but not under 50 psi or 10 psi. The test was allowed to proceed anyway because of the short time available for the testing program. The assumption was that any remaining dissipation of pore water pressure (swelling) would occur during the shearing test.

Coefficients of consolidation were estimated by fitting theoretical ΔV-t curves to the measured values (see the appendix). The fitted values were:

Pressure psi	Coefficient of Consolidation sq.ft./day
100	0.013
50	0.0017
10	0.0025

The fit was a relatively poor one for the 100 psi pressure, perhaps because of the dominating influence of secondary effects or because of the problems with membrane failure. The values at 50 psi and 10 psi seem more reliable.

Shearing stage. The sample failed after about eight hours of loading, on a plane rotated only 22 degrees from the horizontal (see Fig. CD2.4). For a coefficient of consolidation of 2.5×10^{-3} sq.in./min. and a time to failure of 492 minutes, the calculated degree of consolidation at failure was 60%.

At 50% of the failure stress difference, the secant values of Young's modulus and Poisson's ratio were 4100 psi and 0.25, respectively.

Comments on Test CD3

Consolidation stage. This sample was subjected to a single pressure of 100 psi. The membranes leaked, thus destroying measurements of volume change. The test was dismantled and set up again using new membranes. The wet weight of the sample for the second set-up was about 2.3 grams more than the original wet weight so the sample swelled by at least 2.3 cc of water.

The sample reconsolidated, essentially in accord with theory, and the calculated (fitted) coefficient of consolidation was 0.0014 sq.ft./day

Shearing stage. The sample reached the peak stress difference after about 785 minutes. The estimated degree of consolidation at failure was 52%. The strain at failure was 4.3%. The sample failed on a surface at an angle of about 36 degrees from the horizontal (Fig. CD3.4 in appendix).

At 50% of the peak stress difference, secant values of Young's modulus and Poisson's ratio were 18,000 psi and 0.15, respectively.

Comments on Test CD4

Consolidation stage. The sample for test CD4 was subjected to an initial 100 psi consolidation pressure and was then rebounded to 50 psi. The sample was probably not fully consolidated under 100 psi but the pressure was reduced anyway to obtain preliminary data. The time-volume curve at 50 psi exhibited strange behavior at an elapsed time of about 1000 minutes when a vacuum was

inadvertently applied to the sample. The sample was swelling under the 50 psi pressure so the reversal in flow direction at a time near 20,000 minutes (two weeks) means that water was flowing out of the sample. The problem was probably membrane leakage because the reverse flow was only about 0.03 cc/day. The reversed flow would have no influence on the effective stresses in the sample, and thus none on strength, but would have an influence on the apparent volumetric strains during the shearing stage.

The fitted coefficient of consolidation was 1.2×10^{-4} sq.ft./day.

Shearing stage. The sample in test CD4 failed at an axial strain of 3.4%, in 635 minutes, on a failure plane oriented at 39 degrees from the horizontal (Fig. CD4.4). The calculated degree of consolidation at failure was 15%.

The failure time was too short because time was running out on the testing program. The consolidation stage should have been shorter and the shearing stage longer but we wanted information, for at least one sample, on the consolidation time required to achieve essential equilibrium so we left this specimen under the final pressure for 25 days.

At 50% of the peak stress difference, secant values of Young's modulus and Poisson's ratio were 18,000 psi and 0.17, respectively.

Collective Data for Tests CD2-CD4

Atterberg limits. The Atterberg limits for specimens used in tests CD2 through CD4 are summarized below:

Test No.	Liquid Limit %	Plastic Limit %	Plasticity Index %
CD2	69	29	40
CD3	83	26	57
CD4	82	29	53

The core used for test CD2 seems to have been materially different from the core used for tests CD3 and CD4.

Consolidation data. Because of the problems with membrane leakage, the void ratios could not be calculated with a useful accuracy. The coefficients of consolidation are summarized below:

Test No.	$\bar{\sigma}_3$ psi	c sq.ft./day
CD2	100	0.013
	50	0.0017
	10	0.0025
CD3	100	0.0014
CD4	50	0.00012

Except for the first pressure for test CD2, these coefficients are extremely low. The lowest value was for test CD4 where the pressure was left in place for 25 days and the sample continued to expand slowly. The result was that the times used in the fitting operation also became quite long and the calculated coefficient of consolidation was proportionately lowered. Pressures were applied for shorter times to other samples so there was no way to estimate what would happen to the ΔV-t curves once the next pressure, or the shearing stage, began. Fitting was thus performed with the data available and the best fit curves had comparatively short times and comparatively large coefficients of consolidation.

Data of the type just indicated are highly indicative of dominating secondary effects. The best evidence of the conclusion of primary consolidation would be the dissipation of excess pore water pressures but no such measurements were included in this contract.

If the primary rebound curve merged smoothly with a secondary curve, then volume change could be measured for prolonged periods of time. For such long times, the sample might experience chemical changes, e.g., oxidation of pyrite, that would cause additional long-term effects. In the absence of pore water pressure data, all such effects might be lumped into the coefficient of consolidation which, accordingly, would be extremely low, and which would then not be applicable to field conditions.

Shearing stress-strain behavior. Specimens used for tests CD2 through CD4 exhibit the brittle behavior (Fig. 6.2) expected of highly overconsolidated materials.

The samples in all tests exhibited a relatively steep loading curve initially and then a detectable "break" (reduction in slope) at an axial strain of about 0.5%. This change in slope has been observed for numerous tests on widely different soil and rock materials.

For such highly overconsolidated materials, we were surprised that the samples all decreased in volume up until failure. Highly overconsolidated materials typically compress for axial strains less than perhaps one percent, and then begin dilating.

Volumetric strains are developed due to changes in both mean normal effective stress and shearing stress. In a triaxial compression test, negative volumetric strains (decrease in volume) tend to occur because of the increase in mean normal stress. Expansion for highly overconsolidated materials then results from the shearing stresses. In dense soils with blocky particles, the particles are forced to roll up over each other during shear and thus dilation occurs. In some highly plastic materials, the particles are too flexible to force a volume expansion and compression occurs even for dense materials. Compression may also occur if the material is strong and relatively incompressible because of the presence of cement, but actually has a low density; a condition that does not seem applicable to the Eagleford material at this site.

In direct shear, the specimens of Eagleford shale expanded during shear. In direct shear tests there should be only a small increase in mean normal stress so the predominant influence is the shear. In the case of triaxial compression tests CD2 through CD4, the specimens compressed up to failure indicating the preponderant influence of the mean normal stress.

Failure mode. The samples failed on distinct shear planes that did not coincide with the planes of maximum obliquity, but were apparently controlled by fissures and horizontal planes of weakness.

In the tests where the operator was able to view the sample when the peak stress difference developed, a failure plane did not become noticeable until the stress difference started to decrease.

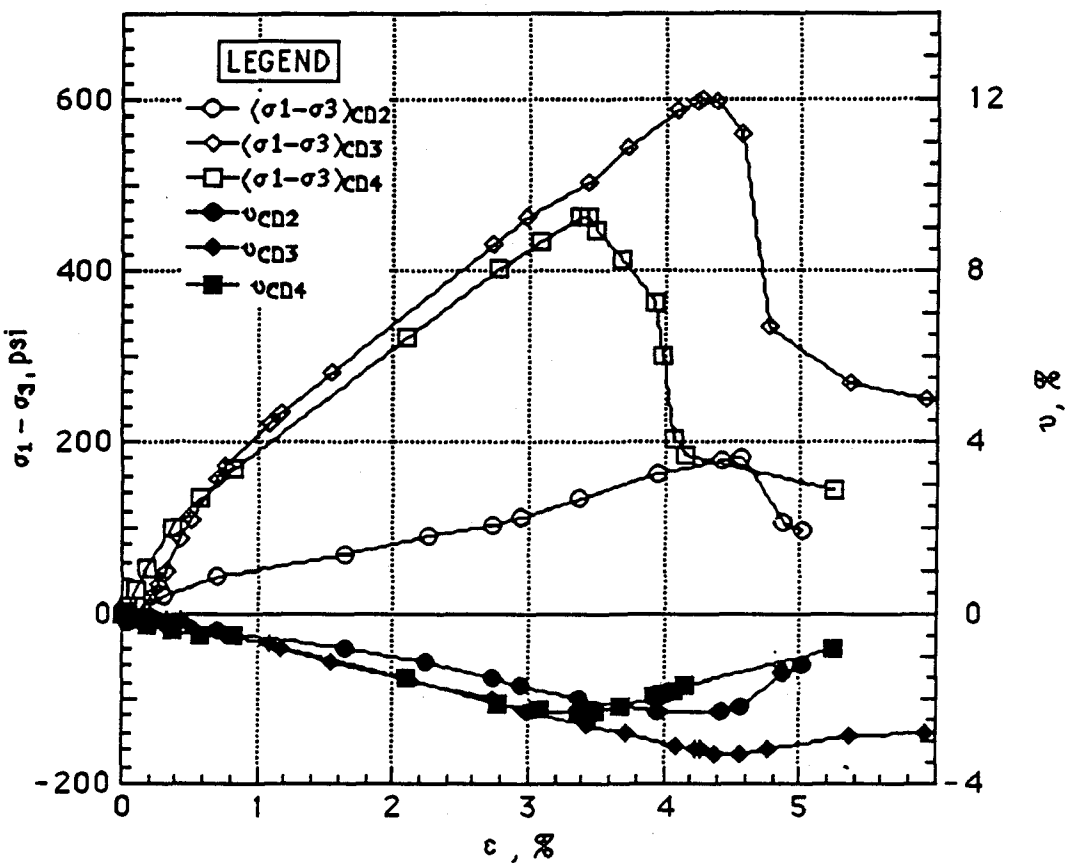

Fig. 6.2 Stress-Strain-Volumetric Strain Curves for Triaxial Tests CD2-CD4 for Eagleford Shale

After the failure plane develops the strains are highly localized so the interpretation of the test can no longer be based on the assumption of uniform stresses and strains. The stress-strain curves are extended beyond their intended usefulness (after the failure plane develops) for qualitative purposes only.

Failure envelope. Tests CD2-CD4 resulted in a failure envelope (Fig. 6.3) defined with $\bar{\phi}$ = 44 degrees and $\bar{c}$ = 36 psi (5200 psf). Scatter of data points may result from:

1. inherent non-homogeneities in the cores

2. variations in the amount of excess pore water pressure dissipation among the different tests

3. variations in strength loss due to differing amounts of sample disturbance

4. a curved failure envelope, i.e., no actual scatter.

It should be noted that in spite of the low theoretical degree of consolidation for the specimen for test CD4 (at 50 psi confining pressure), the stress-strain response (Fig. 6.2) is similar to that of the other specimens. The fact that the specimens were decreasing in volume during shear means that they were generating positive pore water pressures. Such pore water pressures would weaken the specimen. However, the specimen for test CD4 was actually stronger than would be expected compared to the other two tests (Fig. 6.3).

Young's Modulii and Poisson's ratio. The secant values of Young's modulus and Poisson's ratio, at a stress difference of half of the failure value, are summarized below:

Test No.	Consolidation Pressure psi	Young's Modulus psi	Poisson's Ratio
CD2	10	4,100	0.25
CD4	50	18,000	0.17
CD3	100	18,000	0.15

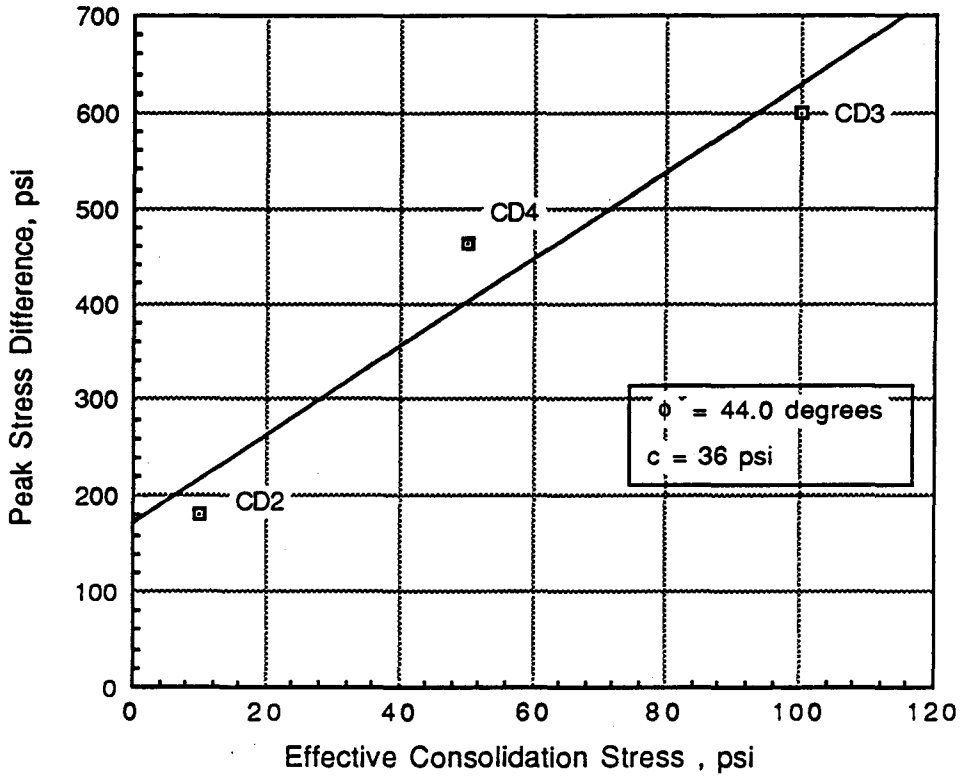

Fig. 6.3 Modified Mohr-Coulomb Diagram for Triaxial Test CD2-CD4 for Eagleford Shale

The data are reasonably consistent. Young's modulus increases as the consolidation pressure increases. Poisson's ratio is lower at the high consolidation pressures because the sample compresses more during shear.

EAGLEFORD SHALE (TESTS CD5-CD8)

Introduction

Tests CD5 through CD8 were performed at different loading (strain) rates at an effective consolidation pressure of 10 psi to study rate effects the "drained" strength of Eagleford Shale. Time did not permit a more extensive testing program.

Comments for Test C5

Consolidation stage. The sample used for test CD5 swelled under confining pressures of 100 psi and 120 psi but equilibrated under 140 psi. It was then rebounded to 50 psi and 10 psi. The sample was subjected to 140 psi for seven days, 50 psi for nine days, and 10 psi for 43 days.

Application of Bishop and Gibson's method to the readings of volume change versus time resulted in the following estimates of the coefficient of consolidation:

Load No.	Pressure psi	Coeff. of Consol. sq. ft./day
3	140	0.00024
4	50	0.00063
5	10	0.00010

The coefficient of consolidation for load number 5 is lower in part due to the longer swelling time. Even after 43 days the volume change-log time curve did not indicate the completion of what would appear to be primary consolidation. As discussed for the previous test series, secondary effects may be dominating the behavior.

Shearing stage. The stress-strain curve rose steeply only for the first 0.2% and then rose at a relatively uniform rate to the peak at 4% axial strain (Fig. 6.4). In spite of the high overconsolidation ratio, the sample compressed up until failure. The failure plane was oriented at 42 degrees from the horizontal (Fig. CD5.4 in appendix). The time to failure was 1138 minutes and the theoretical degree of consolidation at failure was 20%.

The calculated final water content, based on the measured initial water content and the measured volume changes, was 21.1%. The measured final water content was 18.6%. The difference is believed to have resulted from the failure mode. After failure, the sample broke into blocks that slid on each other, creating water-filled voids between blocks and perhaps between the sample and the membranes. The water removed from the pipet to occupy these macrovoids did not show up on the measured final water content of the blocks. It appears that the water content at failure might best be approximated as the final measured water content without correcting for the apparent change in volume after failure, that volume change perhaps representing mostly trapped water around the sliding blocks.

At half of the failure stress difference, the secant values of Young's modulus and Poisson's ratio were 9000 psi and -0.02, respectively. The very low value of Poisson's ratio means that the specimen essentially crushed, with negligible lateral strain, during the early part of loading. Secant values of Poisson's ratio rose to as high as 0.49 during later stages of shear.

Comments on Test C6

Consolidation stage. The specimen used for test CD6 was subjected to isotropic consolidation pressures of 140 psi (7 days), 50 psi (9 days), and 10 psi (25 days).

The Bishop and Gibson (1963) consolidation theory was used to obtain the following coefficients of consolidation:

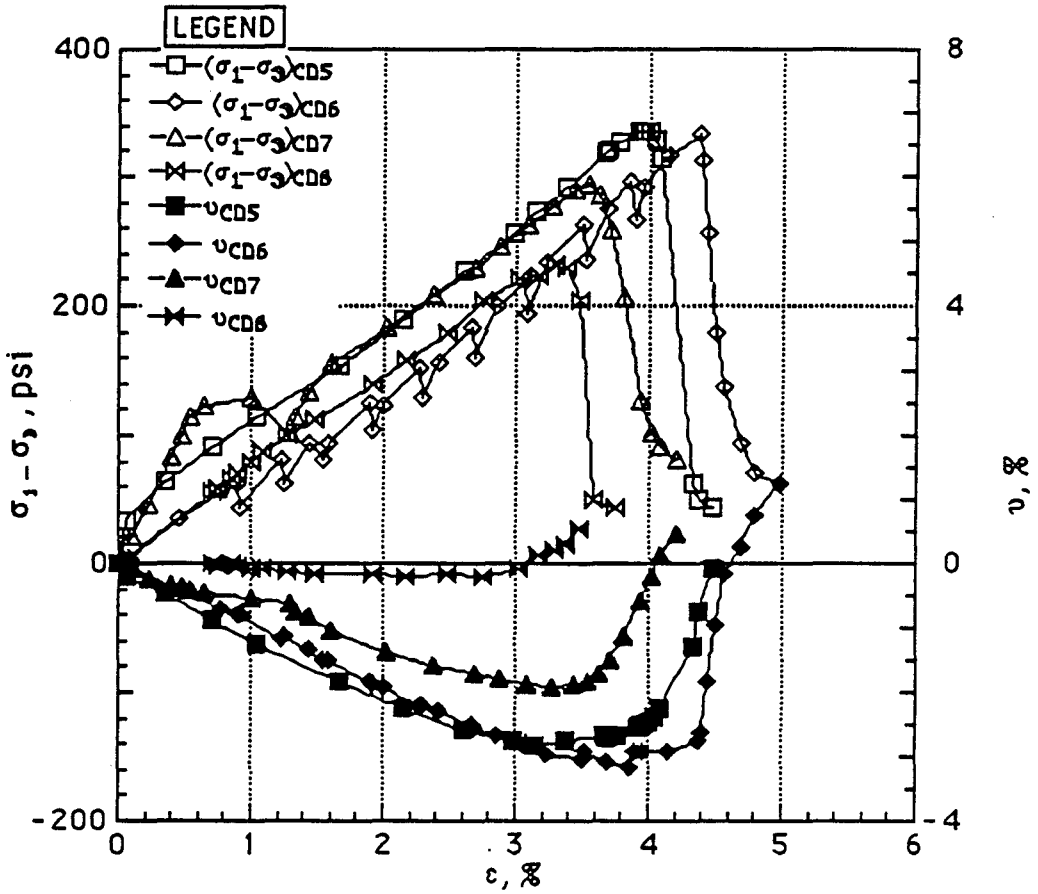

Fig. 6.4 Stress-Strain-Volumetric Strain Curves for Triaxial Tests CD5-CD8 for Eagleford Shale

Load No.	Pressure psi	Coeff. of Consol. sq. ft./day
2	50	0.00053
3	10	0.000045

The fitted coefficient of consolidation using the t_{100} fitting method for load number 3 was 0.0000605 ft^2/day.

Shearing stage. The stress-strain behavior of the specimen for test CD6 is quite similar to that for specimen used in CD5 (Fig. 6.4). The sample failed on two failure planes (see appendix) oriented at 68 and 73 degrees from the horizontal (Fig. CD6.4 in appendix), and passing through the top cap.

The failure time was 15,933 minutes (11 days) with a theoretical degree of consolidation at failure of 45%. The loading press was unable to load the sample at a strain sufficiently slow to achieve the desired shearing time so we stopped the press at selected times. During the non-loading periods, creep and consolidation resulted in small amounts of unloading (Fig. 6.4). In some cases the sample continued to consolidate by as much as 0.04 cc in 15 hours after the press was turned off, while in other cases the sample swelled by up to 0.04 cc. Large plastic strains developed at stress levels significantly less than the peak strength.

Unfortunately the sample in CD6 failed through the top cap so the actual peak stress difference of a "non-top cap failure" mode at the same strain rate is unknown. The failure planes did not become evident until after the peak stress difference had been reached so it may be possible that the failure mode did not significantly affect the measured strength.

The measured final water content was 19.7% whereas the value calculated from the initial water content and measured volume changes was 21.1%. The explanation seems to be the same as for test CD5.

At half of the failure stress difference, the secant values of Young's modulus and Poisson's ratio were 6600 psi and 0.02, respectively. The very low value of Poisson's ratio means that the specimen essentially crushed, with negligible lateral strain, during the early part of loading. Secant values of Poisson's ratio rose to as high as 0.63 during later stages of shear.

Comments on Test C7

Consolidation stage. The specimen for test CD7 was subjected to its final pressure of 10 psi at once, in an effort to speed up the testing program. Under 10 psi the sample was subjected to 25 days of swelling and approximately 3.67 cc of volume change. However, the triaxial cell developed a leak in the bushing after 12 days. In the process of dismantling the apparatus, a vacuum was accidently applied to the cell fluid, and probably caused both water and air to be sucked from the pipet into the interface between the sample and the membrane. The test was completely dismantled and set up all over again. The volume change-time curve had a sudden shift at the point where the accident occurred (see appendix). This problem should not have affected the shearing behavior.

In spite of the apparent predominant influence of secondary effects, the primary - theory was fit to the data (see appendix) and the coefficient of consolidation was estimated to be 5.6×10^{-4} sq.ft./day.

Shearing stage. During shearing, the bushing in the replacement cell began to leak but the testing time was sufficiently short (22 minutes) that the leak was tolerated without repair.

The stress-strain curves for test CD7 are similar to those for tests CD5 and CD6 (Fig. 6.4) except that the specimen for CD6 is slightly weaker than the others and the decrease in volume is slightly less, both in accord with the short testing time. Failure occurred on failure planes oriented at 35 and 39 degrees from the horizontal, near the base (Fig. CD7.4 in the appendix). The theoretical degree of consolidation at failure was 8% in accord with the desire to have a negligible amount of drainage.

At half of the failure stress difference, the secant values of Young's modulus and Poisson's ratio were 9600 psi and 0.19, respectively.

Comments on Test CD8

Consolidation stage. The specimen for test CD8 was subjected to the final consolidation pressure of 10 psi at once, to speed up the testing program. The sample swelled by 3.12 cc during 12 days. The Bishop and Gibson fitted coefficient of consolidation was 2.5×10^{-3} sq.ft./day. The shape of the swelling curve for CD8 was different from the shapes for other tests involving Eagleford shale (Fig. 6.5). We were unable to find any reason for the behavior.

Shearing stage. The membrane in test CD8 developed a leak during shear. The test was stopped, the cell was disassembled, and the membrane was replaced. The apparatus was reassembled, the confining pressure applied briefly, the load returned to the value it had when failure occurred, and the test continued. It might have been more reasonable to simply discard the sample but time did not permit replacing the test with a new one so we tried to obtain whatever data we could.

The stress-strain response of this sample is different from the previous tests (Fig. 6.4), especially in terms of the volumetric strains developed during shear. The failure plane was oriented at an angle of 62 degrees from the horizontal (Fig. CD8.4 in the appendix). The shearing time to failure was 2340 minutes, with a theoretical degree of consolidation at failure of 91%.

At half of the failure stress difference, the secant values of Young's modulus and Poisson's ratio were 7500 psi and 0.45, respectively.

Collective Consideration of Data for Tests CD5 Through CD8

Atterberg limits. The Atterberg limits for specimens used in tests CD5 through CD8 are summarized below:

Test No.	Liquid Limit %	Plastic Limit %	Plasticity Index %
CD5	80	31	49
CD6	85	29	56
CD7	80	30	50
CD8	77	31	46

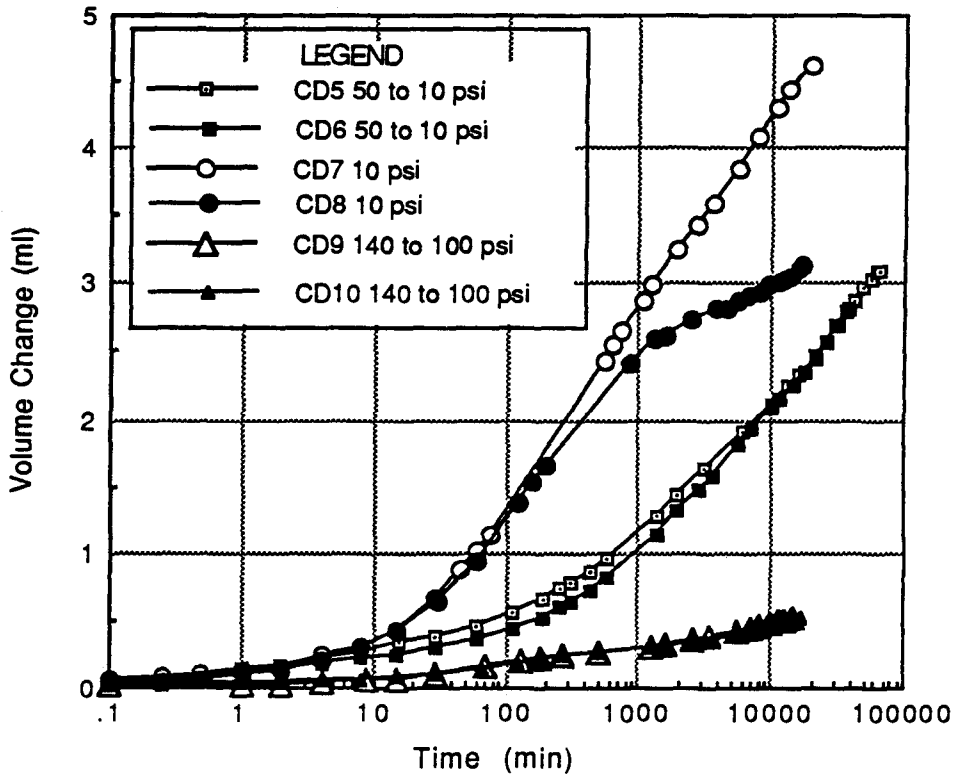

Fig. 6.5 Time-Volume Change Curves for the Last Swell Increments for CD Test on Eagleford Shale

The four samples seem to have been reasonably uniform at least in terms of their Atterberg limits.

Consolidation data. Coefficients of consolidation for tests CD5 through CD8 are summarized in Table 6.3. The values range widely but all are quite low. The value for test CD8 is high, in part, because the late stages of consolidation were considered to be secondary and primary theory was fit to the early part of the curve only.

Table 6.3 Summary of Coefficients of Consolidation for Tests in the Series CD5 through CD8

Test No.	Load No.	Pressure psi	Coeff. of Consol. sq. ft./day
CD5	3	140	0.00024
	4	50	0.00063
	5	10	0.000099
CD6	2	50	0.00053
	3	10	0.000045
CD7	1	10	0.00056
CD8	1	10	0.0025

Shearing data. The measured compressive strengths of samples used in tests CD5 through CD8 are plotted against the time to failure, in Fig. 6.6. Data from tests CD5 through CD7 fit into a tolerably uniform pattern. The measured strength increases with increasing time to failure, in accord with the observation that the samples all compressed during shear, i.e., that they generated positive pore water pressures. The specimen for test CD8 yielded a considerably lower strength. It is possible that the need to dismantle that test during the shearing stage, and then set it up again, caused the strength loss. The same thing happened with the first direct shear test on Taylor marl. The sample for CD8 is different from the others in that it underwent much less compression during the early stages of shear, and dilated more than the other samples.

The secant values of Young's modulus and Poisson's ratio, at a stress difference of half of the failure value, are summarized below:

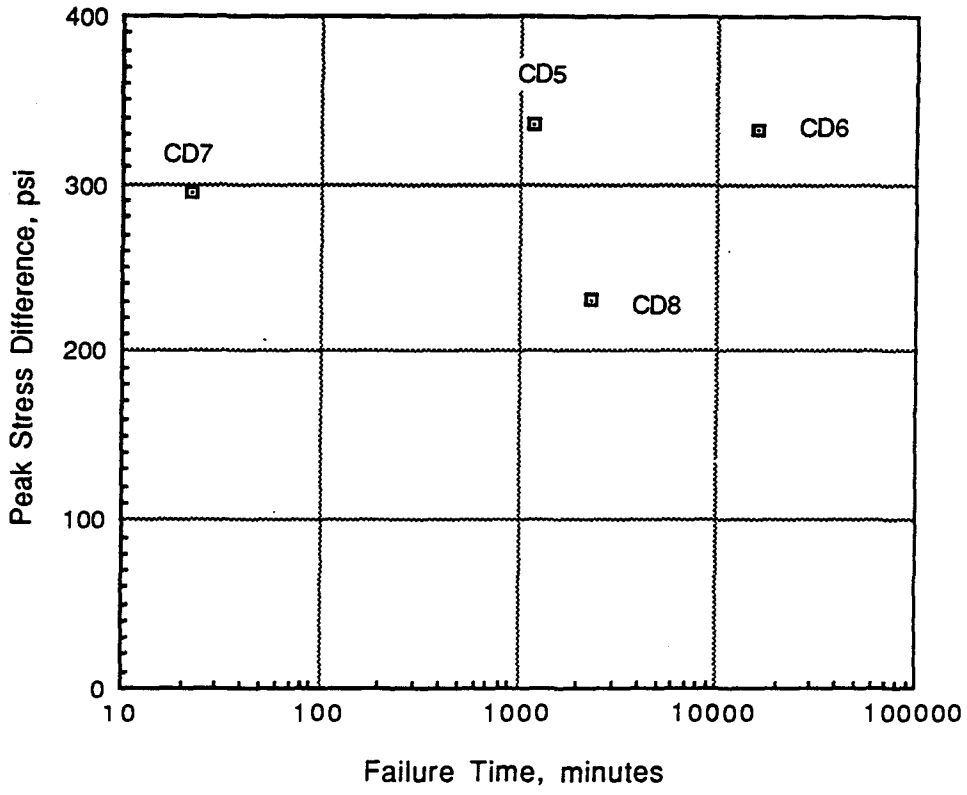

Fig. 6.6 Peak Stress Difference-Log Failure Time for Eagleford Shale at 10 psi

Test No.	Time to Failure minutes	Degree of Consolidation at Failure %	Young's Modulus psi	Poisson's Ratio
CD5	1138	20	9000	-0.02
CD6	15,900	45	6600	0.02
CD7	22	8	9600	0.19
CD8	2340	91	7500	0.45

The lack of relationship between the calculated degrees of consolidation at failure and the times to failure is the result of a wide range in coefficients of consolidation.

The failure modes of the samples were not generally in accord with theory, apparently as a result of severe anisotropy and possibly due to the presence of fissures. The effect that the strange failure modes had on the compressive strengths is unknown.

The data seem to indicate that shearing times to failure of the order of 1000 minutes would be adequate. For coefficients of consolidation ranging from 0.0025 sq.ft./day down to 0.000045 sq.ft./day, the theoretical times to failure for 95% consolidation range from 3 days to 175 days. Several possible explanations can be developed for the relationship between the measurements and the theory:

1. the long testing times are appropriate and all of the tested performed here had such short times that they are effectively undrained and thus yielded similar strengths. This argument cannot be rejected unless pore water pressure data exist for externally drained samples. However, theory would probably indicate that the influence of time to failure should have been more than we found for tests with times to failure up to 20,000 minutes (two weeks).

2. the strengths of these materials under undrained and fully drained conditions do not differ significantly, i.e., only small excess pore water pressures would be generated in undrained tests. In such a case, the strengths under drained and undrained conditions would not differ significantly and scatter associated with non-uniform samples assumes a dominant role. We think this situation may be applicable to the

Eagleford samples, but we were not assigned any undrained tests and thus cannot make direct comparisons.

3. secondary effects exert a major influence over the volume change characteristics so the fitted coefficients of consolidation are far too low. We consider this factor to be a major one.

EAGLEFORD SHALE (TESTS CD9 AND CD10)

Purpose of these Tests

The previous series of tests utilized samples at a confining pressure of 10 psi. Such samples would be highly overconsolidated. We considered it desirable to conduct a duplicate series of tests using a higher confining pressure to determine the overall applicability of the data.

Accordingly, tests CD9 and CD10 were performed at different strain rates at an effective consolidation pressure of 100 psi.

Discussion of Test CD9

Core condition. The outer 0.1 inch of the original core was clearly softened, probably by contact with drilling fluid, so the whole specimen may have been softened somewhat.

Consolidation stage. The sample used for test CD9 was subjected to isotropic consolidation pressure of 140 psi for three days and seemed to come to equilibrium. Then it was rebounded to 100 psi for nine days. The small relative stress change would normally be expected to result in substantial secondary effects.

In test CD9 a thicker commercial membrane (Wykeham Farrance 10500, 0.012"-0.18" thick) was used but the slit plastic sheet was

still used to protect the membrane. The thicker membrane may have reduced the rate of membrane leakage.

The curve of volume change versus log(time), under a pressure of 100 psi, had a small inflection in the middle (see appendix). If Bishop and Gibson's theory is fit to the pre-inflection part of the curve, thus believing that the latter part is secondary, then $c=3.7x10^{-3}$ sq.ft./day. If the theory is fit to the whole curve, then $c=5.0x10^{-4}$ sq.ft./day, but the shapes of the measured and theoretical curves differ significantly. The coefficient of consolidation computed using measured permeability and volumetric compressibility is 3.90×10^{-2} ft^2/day.

Shearing stage. The specimen failed (Fig. 6.7) at an axial strain of 2.7%, on a failure plane 47 degrees (Fig. CD9.4 in the appendix) from the horizontal in 22 minutes. The theoretical time to failure, based on the fitted coefficients of consolidation and for 95% consolidation at failure, would range from 2 days to 16 days. The predicted time to failure based on measured hydraulic conductivity and triaxial compressibility was 220 minutes. The calculated degree of consolidation at failure, based on $c=3.7x10^{-4}$ sq.in./min., was 20%.

At a stress difference of 50% of the failure value, the secant values of Young's modulus and Poisson's ratio were 27,000 psi and 0.38, respectively.

The initial water content was 15.7% and the measured final water content was 15.6 %. The final water content, calculated from the initial water content and measured amounts of inflow or outflow, was 15.8%. After the failure plane developed, the tendency of the sample to break into distinct blocks was less than for tests performed at 10 psi and the membrane is stretched more tightly over the sample by the 100 psi confining pressure, so that water can not move in between the sample and the membrane. Thus, the measured and calculated final water contents agreed more closely than for tests performed at smaller pressures.

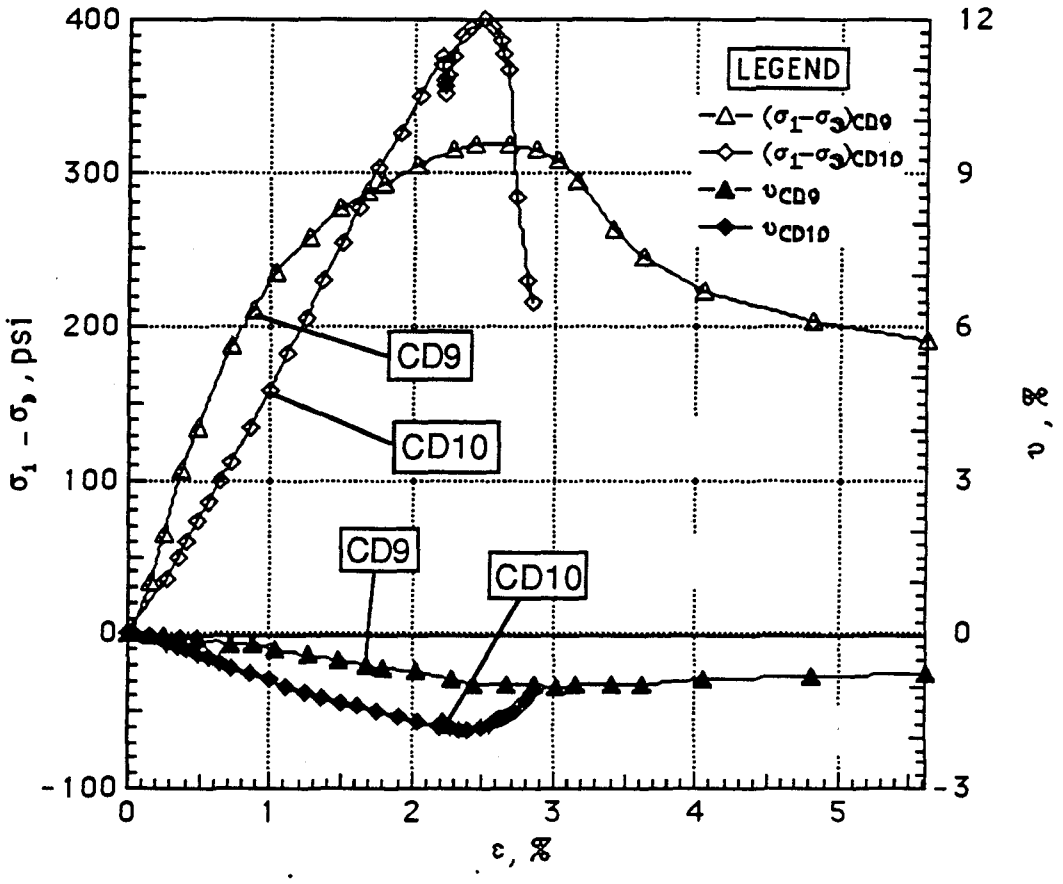

Fig. 6.7 Stress-Strain Behavior of Eagleford Shale in Tests CD9 and CD10

Comments on Test CD10

Consolidation stage. The specimen for test CD10 was also consolidated initially under 140 psi (two days), and then rebounded under 100 psi (ten days). In test CD10 the thicker commercial membrane was used but the slit plastic sheet was not used to protect the membrane.

As for test CD9, the ΔV-log(t) curve, for a pressure of 100 psi, had a small inflection in the middle and primary consolidation could be assumed to occur in the first part or over the whole curve. The fitted coefficients of consolidation then ranged from 3.0×10^{-3} sq.ft/day (first part) down to 2.0×10^{-4} sq.ft./day (poor fit to whole curve).

Shearing stage. We chose the strain rate to produce what we thought would be a drained failure and also to complete the testing phase in a reasonable amount of time.

The shearing stage was stopped (the press was turned off) for approximately 16 hours to look for evidence of dissipation of excess pore water pressures during shear. During the time the press was off, the pipet indicated swell on the order of 0.01 cc. Because the sample had previously been compressing, the swell was apparently the result of the small reduction in stress difference, from 376 psi (mean stress 225 psi) to 352 psi (mean stress 217 psi). There was no evidence of dissipation of any major amount of pore water pressure.

The specimen in CD10 failed (Fig. 6.7) at an axial strain of 2.50 %, on a failure plane oriented at 37 degrees from the horizontal (Fig. CD10.4 in the appendix) in 4318 minutes (3 days). The calculated degree of consolidation at failure, using $c=3.0 \times 10^{-4}$ sq.in./min., was 96%.

At a stress difference of 50% of the failure value, the secant values of Young's modulus and Poisson's ratio were 16,600 psi and 0.06, respectively.

The initial water content was 15.8 % and the measured final water content was 15.2 %. The final water content, calculated from the

initial water content and the measured amounts of inflow or outflow of water, was 15.4% (a good correlation at 100 psi).

Comparison of Tests CD9 and CD10

Atterberg limits. The Atterberg limits for the two specimens were:

Test No.	Liquid Limit %	Plastic Limit %	Plasticity Index %
CD9	64	28	36
CD10	67	30	37

The two samples seem to have been reasonably uniform, at least in terms of their Atterberg limits, but to differ significantly from the material used for the test at 10 psi of confining pressure.

Influence of shearing time on Young's modulus. Stress-strain curves for samples used in tests CD9 and CD10 are compared in Fig. 6.7. Young's modulus was clearly higher for test CD9 with the shorter loading time. The reason for this difference in modulus is easily understood if we think of a constant load test. A stress difference is applied instantaneously and an axial strain is measured, thus yielding a modulus under undrained conditions. If the stress is maintained, the sample will deform, regardless of the overconsolidation ratio, thus increasing axial strain and decreasing the modulus.

The compressive volumetric strains are larger for the sample in test CD10 because more time was available for discharge of water.

It appears that the sample in test CD10 also had time to dilate and suck in water when failure occurred, and thus it lost strength rapidly after failure. The sample with the short shearing time (CD9) could not compress as much during initial loading, and thus was weaker at failure, but neither could it imbibe water rapidly at failure and thus it did not lose strength as rapidly (rapidly in terms of axial strain rather than time).

Influence of shearing time on strength. The compressive strengths of the two specimens are plotted against the time to failure in Fig. 6.8. It is unfortunate that there was neither sufficient time, nor sufficient core, to test specimens at intermediate strain rates.

The calculated degrees of consolidation at failure were 20% for test CD9 and 96% for test CD10. The compressive strengths rose from 318 psi for CD9 to 400 psi for CD10, a difference of 26%. For normally consolidated materials, we would normally expect a 100% increase in going from an undrained strength to a fully drained strength. The small difference between the strengths of specimens CD9 and CD10 may indicate that only small excess pore water pressures are generated in triaxial compression on this material under a confining pressure of 100 psi. With the usual scatter in properties for natural materials, and only two tests, the difference may be controlled by differences in material properties.

COLLECTIVE DISCUSSION OF TESTS ON EAGLEFORD SHALE

Time-Dependent Chemical Changes

The existence of pyrite in the cores indicates that the material is in a reducing environment in the field. The laboratory environment is an oxidizing one so chemical changes are anticipated when samples are exposed to the laboratory environment for prolonged periods of time. The only obvious change that we detected was the presence of a strong odor from triaxial samples when they were being dismantled. The source of the odor was not determined. Chemical changes may have occurred in direct shear and consolidation samples as well but any gases generated in the process could easily escape during the test.

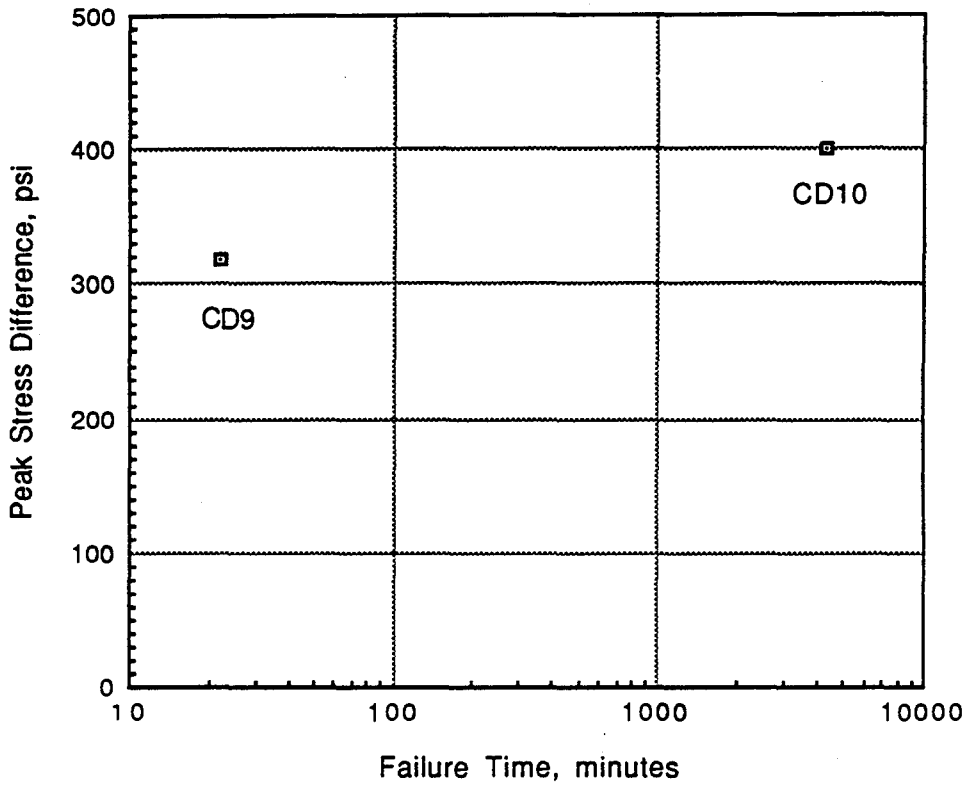

Fig. 6.8 Peak Stress Difference-Log Failure Time for Eagleford Shale at 100 psi

Consolidation Properties

Effects of membrane leakage. Measurement of the stress-strain behavior of specimens from the SSC site under isotropic stresses is subject to potentially large errors. The material is relatively incompressible and thus undergoes relatively small changes in void ratio (strains) under applied stresses. Membrane leakages that are too small to be of concern with more compressible materials may result in measured volume changes that are a significant fraction of the actual material volume changes.

A first source of membrane leakage is gas diffusion. If the sample contains free gas bubbles and the cell is filled with deaired water, then the gas in the sample will diffuse through the membranes and dissolve in the cell water. With prophylactic membranes, we have generally found that equilibrium is established in about one to two weeks. We recorded flows of water back into samples from the pipets, after a stage of consolidation, and believe these may have been due to gas diffusion.

Water leakage occurs through membranes and bindings, more or less in accord with Darcy's law. Poulos (1964) measured a hydraulic conductivity of Ramses membranes as about 5×10^{-16} cm/sec. For a sample with a height of 3 inches, a diameter of 1.5 inches, and for a membrane with an average thickness of 0.002 inch subjected to a pressure differential of 100 psi, the leakage rate is 0.005 cc/day. For Trojan membranes, we have measured leakage rates of about 0.006 cc/day under a pressure difference of 40 psi so we would expect rates of about 0.015 cc/day for 100 psi, but this rate includes binding leakage. The two sets of measurements thus yield more or less comparable results.

When there are salt concentration gradients across a membrane, the osmotic leakage occurs from the side with low salt concentration to the side with high salt concentration, i.e., generally from the triaxial cell into the sample. For samples with a single Trojan membrane and a one-molar salt solution in the sample, we measured a leakage rate of 0.032 cc/day under a negligible cell pressure of 5 psi.

For dual Trojan membranes, as used for most of the tests here, the pressure leakage rate would be about (0.015 cc/day)/(100 psi) =

0.00015 cc/day/psi for one membrane, or probably about 0.000075 cc/day/psi for dual membranes, as used on this project. We do not know the salt concentration in the pore water and thus cannot calculate osmotic leakage rates. However, for dual Trojan membranes, we might anticipate rates of about 0.010 cc/day. Thus, we anticipate a leakage rate of about:

$$q = 0.010 + 0.00015\Delta p \qquad (6.12)$$

where q is leakage in cc/day and Δp is the pressure drop in units of psi. For the cell pressures of 10, 50, 100, and 140 psi, the leakage should be about 0.012, 0.018, 0.025, and 0.031 cc/day, respectively.

The above leakage rates were assumed to occur for each of the tests CD2 through CD8 where dual prophylactic membranes were used. For the consolidation phases, the calculated total leakage represented the following percentages of the measured volume change: CD2 (4%), CD3 (5%), CD4 (33%), CD5 (10%), CD6 (14%), CD7 (8%), CD8 and (4%).

The measured rebound curve for test CD4 under 50 psi of cell pressure, is compared with the curve corrected for leakage rates of 0.018 cc/day (value assumed for 50 psi of cell pressure) and 0.025 cc/day in Fig. 6.9. It appears that the flow reversal at about 20,000 minutes was due to the leakage rate exceeding the swelling rate for this sample but that the actual leakage rate is in excess of 0.25 cc/day. Higher leakage rates could result from a variety of causes, e.g., different membrane properties from those used in the previous studies, a higher electrolyte concentration in the sample than assumed in the calculations, looser bindings than used in previous studies, and tiny holes in the membranes (perhaps just thin spots) caused by sharp pyrite particles. Further, effects of gas diffusion leakage have not been included because we have no record of the extent to which the cell water was deaired nor details associated with gases in the samples.

No attempt will be made to correct measured volume changes for membrane leakage, in general, but the effects of leakage will be considered in cases where leakage might influence the discussion.

Stress-strain curves. Problems with membrane rupture and gas diffusion through the membranes makes it difficult to determine reasonably accurate one-dimensional stress-strain [e-log($\bar{\sigma}$)] curves

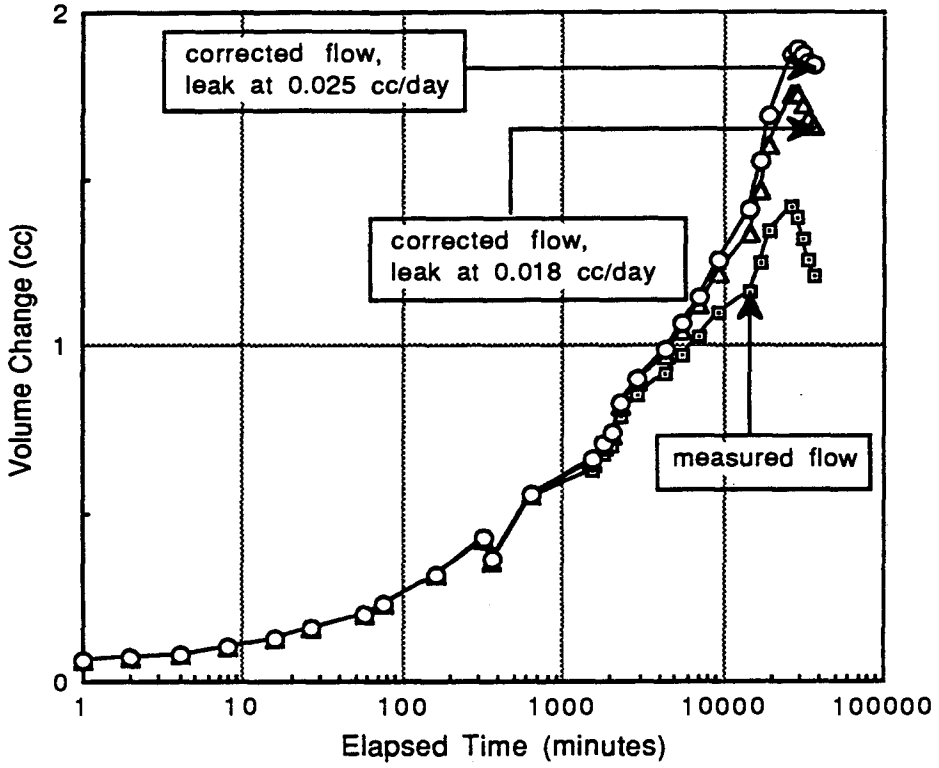

Fig. 6.9 Measured and Corrected Consolidation Curves for Test CD4 under 50 psi of Cell Pressure

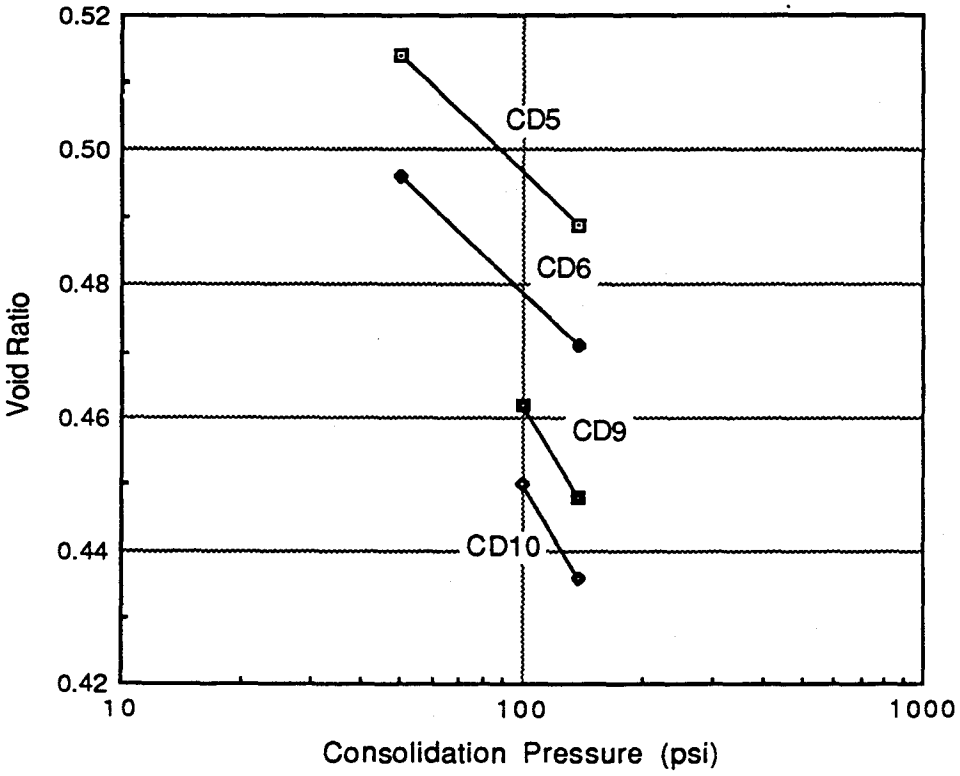

Fig. 6.10 Comparison of Triaxial Rebound Curves for Eagleford Shale

from the triaxial tests. After consideration of all of the data, we concluded that tests CD5, CD6, CD9, and CD10 were likely to yield the most accurate data. We used initial void ratios and volumes of solids from the original set-up data forms (see appendix), and corrected the measured volume changes for membrane leakage using the Eq. 6.12. The resulting stress-strain curves are shown in Fig. 6.10. The differences in void ratios between the different samples at a given effective stress are small and may be real or may result from minor errors in specific gravity or other causes (the range in void ratio at 100 psi is only 0.05). Of more importance is the slope of the swelling curve. For tests CD5 and CD6 the swelling index (slope of e-log($\bar{\sigma}$) curve) were both 0.056. For tests CD9 and CD10 the rebound slopes were both 0.096.

Coefficients of consolidation. Coefficients of consolidation are summarized below for all triaxial tests with Eagleford shale.

Test No.	Starting Stress psi	Ending Stress psi	Stress Ratio	c sq.ft./day	Consol. time days
CD2	-	100	-	0.013	1.0
	100	50	2.0	0.0017	0.9
	50	10	5.0	0.0025	0.9
CD3	-	100	-	0.0014	1.9
CD4	-	50	-	0.00012	25.2
CD5	-	140	-	0.00024	7.1
	140	50	2.8	0.00063	9.0
	50	10	5.0	0.00010	45.0
CD6	140	50	2.8	0.00053	9.0
	50	10	5.0	0.000045	26.0
CD7	-	10	-	0.000056	24.5
CD8	-	10	-	0.0025	11.6
CD9	140	100	1.4	0.0037	9.9
CD10	140	100	1.4	0.0030	11.8

Taken collectively, they indicate a range of almost 300 times in the coefficient of consolidation. Based on earlier discussion and general experience, some of the following factors are involved:

1. the cores actually had a variation in material properties
2. coefficients were low in cases where measurements were taken for long periods of time and the measured ΔV-log(t)

curve did not show evidence of a changeover from primary to secondary consolidation, e.g., CD4. In such cases, the fitted theoretical curve was forced to indicate measurable consolidation out to large times and thus the coefficient of consolidation was low.

3. in cases where the ΔV-log(t) curve could be interpreted to show a changeover from primary to secondary consolidation, e.g., CD9 and CD10, the theoretical curve was fitted to the early part of the measured curve and coefficients of consolidation were relatively large. Note that the evidence of changeover from primary to secondary was a tiny effect that could have been nothing more than a very minor reading error that left one reading slightly out of line with the others.
4. in one-dimensional consolidation testing, secondary effects become increasingly important as the stress ratio decreases and as the consolidation time for the previous load increases.
5. for volume changes as small as those measured here, gas diffusion through the membranes, evaporation from the top of the pipet, and a number of other sources of error can become detectable. We made gradual adjustments to experimental procedures to minimize such problems but separate studies are probably needed to isolate such unusual problems.
6. we have not examined the problem of partially draining filter paper because that would require a special set of tests to measure hydraulic conductivity of the paper as a function of stress level.
7. we have not made measurements to determine the influence of anisotropy on consolidation properties.
8. some of the high values of the coefficient of consolidation could have resulted from the presence of undetected fissures or tiny seams of more pervious material that would have allowed more rapid internal drainage.

Shearing Properties

Failure data for all of the triaxial tests with Eagleford shale are collected together in Fig. 6.11 (along with data for test CD1 on Taylor marl). The two failure envelopes shown in the figure are defined by:

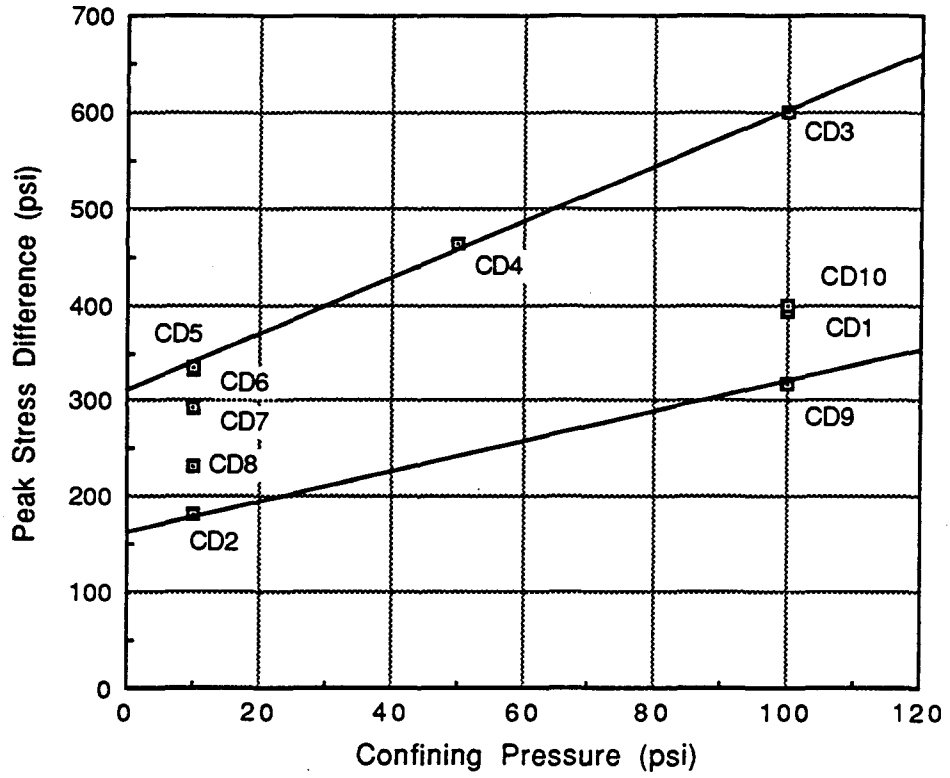

Fig. 6.11 Modified Mohr-Coulomb Diagram for all Triaxial Compression Tests

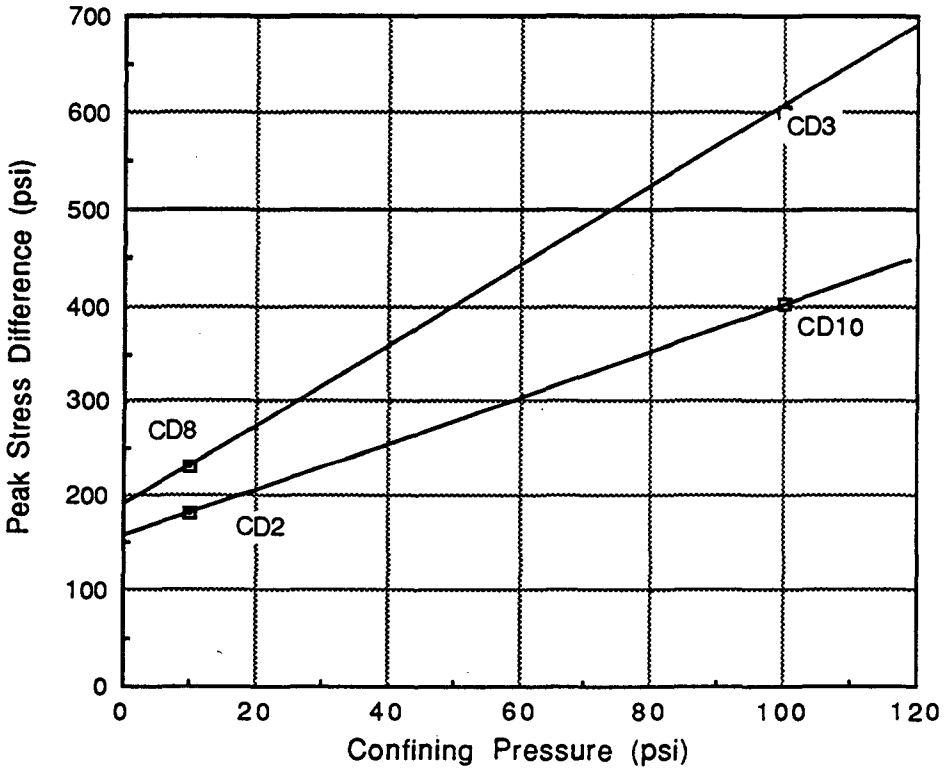

Fig. 6.12 Modified Mohr-Coulomb Diagram for all "Good" Triaxial Compression Tests on Eagleford Shale

Envelope	$\bar{\phi}$ (deg.)	$\bar{c}$ (psi)
lower limit	26	52
upper limit	37	76

However, some of these specimens should be given a low confidence level because they were deliberately tested in a short time period (CD4, CD5, CD9). Others should have reduced confidence because of failure planes at angles considerably different than the Mohr-Coulomb failure planes (CD2), and failure through the top cap (CD6), both apparently brought on by anisotropy caused by fissile surfaces and fissures. Remaining tests (CD2, CD3, CD8, CD10) would yield a somewhat more narrowly defined failure envelope (Fig. 6.12).

The usual interpretation of Mohr-Coulomb failure envelopes involves the assumption that the planes of maximum deformation are oriented at an angle of $45+\frac{\bar{\phi}}{2}$ from the horizontal. It is clear that the failure planes actually ranged widely in slope but did not, in general, coincide with the Mohr-Coulomb planes. An alternative interpretation of the data is to calculate the normal and shearing stresses on the actual failure planes using the standard equations:

$$\sigma = \frac{1}{2}(\sigma_1+\sigma_3) + \frac{1}{2}(\sigma_1-\sigma_3)\cos(2\alpha) \qquad (6.13)$$

$$\tau = \frac{1}{2}(\sigma_1-\sigma_3)\sin(2\alpha) \qquad (6.14)$$

where α is the angle between the failure plane and the plane upon which σ_1 acts, i.e., the angle between the failure plane and the horizontal.

A Mohr-Coulomb diagram using stresses calculated on the failure plane(s) (Fig. 6.13) yields, by linear regression analysis, $\bar{\phi}$=25 deg. and $\bar{c}$=62 psi. If only "good" data are used (Fig. 6.14), then $\bar{\phi}$=29 deg. and $\bar{c}$=29 psi.

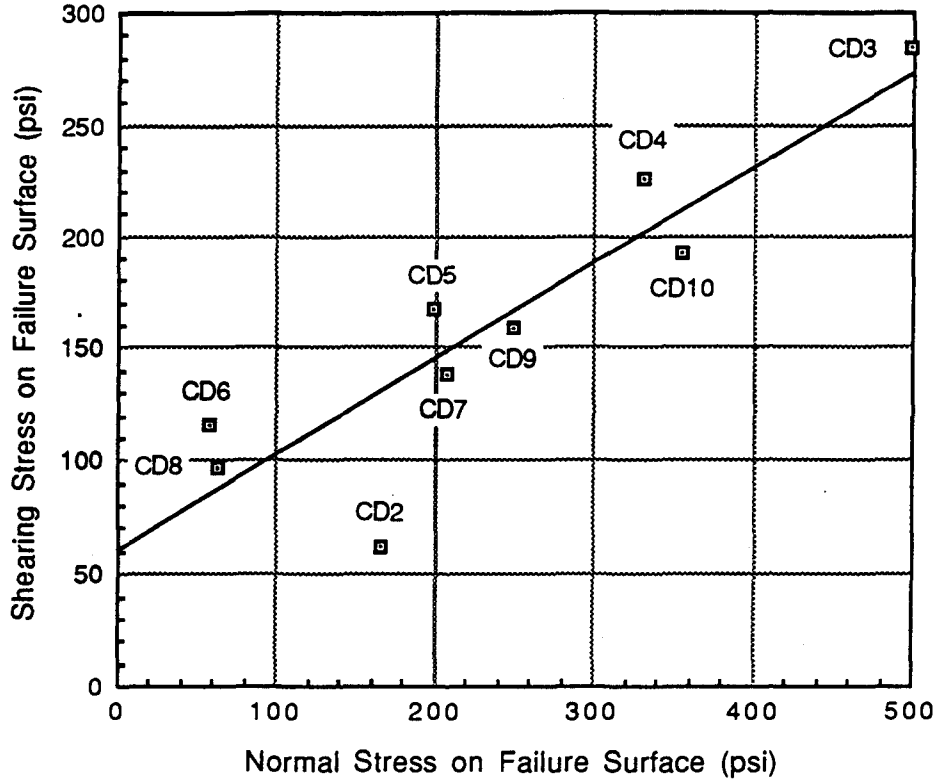

Fig. 6.13 Coulomb Diagram for Specimens of Eagleford Shale

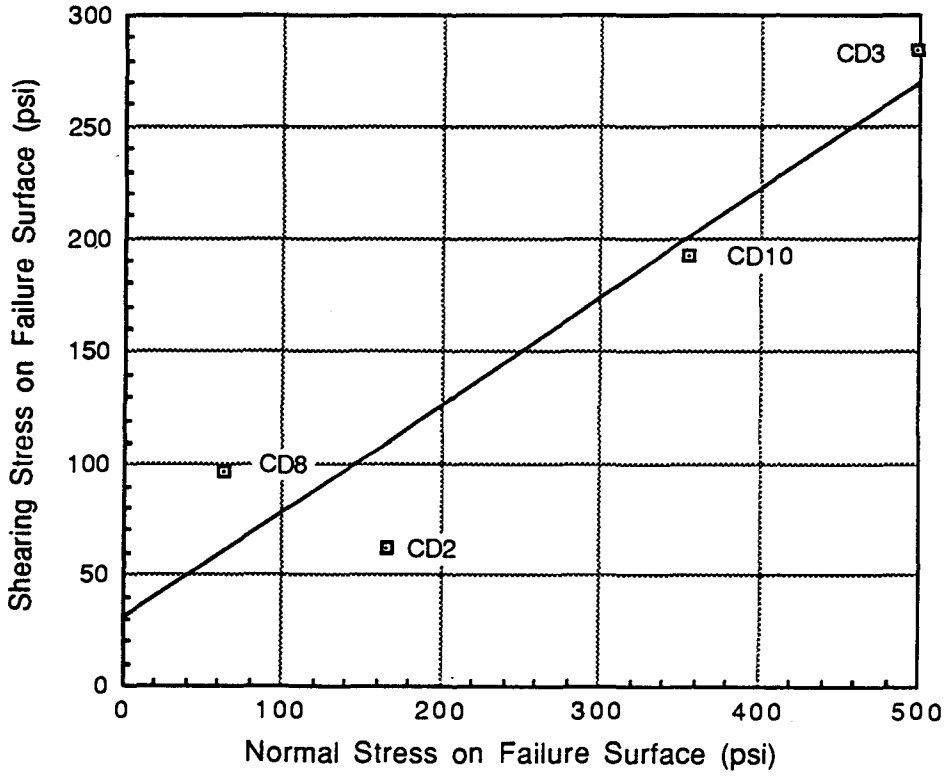

Fig. 6.14 Coulomb Diagram for Specimens of Eagleford Shale using only "Good" Tests

MODELLING OF STRESS-STRAIN BEHAVIOR

Introduction

The main function of this project was to engage in preliminary work to develop testing techniques rather than to engage in studies of modelling the stress-strain behavior of the material at the SSC site. Nevertheless, values of Young's modulus and Poisson's ratio were easily calculated in the spreadsheets and included in the appendices. It should be emphasized that the definitions used were for secant values and that it would have been more rational, from a modelling point of view, to engage in a number of load-unload cycles to try to separate elastic and plastic components of the deformations. Such experimental measurements could not be made within the constraints of this project. Thus, we will mention simply the secant values of Young's modulus and Poisson's ratio at the 50% stress level.

Secant Young's Modulus

The secant Young's modulus (E) generally ranges from 5000 psi to 25,000 psi (Fig. 6.15) and increases as the confining pressure increases. From previous discussion, it is clear that E is higher for undrained loading than for drained loading, at the same applied stress difference. Indeed, in spite of usual scatter, the highest values of E are generally for the shortest testing times (tests CD3, CD4, CD7, and CD9 in Fig. 6.15), with CD2 being an exception. Tests with longer times to failure (CD5, CD6, CD8, and CD10) tended to have values approximately along the line drawn in Fig. 6.15. Note that test CD1 was actually for Taylor marl.

Secant Poisson's Ratio

Values of Poisson's ratio scatter widely (Fig. 6.16). However, it may be noted that three of the tests with longer times to failure (CD5, CD6, and CD10) plot in the lower part of the scatter band. The other test with a longer testing time, CD8, had strange volume change

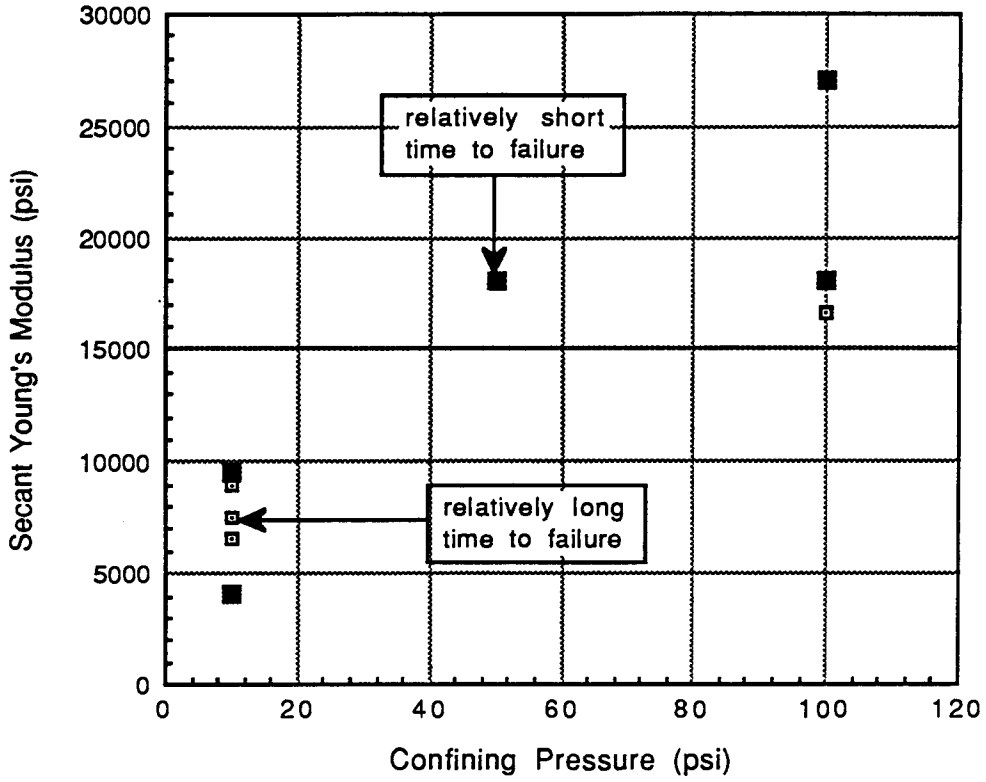

Fig. 6.15 Secant Values of Young's Modulii Defined at the 50% Stress Level

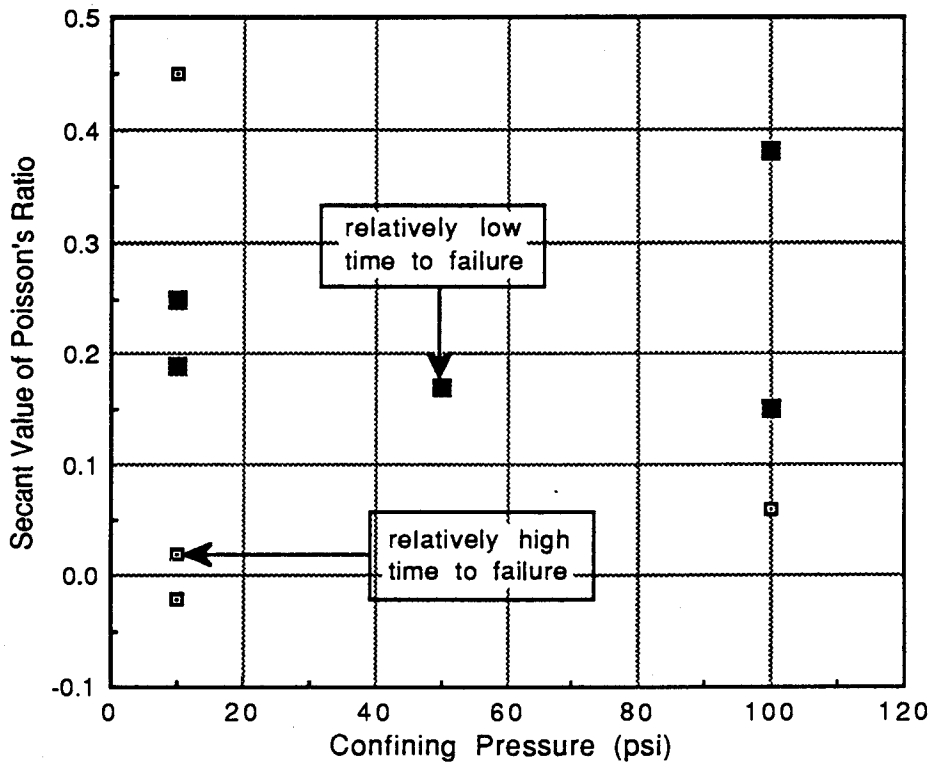

Fig. 6.16 Secant Values of Poisson's Ratio Defined at the 50% Stress Level

characteristics during consolidation, almost as if drainage became partially blocked. It had a relatively low compressive strength and is now seen to have an unreasonably high value of Poisson's ratio, all indicative of retarded drainage. Tests with shorter shearing times (CD2, CD3, CD4, CD7, CD9) have higher values of Poisson's ratio. For an undrained test with saturated material, Poisson's ratio is essentially 0.5. The data in Fig. 6.16 thus clearly show a drainage effect. Under fully drained conditions, Poisson's ratio, at the 50% stress level, tends to be between 0 and 0.1 and may increase as the confining pressure increases.

SECONDARY EFFECTS

In the absence of any measurements of pore water pressures, it is not possible to decide when primary effects have damped out and secondary effects have become dominant. The shapes of the ΔV-log(t) curves often indicate that primary effects are not governing volume change behavior. Further, the measured values of hydraulic conductivity in the one-dimensional consolidation tests were substantially higher than the values of hydraulic conductivity obtained by fitting Terzaghi's theory to measured time-settlement curves, indicating important secondary effects.

With respect to shear, secondary effects are of interest in trying to estimate shearing times that will result in a reasonable dissipation of excess pore water pressures generated during the shearing stage.

One way to estimate the influence of secondary effects during primary consolidation is to use measured values of hydraulic conductivity (k) from one-dimensional consolidation tests, and measured volumetric strains in the triaxial tests to estimate coefficients of consolidation. It is recognized that drainage is mainly in the horizontal direction in the triaxial specimen but is restricted to the vertical direction in the one-dimensional test, and that the soil is probably highly anisotropic to hydraulic conductivity. Further, the states of stress differ. Nevertheless, in the absence of other information, we will define the coefficient of consolidation using:

$$c = \frac{k}{(\gamma_w)(m_v)} \tag{6.15}$$

$$m_v = \frac{\delta V}{(V_0)(\delta \bar{\sigma})} \tag{6.16}$$

where k is the measured hydraulic conductivity, γ_w is the unit weight of water, δV is the volume change, V_0 is the initial volume, and $\delta \bar{\sigma}$ is the change in effective stress for the load increment.

As an example, consider load number 5 in test CD5. The sample volume was 83.4 cc, the volume change was 3.09 cc, and the change in effective stress was 40 psi so the volumetric strain, $\Delta\varepsilon$, was:

$$\Delta\varepsilon = \frac{3.09 \text{ cc}}{83.4 \text{ cc}} = 0.0371$$

and the volumetric compressibility, m_v, is:

$$m_v = \frac{0.0371}{40 \text{ psi}} = 9.26 \times 10^{-4} \frac{\text{sq.in.}}{\text{lb}} = 6.43 \times 10^{-6} \frac{\text{sq.ft.}}{\text{lb}}$$

The measured hydraulic conductivity was estimated to be 5.7×10^{-7} ft/day based on measurements in consolidation test C9 under load number 10. The calculated coefficient of consolidation is then:

$$c = \frac{5.7 \times 10^{-7} \text{ft/day}}{(62.4 \text{ lb/cu.ft})(6.43 \times 10^{-6} \text{ sq.ft/lb})} = 1.42 \times 10^{-3} \text{ ft}^2\text{/day}$$

which is over 14 times larger than the value, 9.33×10^{-5} sq.ft./day, obtained from experimental volume change-time readings in the triaxial test.

The difference becomes even greater if we assume that the horizontal hydraulic conductivity exceeds the vertical value. In addition, if some of the volume change under load number 5 is due to secondary consolidation, diffusion, and membrane leakage problems, the volumetric compressibility due to primary consolidation is smaller than 6.43×10^{-6} ft^2/lb.

The predicted times to failure, for 95% consolidation, come from Eq. 6.9b The time to failure, calculated using the fitted theoretical curve is:

$$t_f = \frac{(1.5/12)^2}{(40)(9.33\times10^{-5})(0.05)} = 84 \text{ days}$$

whereas using the coefficient of consolidation calculated using the measured hydraulic conductivity:

$$t_f = \frac{(1.5/12)^2}{(40)(1.42\times10^{-3})(0.005)} = 5.5 \text{ days}$$

For test CD6, the required time to failure using the fitted theoretical curve is 112 days but using a coefficient of consolidation calculated using the measured hydraulic conductivity the time to failure is about 4.5 days.

SUMMARY AND CONCLUSIONS

The following conclusions seem warranted based on the triaxial compression tests with rocks from the SSC site:

1. the rocks contain fissures and weak horizontal planes, resulting in failure modes that are not in accord with Mohr-Coulomb assumptions.

2. even small samples of the size used here, require very long periods of time to come to equilibrium during the swelling process. We were not able to wait for equilibrium to be established but we maintained constant pressure on one specimen (CD5) for a month and a half and the ΔV-log(t) curve showed no sign of transition from primary to secondary consolidation.

3. The time required for primary consolidation varies with the square of the sample size but secondary effects should not scale at all. If our observed ΔV-log(t) behavior is of a secondary type, then times will not be significantly longer for larger sample sizes than for the sizes used here. With larger samples, it might be possible to achieve more consistent behavior by having a random distribution of perfections in all samples.

4. Attempts to fit primary consolidation theory to volume change-time curves led to coefficients of consolidation that were among the lowest we have ever seen. The fitted coefficients tended to decrease as the time duration of measurements increased. The range in coefficients of consolidation that we observed was generally from 1.3×10^{-3} sq.ft./day down to 5×10^{-5} sq.ft./day. For shallow clays, we generally expect coefficients of consolidation to be in the range of 1 sq.ft./day down to 0.001 sq.ft./day.

5. the material in the cores was stiff, with secant values of Young's modulus, at the 50% stress level, generally in the range of 5000 psi to 20,000 psi.

6. values of Poisson's ratio are low, under drained conditions. Typical values are in the range of zero to 0.1.

7. the lack of sufficient time and number of tests, coupled with the heterogeneity of the material, makes it difficult to recommend a reasonable testing time to achieve adequate drainage during shear. However, times to failure should not be less than about twenty four hours and should preferably be in the range of four to seven days, pending collection of more definitive information.

8. as a result of the apparently random distribution of surfaces of weakness in samples, the shearing strengths scattered widely. The apparent scatter was further increased by the deliberate performance of tests with widely varying shearing times. When we used the best four triaxial compression tests, and calculated stresses on the apparent failure planes, we found that the failure envelope would be defined using $\bar{\phi}=29$ degrees and $\bar{c}=29$ psi.

9. several experimental problems developed that are particularly relevant to material as incompressible as the Eagleford shale. One was membrane leakage. We were forced to use relatively heavy "commercial" membranes to retard leakage. Consideration should be given to taking further steps to reduce leakage, e.g., using a cell fluid with the same osmotic pressure as the pore fluid of the samples or switching to a cell fluid that is less likely to leak through the membranes.

10. the time required to shear a sample, under drained conditions, increases essentially with the square of the sample size. Nevertheless, there are advantages in testing larger samples when the material is fissured. Samples large enough to contain a random distribution of fissures are more likely to represent field conditions than are small samples where the existence, or lack thereof, of a fissure exerts a strong influence on behavior.

SECTION 7

COMPARISON OF DATA ON ENGINEERING PROPERTIES OF THE EAGLEFORD SHALE MEASURED USING DIFFERENT TESTS

INTRODUCTION

In previous sections, we deliberately concentrated on a single test or single test type, and avoided making more general comparisons. The more general comparisons are included in this section. This section does not contain a summary of data presented previously.

We will avoid discussions the experimental problems when these problems were discussed previously. Instead, we will try to develop an understanding of the measured properties. We will attempt to compare tests that do not have obvious interpretation problems (membrane leakage, non-standard load increment ratios, etc.).

ATTERBERG LIMITS

The Atterberg limits were used as a means of estimating the uniformity of the cores among the different tests.

It was apparent, at once, that Atterberg limits were consistently lower for samples used in one-dimensional consolidation tests as opposed to triaxial compression tests. Differences between consolidation and direct shear were less clear. Summary data are presented in Table 7.1. The locations of the specimens used in the various tests were selected to try to use uniform material for paired tests, e.g., for a one-dimensional consolidation test and a

triaxial test on adjacent pieces of core. As a result, the differences are surprising.

It was noticed, on several occasions, that the samples used in the triaxial tests had a distinct organic odor when the tests were dismantled. No such odor was noticed for samples used in other tests. Clearly, any odoriferous material could escape readily in one-dimensional consolidation and direct shear tests but would tend to be trapped inside the membrane for triaxial tests.

Table 7.1 Summary of Atterberg Limits for Various Test Series*

Core ID	Test Type	N	LL %	PL %
11	Consolidation	2	68	26
	Triaxial	4	80	30
13	Direct Shear	10	85	31
	Consolidation	1	88	30
14	Consolidation	1	75	29
	Triaxial	3	85	30
15	Consolidation	2	62	28
	Triaxial	2	66	29

* N=number of tests used in calculating the average liquid limit (LL) and plastic limit (PL)

If the differing Atterberg limits resulted from some type of chemical reaction, or growth of organic matter, then we would expect that limits might differ for adjacent consolidation tests in which one was tested in the usual way and one was subjected to hydraulic conductivity tests. Paired data are shown in Table 7.2. The data are inconsistent and thus suggest that flushing deaired water through the samples had little, if any, influence on the Atterberg limits.

Plots of Atterberg limits versus total time in the apparatus did not indicate any consistent influence of time on limits (Fig. 7.1).

Our present inclination is to believe that some organic process occurs during the triaxial tests, that causes a change in the Atterberg limits. It would be interesting to know if such changes

are actually occurring and, if so, are they also occurring in the cores during storage.

Table 7.2 Comparison of Atterberg Limits on Paired Tests With and Without Measurement of Hydraulic Conductivity

Formation	Measure k	Test Number	LL(%)	PL(%)
Taylor	no	C3	66	29
	yes	C2	69	29
bentonite	no	DS14-16	114	55
	yes	C5	110	53
Eagleford	no	C6	88	30
	yes	C7	75	29
Eagleford	no	C8	64	25
	yes	C9	64	25
Eagleford	no	C10	59	28
	yes	C10	66	27

STRESS-STRAIN BEHAVIOR

Stress-strain properties cannot be measured in direct shear tests. Axial strains in one-dimensional compression are obviously much smaller than axial strains in triaxial compression tests where the radial boundaries are subjected to constant stress, so such comparisons do not seem particularly fruitful.

The e-log($\bar{\sigma}$) relationship from consolidation tests is a stress strain relationship (Δe is strain defined using the height of solids), thus allowing comparison of e-log($\bar{\sigma}$) relationships for one-dimensional consolidation tests and for triaxial tests both during consolidation and during shear.

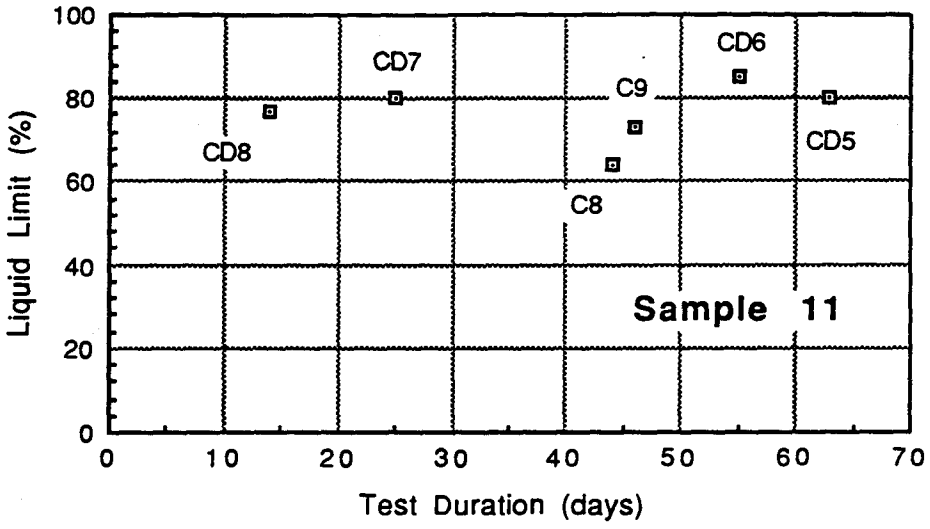

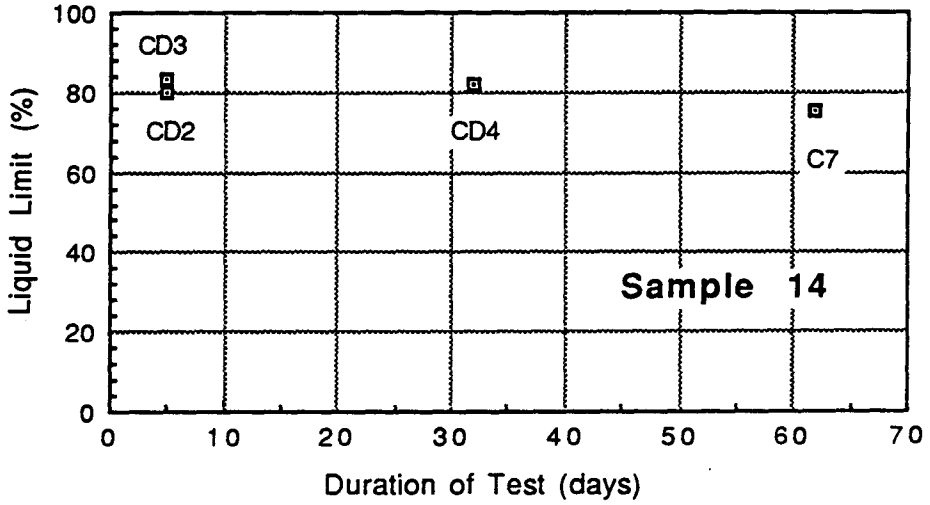

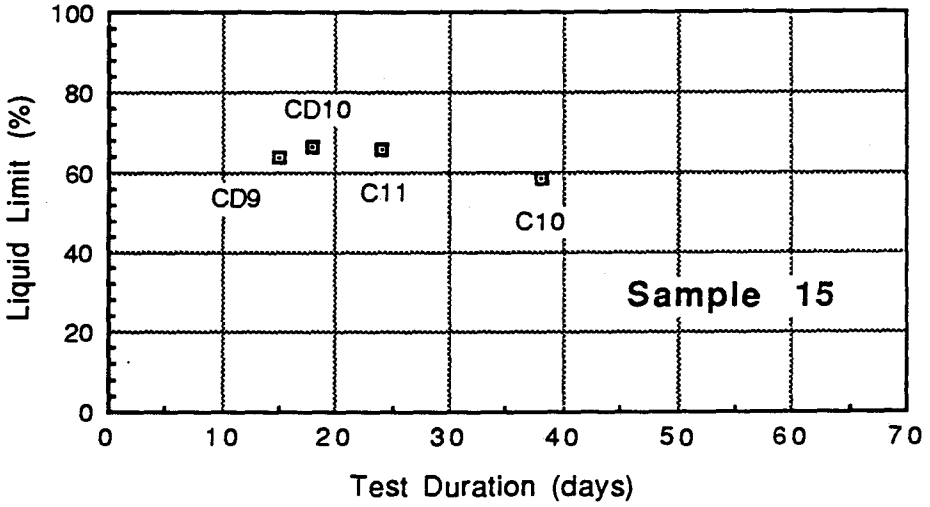

Fig. 7.1 Influence of Testing Time on Liquid Limits of Eagleford Shale

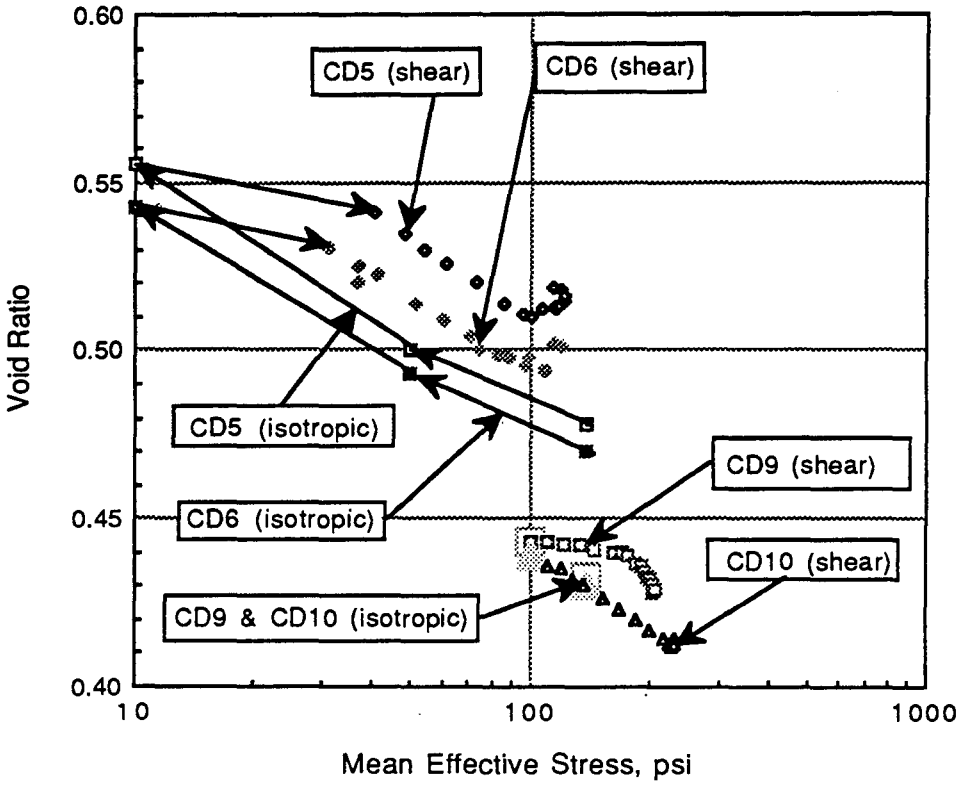

Fig. 7.2 Void Ratio-LogMean Effective Stress Curves during Isotropic Consolidation and Shearing for Tests CD5-CD6 & CD9-CD10 for Eagleford Shale

The only tests in triaxial compression that did not have leakage problems were CD5, CD6, CD9, and CD10 (on Eagleford shale). Tests CD5 and CD6 exhibited essentially the same stress-strain behavior (Fig. 7.2) so only one (CD5) will be used in later comparisons. Further, CD9 and CD10 exhibited the sample response under isotropic stresses (Fig. 7.2). However, CD9 was sheared so rapidly that it had little time to drain during the shearing stage (Fig. 7.2). Consequently, only test CD10 will be used in later comparisons.

In the absence of information on the overall state of stress in the one-dimensional consolidation test, we will use the vertical effective stress in the diagrams. The mean effective stress will be used for triaxial tests. The choice of these definitions of stress clearly does not imply that the void ratio is solely a function of either the vertical effective stress nor the mean effective stress; the choice was based on the available data.

For stresses near 10,000 psf, the slopes of the swelling curves for the triaxial and one-dimensional samples are essentially the same (Fig. 7.3). For smaller stresses, the slope flattens out considerably for the one-dimensional test but steepens for triaxial test CD5. Several explanations may be used for the differing stress-strain response:

1. The rings used in the consolidation tests were polished, greased, stainless steel. Nevertheless, the first thought is that ring friction in the one-dimensional tests has prevented free swell. We believe that ring friction alone can be the cause of the difference in slopes.
2. If the void ratio is mainly controlled by the mean stress, and K_o is considerably in excess of one for the one-dimensional rebound curve, then the stresses used with the one-dimensional curve should be increased proportionately. This effect is too small to be a sole explanation of the difference in slopes but it may be a contributing factor.
3. A less likely explanation is that the triaxial specimen is undergoing some type of chemical change that is causing increased rebound.

The shearing stage of triaxial test CD5 yields a curve that forms a hysteresis loop with the rebound curve and resembles the curves from one-dimensional consolidation tests. The hysteresis loop for the triaxial test may then be partially explained by the low

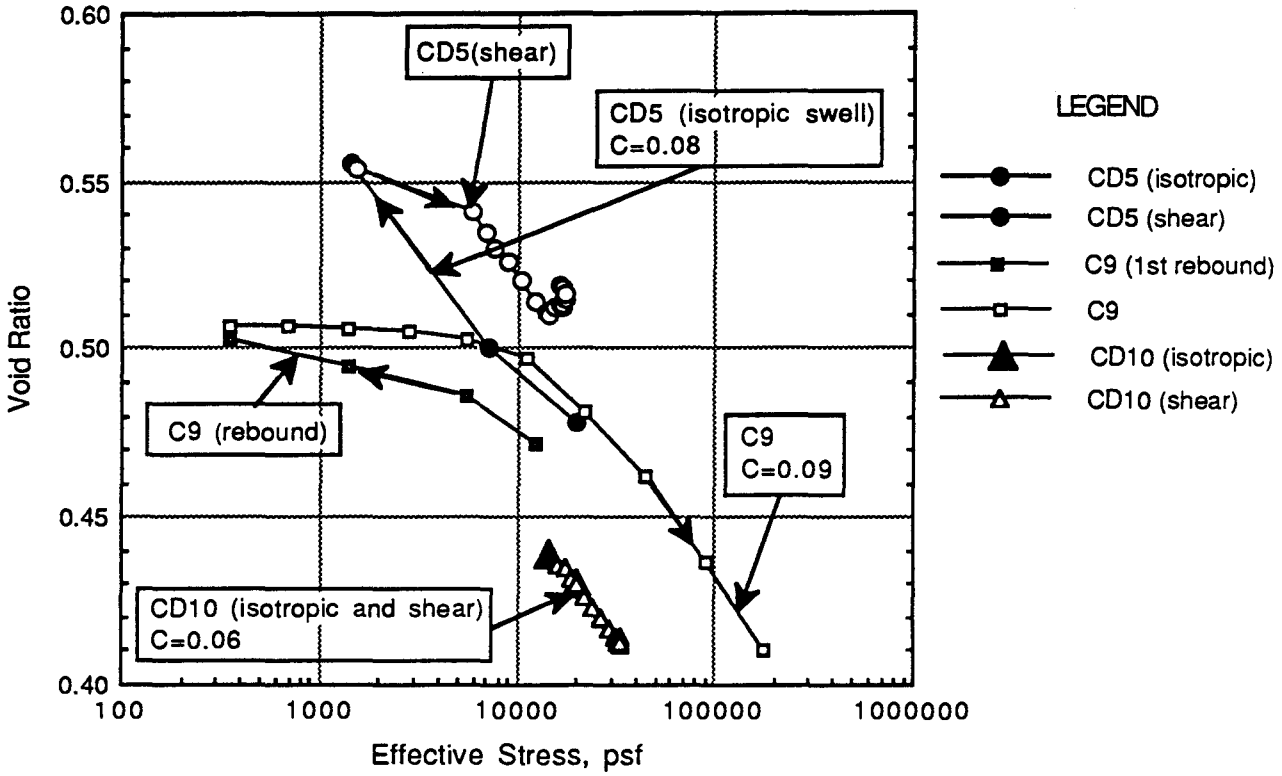

Fig. 7.3 Void Ratio-Log Effective Stress Curves During Consolidation and Shearing for Tests CD5, CD10, and C9 for Eagleford Shale

Poisson's ratio during the early stages of shear. With only a small lateral strain, the triaxial and one-dimensional responses might be expected to be qualitatively similar.

Further, the triaxial sample may have had significant excess pore water pressures early during shear, thus compressing less than it should have for the case of full drainage. However, we stopped the loading for test CD6, about once each day, for a number of hours, and found no evidence of volume change caused by dissipation of pore water pressures, so there may have been only small excess pore water pressures in both CD5 and CD6.

Based on data in Fig. 7.2, it appears that the slopes of the semi-logarithmic stress-strain curves are essentially the same in one-dimensional and triaxial compression except in the low stress range where ring friction may be a problem in the one-dimensional tests.

During a major part of the loading in the triaxial compression test, the stress-strain response measured in the e-log($\bar{\sigma}_{oct}$) diagram (Figs. 7.2 and 7.3) is qualitatively similar to the response in one-dimensional compression. At failure the samples dilate.

COEFFICIENTS OF CONSOLIDATION

The coefficients of consolidation were also similar for tests CD5 and CD6, so only CD5 will be used in later comparisons. Similarly, CD9 will be used to represent CD9 and CD10.

Coefficients of consolidation from one-dimensional test C9 and triaxial test CD5 are compared in Fig. 7.4, and tests C10 and CD10 in Fig. 7.5. The small number of points for the triaxial data results from the fact that CD9 was rebounded from 140 psi to 50 psi and then to 10 psi, thus providing data for only two coefficients of consolidation. Test CD10 involved rebound from 140 psi to 100 psi and thus gave data for only a single point.

The coefficients of consolidation were significantly lower for the triaxial tests than for the one-dimensional tests (note the use of a log scale for the coefficient of consolidation). Several factors enter into the differences between the coefficients:

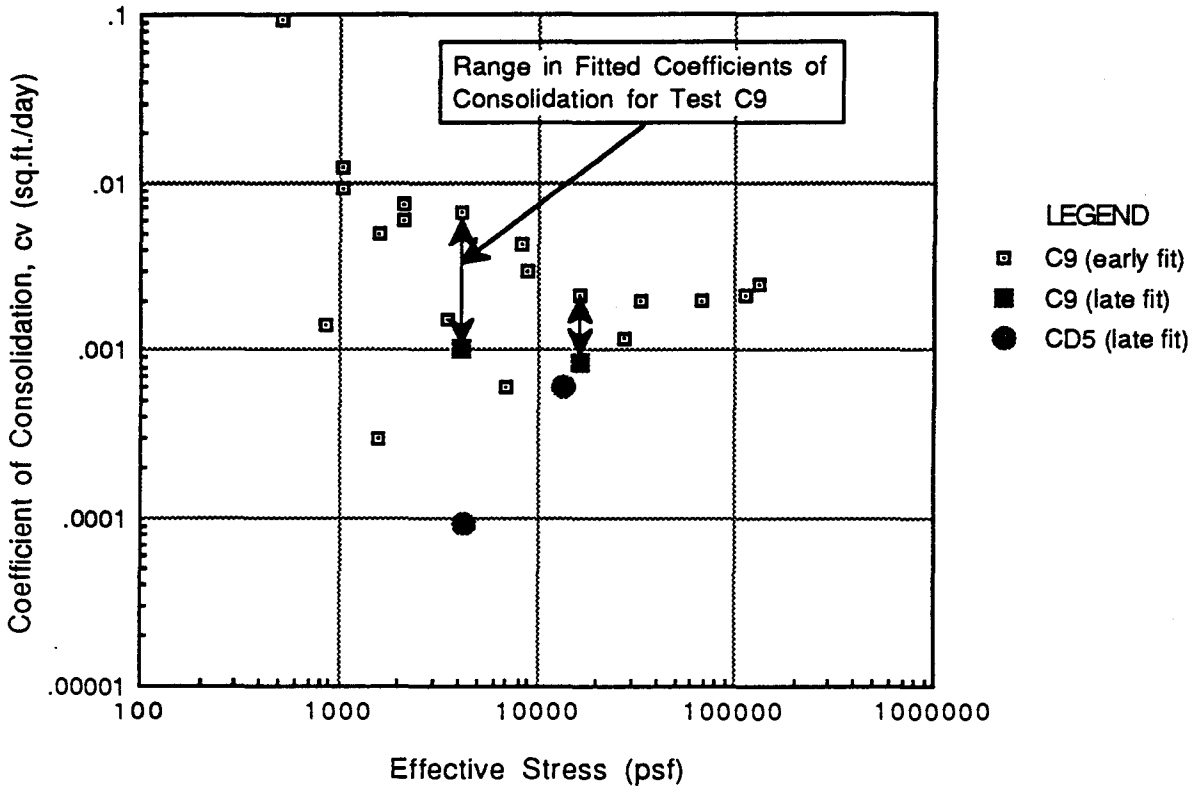

Fig. 7.4 Comparison of Coefficients of Consolidation-Effective Stress Data for Tests C9 and CD5

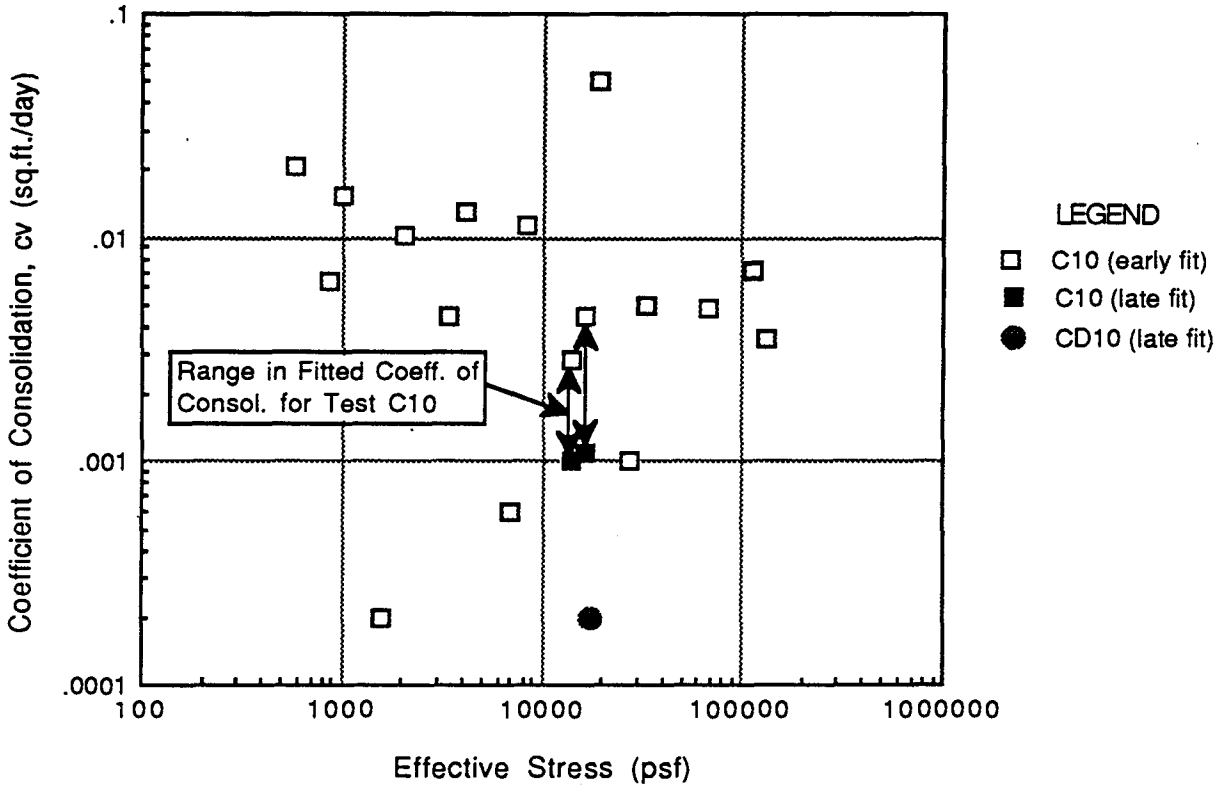

Fig. 7.5 Comparison of Coefficients of Consolidation-Effective Stress Data for Tests C10 and CD10

1. A range in coefficients can be obtained depending on where primary consolidation is assumed to end. For the one-dimensional consolidation tests, we generally began with root-time plotting and concluded that primary consolidation ended well before the final settlement reading. For triaxial consolidation, the ΔV-log(t) plots showed no evidence of the end of primary consolidation and we generally fit to the entire curve. The result is a tendency to obtain lower coefficients for the triaxial tests. Of course, if the triaxial volume change curves had indicated the end of primary at an earlier stage we would have fit to the early part of the curve.

2. The initial void ratios were different for some the tests (CD10 vs C10). Differences in coefficients of consolidation, as a result of different permeabilities and compressibilities, are expected. if the void ratios differ between two tests. The coefficients of consolidation are plotted against void ratio in Figs. 7.6 and 7.7.

3. The coefficient of consolidation varies directly with hydraulic conductivity and inversely with compressibility (Eq. 4.6). In the low-stress range, the compressibilities differ markedly between the one-dimensional tests and the triaxial tests (Fig. 7.3), thus probably being the major factor in causing the different coefficients of consolidation.

4. The coefficient of consolidation calculated by fitting a primary consolidation theory to experimental data is too low because of secondary effects that occur during primary consolidation (see discussion of measured and computed hydraulic conductivities in Section 5). If the secondary effects are larger in one-dimensional tests, as some expect, then coefficients should be lower in the one-dimensional tests.

5. We suspect that the hydraulic conductivities are larger in the horizontal direction than vertically. The triaxial samples probably drain horizontally, preferably, and the one dimensional specimens clearly drain vertically.

6. For some materials, the lateral filter paper drains, used in the triaxial tests, are not freely draining, thus reducing the apparent coefficient of consolidation. For the low coefficients

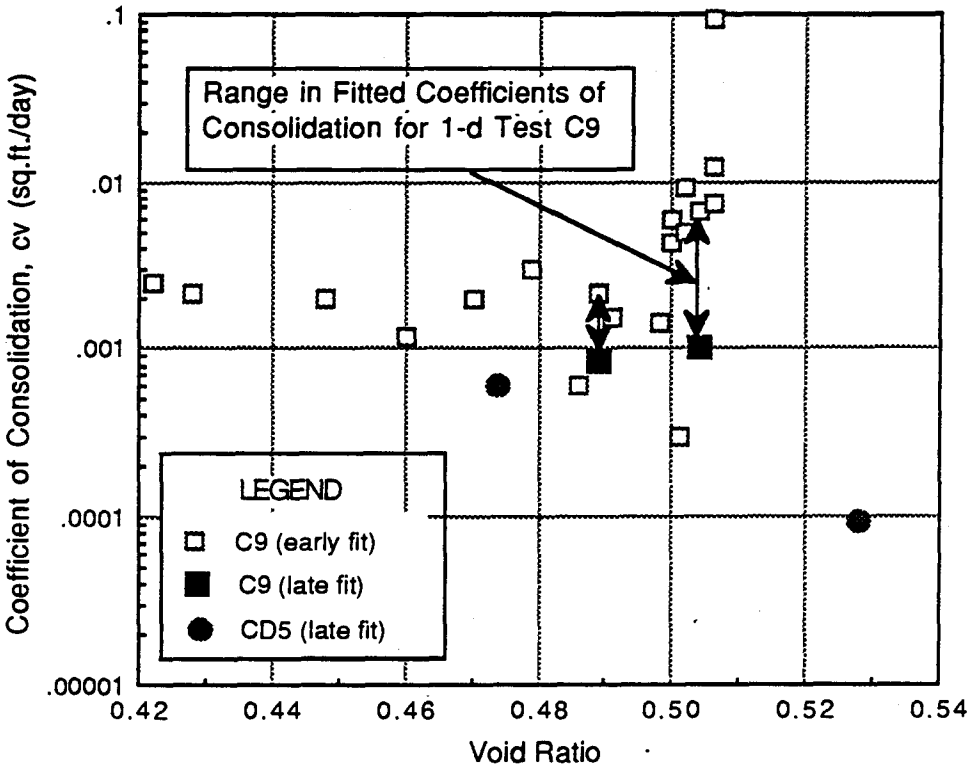

Fig. 7.6 Comparison of Coefficients of Consolidation-Void Ratio Data for Tests C9 and CD5

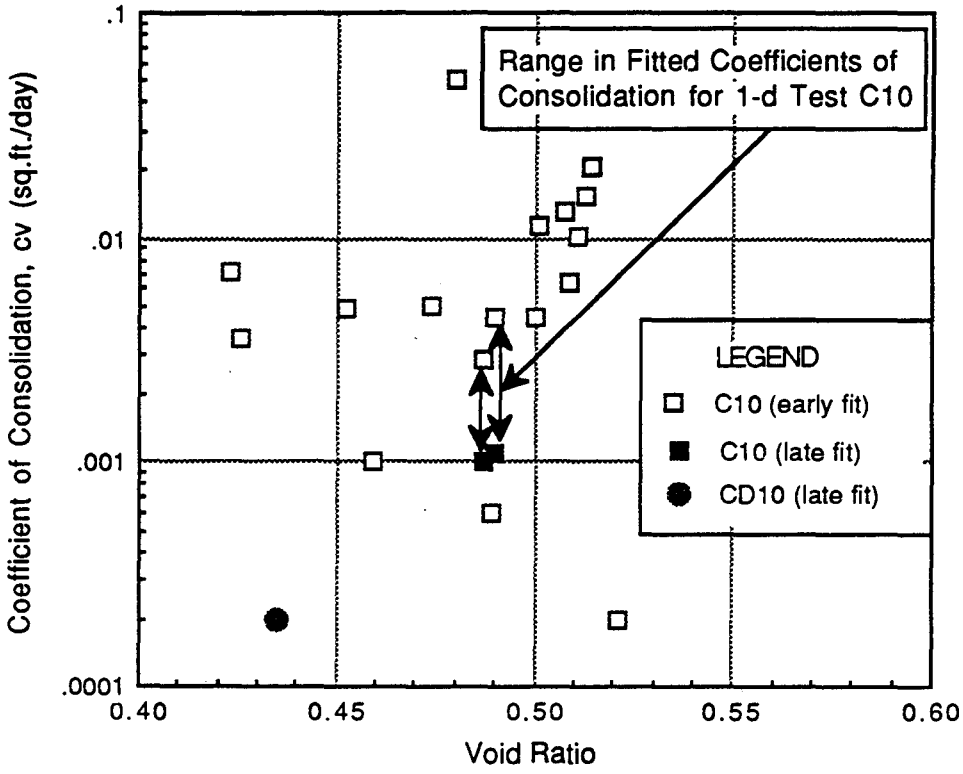

Fig. 7.7 Comparison of Coefficients of Consolidation-Void Ratio Data for Tests C10 and CD10

we have encountered, we do not believe that filter paper drainage is the problem but we have performed no tests to verify this assumption.

7. Membrane leakage due to pressure differences across the membrane and/or water chemistry difference between the specimen and cell water, add uncertainty to the volume-time data obtained in the triaxial tests.

We believe that a combination of these factors is influencing our results but that factors 1 and 3 in the above list are probably the most important.

FAILURE ENVELOPES FOR EAGLEFORD SHALE

A minor difficulty arises in trying to compare failure envelopes between direct shear and triaxial compression tests. Mohr's circles cannot be defined from direct shear tests so neither the Mohr-Coulomb nor modified Mohr-Coulomb diagrams can be used. One option is to plot a standard Mohr-Coulomb diagram with Mohr circles and pick off the normal stress and shearing stress at the intersection of each Mohr circle and the failure envelope. Problems develop in defining the tangent point when the data scatter widely.

We have decided to use the normal and shearing stresses calculated on the planes of maximum deformation (failure planes) in the triaxial tests and thus to use standard Coulomb diagrams for the comparisons.

Both triaxial and triaxial tests were performed at a wide range in deformations rates. Only the tests involving high degrees of consolidation at failure will be used for the comparisons. In addition, we will not include tests where there were obvious problems.

The triaxial tests to be included are CD2, CD3, CD4, CD5, CD7, and CD10. The direct shear tests are DS4, DS7, and DS10. The direct shear data are at a much lower stress level than the triaxial tests

(Fig. 7.8) because there was no increase in normal stress on the failure surface during shear. In the triaxial tests, there were large increases in normal stress, particularly in a few cases where the failure plane was relatively flat. In any case, a single failure envelope has been drawn in, by eye, with a cohesion intercept of 4000 psf and a slope ($\bar{\phi}$) of 28 degrees.

The apparently good agreement between the direct shear residual envelope and the Coulomb envelope from CD tests may not be an accident. The fact that the samples in the CD tests reach peak stress difference before the failure envelope develops probably indicates that yielding of the elements along the failure plane started occurring before peak stress difference was reached. The elements adjacent to the first element that yielded will yield in a progressive progressive fashion until the failure plane develops. By the time the peak stress difference has been reached some percentage of the elements along the failure plane have yielded. Some of these elements may reached a residual stress condition due to localized movements. The apparent peak stress then starts to decrease and once all elements have yielded the failure plane develops.

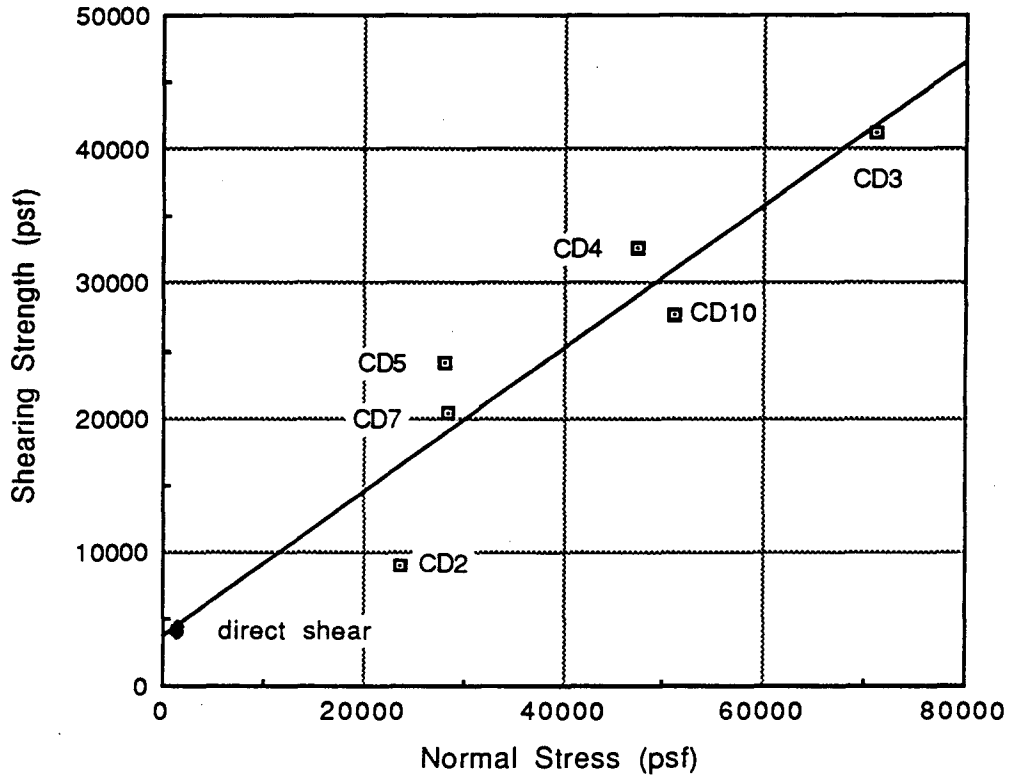

Fig. 7.8 Failure Envelope Involving Both Direct Shear and Triaxial Shear Data

REFERENCES

Bishop, A. W. (1961), "The Measurement of Pore Pressure in the Triaxial Test," *Pore Pressure and Suction in Soils*, Butterworths, London, pp. 38-46.

Bishop, A. W. and R. E. Gibson (1964), "The Influence of Provisions for Boundary Drainage on Strength and Consolidation Characteristics of Soil Measured in the Triaxial Apparatus," ASTM STP No. 361, pp. 435-458.

Bishop, A. W. and D. J. Henkel (1957), *The Measurement of Soil Properties in the Triaxial Test,* Edward Arnold Ltd., London, 190 pp.

Gibson, R. E. and D. J. Henkel (1954), "Influence of Duration of Tests at Constant Rate of Strain on Measured Drained Strength," *Geotechnique,* Vol. 4, pp. 6-15.

Section 8

POSTMORTEM

INTRODUCTION

This project had certain goals, as outlined in Section 1. Although we more than satisfied the contract, our own goals were unattainable. Nevertheless, a great amount of progress was made. In the process of running the tests, we uncovered a number of aspects of both the experimental program and material properties that were left in doubt. This postmortem section is written with the intent of listing some of these problems and discussing methods that might be used to reduce the current level of uncertainty.

We have had a lot of experience testing soils in the laboratory and have apparatus that functions well for such materials. We have much less experience with soft, but relatively incompressible rocks of low hydraulic conductivity, like the Eagleford shale. Further, field experience with such a material, on a long term basis, is severely lacking so it is difficult to rely on empirical methods. If there is to be a rational approach to estimating both short-term and long-term, stability and movements, we need both realistic modelling techniques and a reasonable understanding of material properties, and a reliable and economical way of measuring those properties.

This project was concerned with experimental measurements rather than with modelling. Consequently, we will not discuss modelling in this final section except to note that the experiments are ultimately intended to obtain properties for the models. In this report, we have been concerned with the simplest types of models where one-dimensional consolidation properties and shearing strength suffice. For a project of the nature of the SSC project, more sophisticated modelling will probably be required and tests are needed that

produce the types of data those models require. We will comment on needs for both simple models and the more sophisticated ones.

HYDRAULIC CONDUCTIVITY

The hydraulic conductivity is a property needed for any model that involves water movement in the rock.

With fissile surfaces, it seems almost certain that the soil is highly anisotropic with respect to hydraulic conductivity. Laboratory tests should be used to obtain an estimate of anisotropy in hydraulic conductivity in the cores.

We have measured horizontal hydraulic conductivities in clays using a radial flow consolidation cell in which water could be introduced through a central drain and would flow radially to an outer porous boundary. Existing equipment was designed for cores 2.5 inches in diameter. It seems probable that a modified apparatus could be developed for tests on cores of the rock from the SSC site.

An alternative method, that has been used on a number of occasions, is to trim samples into consolidation rings with the specimen rotated 90 degrees from the field position. This technique is inferior to the previously mentioned approach because: (1) the flow distances are relatively short and may not behave like longer surfaces in the field, (2) the stress state is rotated from the field condition and may cause particle rotations that are not representative of field conditions, and (3) microfissures may open up during trimming and will be parallel to the flow direction, thus making it essentially impossible to close them up when a rigid wall permeameter is used. Flexible wall permeameters may be used provided that care is taken to cover the effects of membrane leakage.

ONE-DIMENSIONAL CONSOLIDATION

A variety of problems developed even in the simple one-dimensional tests used here. The same problems exist in more sophisticated testing where obtaining the required data may be much more difficult than in these comparatively simple tests.

For convenience of reference, the items are numbered.

1. Our calculated degrees of saturation were generally in the range of 90 to 98 percent. A set of preliminary consolidation tests could be performed using samples that have been backpressured to ensure saturation. It is probable that the material in the field, under several hundred feet of water head, is saturated. The interest is to see if the consolidation behavior was in any way seriously influenced by lack of saturation.

2. Incremental consolidation tests are relatively time consuming. If a backpressure device is used, then a few consolidation tests should be performed using an automated device that follows an incremental loading, constant gradient, or constant rate of strain procedure. Such tests usually proceed much faster than the standard consolidation tests but they provide essentially no information on secondary effects. If this approach is successful, they more tests can be run in a short time.

3. Strain rates in the laboratory are far higher than in the field. Consequently, viscous material characteristics, e.g., secondary effects in consolidation, may exert a dominant influence on laboratory properties but a negligible effect on field behavior. As a minimum, it seems useful to try to fit one or more primary/secondary consolidation models to some of the data to get an idea of how field rates might differ from laboratory rates.

TRIAXIAL CONSOLIDATION

Long-Term Consolidation Behavior

Measurement of properties of the material under consolidated-undrained or drained conditions requires that the specimens first be consolidated. Our preliminary measurements indicate that rebound may continue for more than a month. It is not clear whether this response is a real measure of soil properties or results from some other, perhaps extraneous, cause. Relevant studies include:

1. It is not known whether the long term rebound is a primary or secondary phenomenon. One approach to resolving the question is to measure pore water pressures on the axis of the samples as they are draining through the radial boundary, thus providing definitive information on when excess pore water pressures have dissipated. The measurements are likely to be difficult because the low compressibility of the rock requires a measurement system of unusually low compliance.

2. As in the one-dimensional consolidation tests, the effects of low degrees of unsaturation are uncertain. In rebound, the gas bubbles would prevent the development of the anticipated negative pore water pressures and thus slow the initial stages of rebound. In turn, they would expand as the pressure tends to equilibrate, thus lengthening the long term response. A few comparative tests should be performed to determine the effects of backpressuring to ensure saturation.

Influence of Stress States

Modelling under realistic field conditions may require estimates to be made of the effects of following stress paths other than simple triaxial compression. As a minimum, it seems useful to perform some triaxial extension tests in pairs with compression tests on sections of adjacent core to provide preliminary information on the effects of stress state on stress-strain and strength properties. For these rocklike materials, it may be necessary to use elevated triaxial cell pressures.

Membrane Problems

We had unusual problems with membrane leakage. We should look into methods of preventing water leakage by using the same chemistry in the cell water as in the pore water, and perhaps by using butyl or other types of membranes that would be too strong for soil samples but would work fine with soft rocks. We might also want to consider use of mercury as the cell fluid to stop gas diffusion.

SIZE EFFECTS

For fissured materials, the measured strengths of small specimens tend to scatter widely. Some specimens may have no fissures, or at least none with orientations to weaken the specimen, and the measured strength is high. In other cases, major fissures may be aligned with the potential failure planes and result in very low strengths. As the sample size increases, each sample is likely to have a distribution of fissures that more and more closely approximates field mass conditions and the scatter in the strengths should reduce. We have performed one study of the Beaumont formation in Houston to get an estimate of size effects.

We have little idea of what the size effects are for this material. If block samples become available in quantity, we could perform triaxial compression tests with samples of different sizes.

STRENGTH ANISOTROPY

The fissile nature of these sample guarantees that the samples are anisotropic in terms of shearing strength. Although it would be extremely difficult to do, we believe that shear tests should be performed with samples in different orientations so that the strength anisotropy in the field can be taken into account during the

analyses. The Pepper shale at Waco is known from field experience to be highly anisotropic and the lack of attention to this anisotropy was a major contributing cause to the failure of the Waco dam.

OTHER TYPES OF SHEAR TESTS

Direct Simple Shear

In the usual direct shear test, the load is applied to the ring that encases the sample. The ring loads one side of the sample. The resulting deformation allows the ring to make contact with the loading cap and thereafter the relatively rigid cap takes more load than does the side of the compressible soil sample. The result, it is hoped, is that shear is transferred from the top cap (and bottom cap) to the flat faces of the specimen. Only by transferring the shearing stresses from the end caps to the sample, can there be a tolerably uniform shearing stress applied to the failure surfaces.

The materials tested on this project were relatively stiff and brittle. The result may have been that an excessive amount of load was transferred to the specimens from the side, resulting in highly nonuniform states of stress on the failure surface and perhaps explaining the bizarre failure surfaces in two of the three tests with the bentonitic shale.

We need to use a device that truly transfers shearing stress to the faces of the sample and which uses the ring simply for confinement, as it is supposed to be used. To prevent the caps from just sliding on the surface of the sample, it will be necessary to design special gripper plates to fit into grooves on the surface of the sample without causing disturbance. It will also be necessary to devise a method of applying load directly to the gripper plates rather than going through the side rings.

Torsion Shear

Release of large in situ lateral stresses by excavation, has often resulted in large scale lateral movements that bring significant

parts of the deposit into a socalled residual condition. The triaxial and direct simple shear devices are not well suited to the measurement of residual properties. Direct shear tests can be used for this purpose by rocking the two halves of the box back and forth on each other or shearing on a precut surface. As a minimum, such tests should be performed.

The device that is better suited to measurement of large-strain shearing properties, is the torsion shear device. A relatively simple torsion shear device could be made even to work with 1.5-inch O.D. cores. It would not provide good measurements of peak strength because of the fact that strains vary radially, but it might provide the best estimate of large-strain conditions where radial variations in strain become irrelevant.

CHEMISTRY

We had problems with the stainless steel used in consolidation rings and top caps for the consolidation tests. Reactions occurred that caused major pitting of the steel. The mortality rate was also far higher on triaxial membranes than we have ever encountered before. We would be interested in knowing more about the chemistry of the Eagleford shale. In particular, the chemistry of the pore fluid is of interest (electrolyte concentration, cations and anions present, pH). It may also be of interest to look for electric currents set up in apparatus by dissimilar metals. These matters seem worth investigating because of their possible effect on metallic objects buried in the material in the field, on a long term basis.